

Thesis for a Degree of Doctor of Engineering

**Magnetic Properties of
Superparamagnetic Fine Particles:
Comparison with Spin Glass**

Teruo BITOH

December 22, 1993

*Division of Chemical and Materials Engineering,
Muroran Institute of Technology*

Contents

Abstract	1
1 Introduction	3
2 Magnetic Properties of Spin Glass and Fine Particles	6
3 Experimental Methods	17
3.1 Samples	17
3.2 Linear and nonlinear susceptibilities	19
3.3 Dc magnetization	27
4 Experimental Results	28
4.1 Linear and nonlinear susceptibilities	28
4.1.1 Temperature dependence	28
4.1.2 Frequency dependence	29
4.1.3 Comparison with Au-Fe alloy	29
4.2 Field-cooled and zero-field-cooled magnetization	44
4.3 Magnetization curve	48
5 Data Analysis	57
5.1 Superparamagnetic blocking model	57
5.1.1 Assumption	57
5.1.2 Linear and nonlinear susceptibilities	58
5.1.3 Field-cooled and zero-field-cooled magnetization	61
5.1.4 Magnetization curve at high temperatures	62
5.2 Analysis for Cu-Co alloy	65
5.2.1 Characteristic relaxation time	65

5.2.2	Volume distribution function	65
5.2.3	Mean particle volume and volume fraction	67
5.2.4	Anisotropy constant	68
5.3	Analysis for Au-Fe alloy	74
6	Discussion	79
6.1	Linear and nonlinear susceptibilities	79
6.1.1	Temperature dependence	79
6.1.2	Frequency dependence	81
6.2	Field-cooled and zero-field-cooled magnetization	88
6.3	Magnetization curve	96
7	Conclusion	98
	Acknowledgements	100
	A Theory of Nonlinear Susceptibility for Spin Glass	101
	References	105
	List of Figures	108
	List of Tables	113

Abstract

It is well known that many disordered magnetic materials exhibit spin-glass freezing at low temperatures. However the nature of the spin-glass freezing is not yet completely understood. The most fundamental question is whether or not this freezing is a phase transition caused by frustrated interaction between spins. Recently, it was found out that ferrofluids, which are stable dispersions of fine ferromagnetic or ferrimagnetic particles, exhibit spin-glass-like behavior at low temperatures. Some interpretations have been proposed for the spin-glass freezing on the basis of a progressive freezing of the moments of superparamagnetic clusters. To solve this problem, detailed studies of magnetic properties not only for typical spin glasses but also for fine particles are required. The author reports the experimental results and the quantitative analysis of the susceptibilities and the magnetization of ferromagnetic fine cobalt particles, which were precipitated in a $\text{Cu}_{97}\text{Co}_3$ alloy. The author also reports the experimental results for a typical spin-glass $\text{Au}_{96}\text{Fe}_4$ alloy, and compared the results of $\text{Cu}_{97}\text{Co}_3$ with those of $\text{Au}_{96}\text{Fe}_4$.

Some characteristic behavior has been observed in $\text{Cu}_{97}\text{Co}_3$ at low temperatures: (1) The linear susceptibility (χ_0) has a maximum. (2) The magnetization exhibits irreversible behavior. (3) The nonlinear susceptibility χ_2 , which is the coefficient of the H^3 term of the magnetization, has a negative peak around the temperature where χ_0 exhibits the maximum. These results are similar to those of the spin-glass $\text{Au}_{96}\text{Fe}_4$ alloy. However, the negative peak in χ_2 is very broad compared with that of spin glass $\text{Au}_{96}\text{Fe}_4$. Furthermore, χ_2 is proportional to T^{-3} at high temperatures. It is clear

that the temperature dependence of χ_2 of $\text{Cu}_{97}\text{Co}_3$ is very different from that of $\text{Au}_{96}\text{Fe}_4$; χ_2 in the spin glass ($\text{Au}_{96}\text{Fe}_4$) shows divergent behavior, while χ_2 in the fine-particle system ($\text{Cu}_{97}\text{Co}_3$) does not.

In order to clarify the difference between the spin glass and the fine-particle system, an analysis has been performed based on the simplified superparamagnetic blocking model with no interaction between the particles. The temperature dependence of the observed susceptibilities and the magnetization of $\text{Cu}_{97}\text{Co}_3$ is well explained quantitatively by the blocking model; the behavior of susceptibilities in fine-particle systems is expressed as the summation of linear and nonlinear terms of the Langevin function, which describes the magnetization of noninteracting fine-particle systems, over the particle volume distribution. On the other hand, the divergent behavior of χ_2 in $\text{Au}_{96}\text{Fe}_4$ cannot be explained by the blocking model. The author concludes that the nonlinear susceptibility χ_2 shows clearly the difference between the spin-glass transition and the progressive freezing of the cluster moments.

Section 1

Introduction

Studies of the magnetic properties of dilute magnetic alloys (*e.g.*, Au-Fe, Cu-Mn) which contain a small amount of magnetic impurities in nonmagnetic metals have been a subject of interest for half a century.¹⁾ It was found in 1964 that the magnetic susceptibility of such alloys measured in a large magnetic field (≈ 1 kOe) shows a broad maximum at low temperature.²⁾

In 1972, Cannella and Mydosh³⁾ observed a sharp cusp in the low-field (≈ 5 Oe) ac susceptibility of Au-Fe alloys. This observation has been regarded as evidence that such alloys undergo upon cooling a magnetic phase transition from a paramagnetic to an unknown new magnetic state, and led to a great deal of experimental and theoretical work. Edwards and Anderson⁴⁾ proposed in 1975 that the phenomenon described above results from a new type of phase transition, called “spin-glass transition.” According to their model, the magnetic impurities are arranged at random in the nonmagnetic matrix. The impurity spins interact with a potential that oscillates as a function of the distance between the spins (Ruderman-Kittel-Kasuya-Yosida (RKKY) interaction). As a result, the spins are frozen randomly in directions (spin-glass freezing) below the transition temperature T_g , because contradictory ordering between two magnetic spins depending on two different paths, called frustration, takes place. The materials exhibiting the spin-glass transition were named “spin glasses.”

The magnetic properties of spin glasses have been studied extensively. However the nature of spin-glass freezing is still not completely understood.

In particular, the behavior of the specific heat led to the most serious problem. According to the phase transition model,⁴⁾ the magnetic specific heat shows a cusp-like peak at T_g . However, such anomaly in the specific heat of spin glasses has not been observed.⁵⁾ This is taken as evidence against the existence of the phase transition. Wohlfarth⁶⁾ insisted that the spin-glass freezing is not the phase transition but a progressive freezing of the moments of superparamagnetic clusters. He considered that the magnetic atoms are formed ferromagnetic clusters. These clusters exhibit paramagnet-like behavior (superparamagnetism) at high temperatures, but the cluster moments are blocked in the direction of the anisotropy axis at low temperatures.

Recently, Chantrell *et al.*⁷⁾ reported that ferrofluids, which are stable dispersions of fine ferromagnetic or ferrimagnetic particles, exhibit spin-glass-like behavior: *e.g.*, susceptibility maximum, irreversibility between field-cooled and zero-field-cooled magnetization, and time-dependent magnetization. They insisted that such spin-glass-like behavior supports the suggestion of Wohlfarth.⁶⁾ However, it is not clear whether or not all the magnetic properties of fine-particle systems are the same as those of typical spin glasses (*e.g.*, Au-Fe alloys).

As reviewed above, the nature of the spin-glass freezing is still controversial. Detailed studies of magnetic properties not only for typical spin glasses but also for fine particles are required to clarify whether or not the spin-glass freezing is the progressive freezing of the moments of superparamagnetic clusters. In this thesis, the author reports the experimental results and the quantitative analysis of the susceptibility and the magnetization of

ferromagnetic fine particles with special emphasis on behavior of a “non-linear susceptibility χ_2 .” In order to compare with dilute spin-glass alloys (*e.g.*, Au-Fe), the author has selected a Cu-Co alloy as a sample. Copper alloys containing a few percent cobalt have been well known to form spherical precipitates of fcc cobalt dispersed in a matrix of almost pure copper, and have been regarded as one of the typical superparamagnetic materials.⁸⁻¹⁰⁾ The author also measured susceptibilities and magnetization of a typical spin-glass Au-Fe alloy, and compared the results of Cu-Co with that of Au-Fe. From detailed susceptibilities and magnetization measurements and data analysis, the author concluded that the origin of the magnetic properties of superparamagnetic fine particles and spin glasses is very different, though some magnetic properties of fine particles are similar those of spin glasses.

This thesis is organized as follows. In Section 2, the author reviews the earlier experimental results of typical spin glasses and fine particle systems, and compare the magnetic properties of fine particle systems with those of spin glasses. The sample preparation and the experimental methods are described in Section 3. The experimental results are reported in Section 4. The quantitative analysis of the experimental data has been performed based on the superparamagnetic blocking model. The methods of the analysis are explained in Section 5, and the results of the analysis are discussed in Section 6. Conclusion is given in Section 7.

Section 2

Magnetic Properties of Spin Glass and Fine Particles

Typical spin glasses such as Au-Fe or Cu-Mn exhibit following characteristic properties:

- (A) The low field ac susceptibility shows a sharp cusp at the freezing temperature T_g (Fig. 2.1(a): from Cannella and Mydosh, 1972).³⁾ In large fields the cusp in the ac susceptibility of spin glasses is rounded off.
- (B) The freezing temperature T_g shifts to higher with increasing the measuring frequency (Fig. 2.2(a): from Mulder *et al.*, 1981).¹¹⁾
- (C) The magnetic contribution to the specific heat exhibits no sharp anomaly at T_g but a broad maximum well above T_g (Figs. 2.3(a) and (b): from Wenger and Keesom, 1976).¹²⁾
- (D) The dc magnetization (or dc susceptibility) below T_g depends strongly on the way the experiment is performed. The zero-field-cooled magnetization (ZFCM) has a cusp at T_g when the sample is cooled above T_g in the absence of a magnetic field and thereafter the dc magnetic field H is applied. On the other hand, the field-cooled magnetization (FCM) below T_g is larger than ZFCM and is nearly independent of temperature when the sample is cooled above T_g in the dc magnetic field (Fig. 2.4(a): from Nagata *et al.*, 1979).¹³⁾
- (E) The dc magnetization below T_g relaxes rather slowly (sometimes over hours). For example, the isothermal remanent magnetization, $IRM(t)$,

which is obtained after suppressing the dc magnetic field H applied at a given temperature $T < T_g$, decays logarithmically ($IRM(t) = M_0 - S \ln(t)$, where M_0 and S are constants) (Fig. 2.5(a): from Holtzberg *et al.*, 1977).¹⁴⁾

- (F) Mössbauer spectra splits roughly at T_g (Fig. 2.6(a): from Violet and Borg, 1966),¹⁵⁾ thereby suggesting the formation of static or quasi-static internal fields below T_g due to frozen-in spins.
- (G) Spin glasses have no conventional long-range magnetic order (of ferromagnetic or antiferromagnetic type).

The properties of (A) and (F) suggest that the spin-glass freezing is a cooperative phenomenon of the spins (*i.e.*, it is the phase transition), but the properties (B) and (C) suggest that this freezing is a progressive freezing of the spins or cluster moments.

On the other hand, it has been reported that many fine-particle systems exhibit following spin-glass-like properties:

- (a) The low field ac susceptibility has a spin-glass-like maximum at low temperature (Fig. 2.1(b): from Gittleman *et al.*, 1974).¹⁶⁾
- (b) The temperature of the peak in the ac susceptibility shifts to higher with increasing the measuring frequency (Fig. 2.2(b): from Dormann *et al.*, 1983).¹⁷⁾
- (c) The specific heat exhibits no sharp anomaly at low temperatures. (Fig. 2.3(c): from Tournier *et al.*, 1962).¹⁸⁾
- (d) The dc magnetization (or dc susceptibility) at low temperatures exhibits spin-glass-like irreversible behavior; the zero-field-cooled magnetization (ZFCM) has a maximum and field-cooled magnetization

is considerably larger than ZFCM at low temperatures (Fig. 2.4(b): from El-Hilo and O'Grady, 1990).¹⁹⁾

- (e) The dc magnetization at low temperatures relaxes rather slowly. For example, the isothermal remanent magnetization decays logarithmically (Fig. 2.5(b): from El-Hilo *et al.*, 1991).²⁰⁾
- (f) Mössbauer spectra splits at low temperatures (Fig. 2.6(b): from Koch *et al.*, 1986).²¹⁾
- (g) In general, fine-particle systems also have no long-range magnetic order.

These properties of the fine-particle systems are very similar to those of the typical spin glasses.

It should be emphasized that in spin glasses, the nonlinear susceptibility χ_2 can show the characteristic critical behavior. The magnetization M is expanded with respect to an applied magnetic field H in the vicinity of a spin-glass transition temperature T_g as

$$M = \chi_0 H + \chi_2 H^3 + \chi_4 H^5 + \dots, \quad (2.1)$$

where χ_0 is the linear susceptibility, and χ_2, χ_4, \dots are the nonlinear susceptibilities. According to the mean field theory, χ_2 diverges negatively at T_g because the spin-glass order parameter susceptibility is not the linear susceptibility χ_0 but the nonlinear susceptibility χ_2 (see, Appendix A).²²⁻²⁴⁾ Since the first measurement of χ_2 in the spin glass,²⁵⁾ the divergent behavior of χ_2 has been observed for many spin-glass materials; *e.g.*, $(\text{Ti}_{1-x}\text{V}_x)_2\text{O}_3$,^{25, 26)} Au-Fe (Figs. 2.7(a) and (b)),²⁷⁻²⁹⁾ Cu-Mn³⁰⁾ and Ag-Mn.³¹⁾ These results are strongly support that the spin-glass freezing is the phase transition.

On the other hand, the nonlinear susceptibility for fine-particle systems has been rarely studied. Fiorani *et al.*³²⁻³⁴⁾ reported that χ_2 of an Fe-Al₂O₃ granular thin film does not show critical behavior (Fig. 2.7(c)). However, their data are available only above the temperature where χ_0 exhibits a maximum, because they obtained χ_2 from dc magnetization data. Direct measurements of χ_2 of fine particles over a wide temperature range are required to clarify the difference between the spin glass and the fine-particle system.

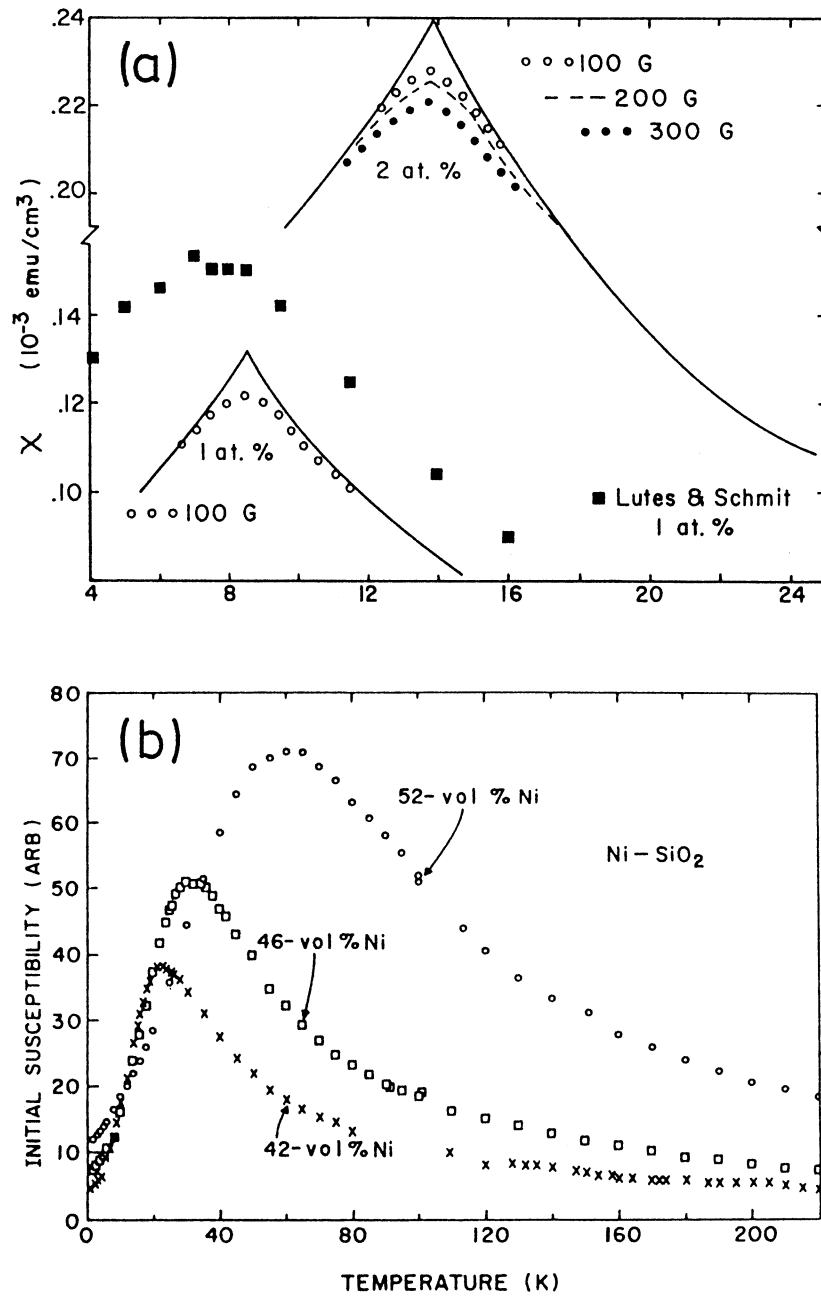


Fig. 2.1. Ac susceptibility of (a) spin-glass Au-Fe alloys (from Cannella and Mydosh, 1972)³⁾ and of (b) Ni fine particles in SiO₂ films (from Gittleman *et al.*, 1974)¹⁶⁾ as a function of temperature. In large fields the cusps in the ac susceptibility of the Au-Fe alloys are rounded off.

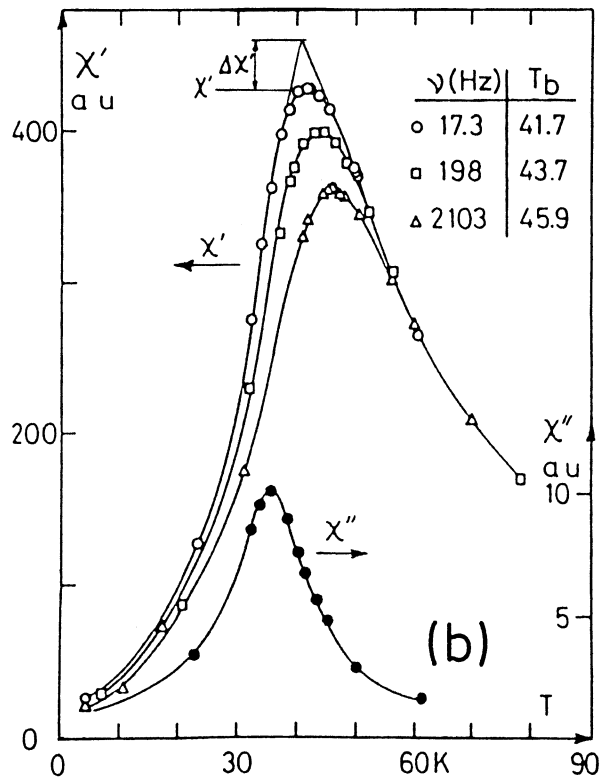
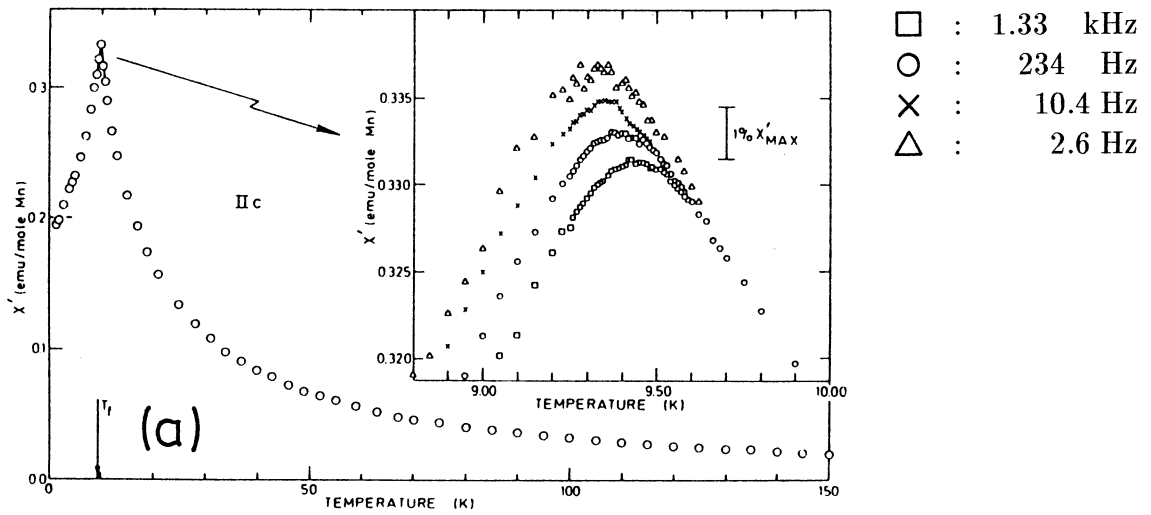


Fig. 2.2. Frequency dependence of ac susceptibility of (a) a spin-glass $\text{Cu}_{99.06}\text{Mn}_{0.94}$ alloy (from Mulder *et al.*, 1981)¹¹⁾ and of (b) Fe fine particles in an amorphous Al_2O_3 film (from Dormann *et al.*, 1983).¹⁷⁾

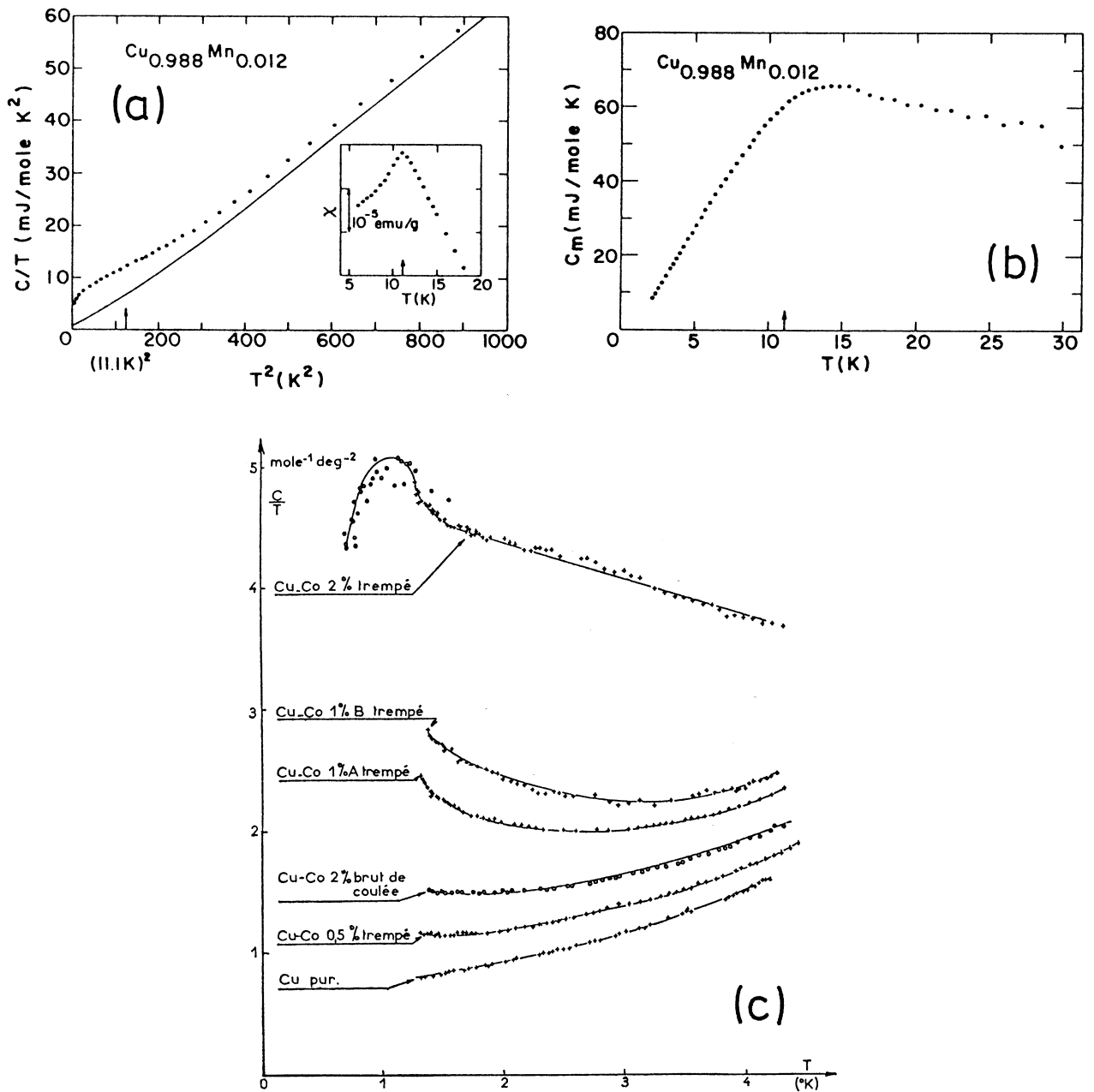


Fig. 2.3. Total ((a) and (c)) and magnetic (b) specific heat of a spin-glass $\text{Cu}_{0.988}\text{Mn}_{0.012}$ alloy ((a) and (b), from Wenger and Keesom, 1976)¹²⁾ and of Co fine particles in Cu-Co alloys ((c), from Tournier *et al.*, 1962).¹⁸⁾ The solid curve in Fig. (a) is calculated nonmagnetic contribution to the specific heat of the alloy. The inset of Fig. (a) shows the ac susceptibility result. The arrows in Figs. (a) and (b) show T_g .

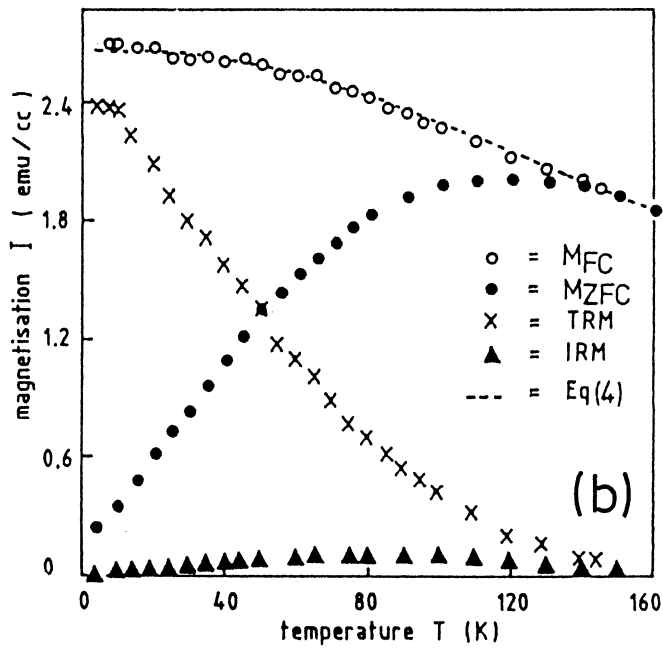
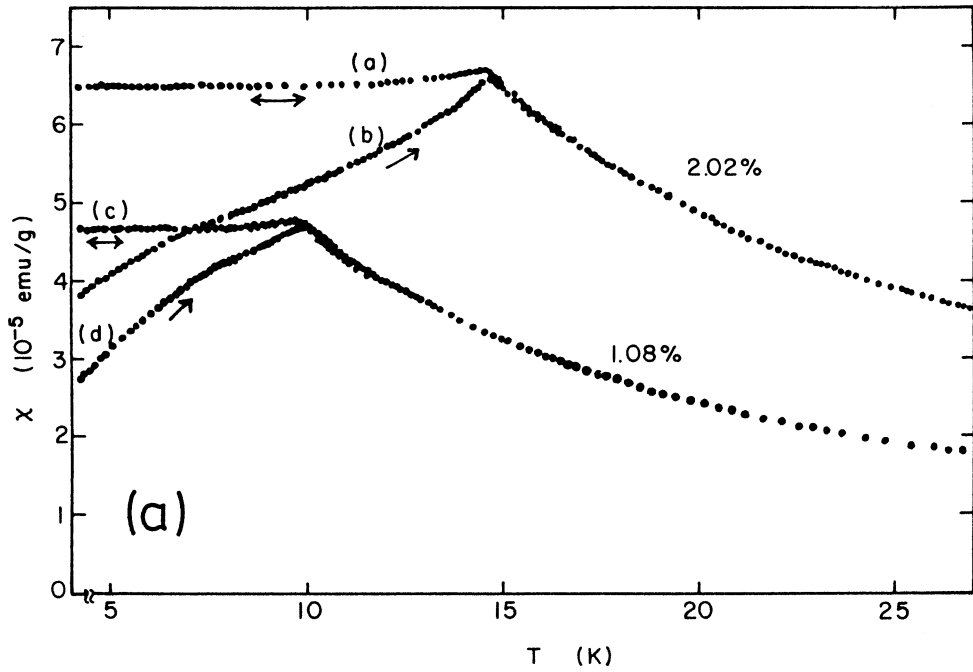


Fig. 2.4. Temperature dependence of field-cooled and zero-field-cooled magnetization (or susceptibility) of (a) spin-glass Cu-Mn alloys (from Nagata *et al.*, 1979)¹³⁾ and of (b) ferrofluid, which comprises stable dispersion of Fe_3O_4 fine particles (from El-Hilo and O'Grady, 1990).¹⁹⁾

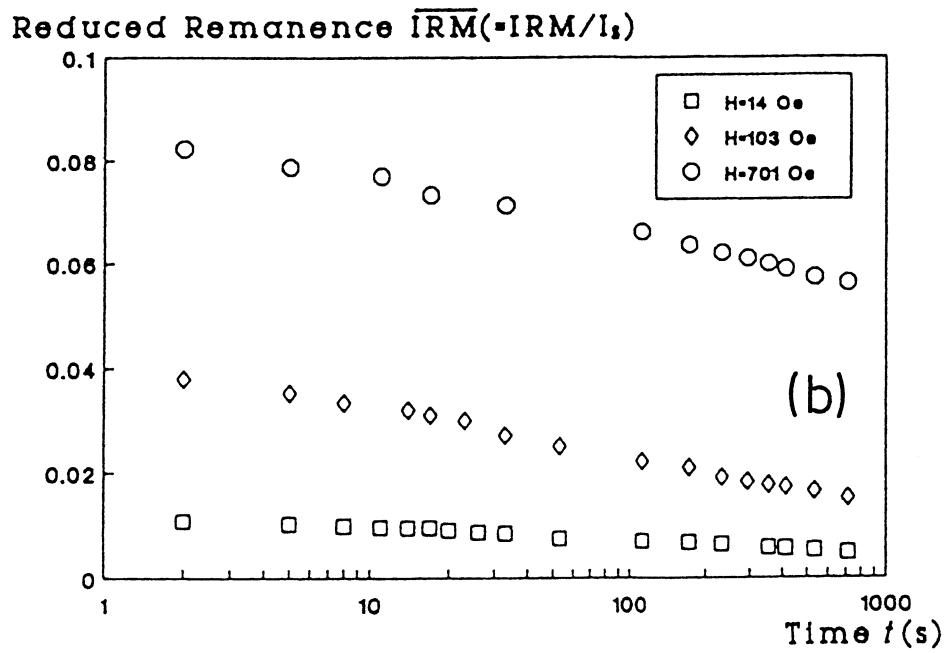
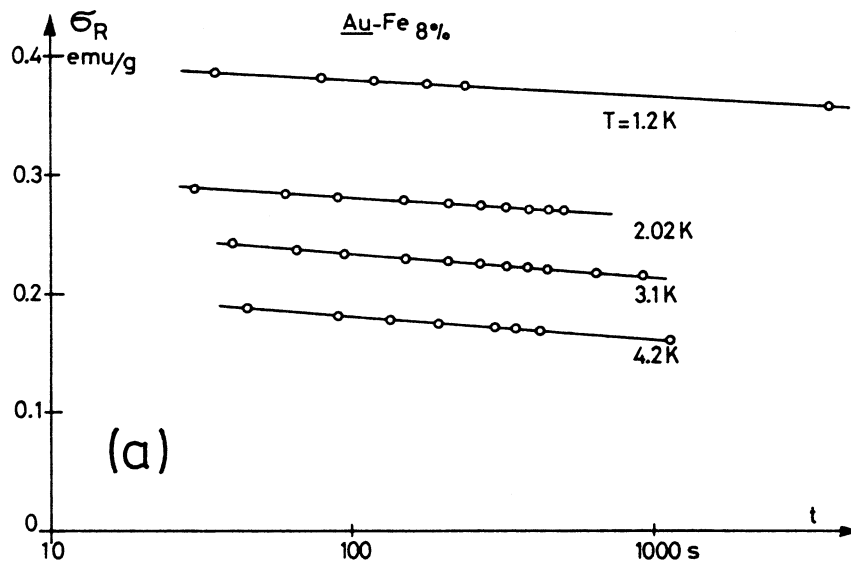


Fig. 2.5. Time decays of $IRM(t)$ of (a) a spin-glass Au_92Fe_8 alloy (from Holtzberg *et al.*, 1977)¹⁴⁾ and of (b) ferrofluid, which comprises stable dispersion of Fe_3O_4 fine particles (from El-Hilo *et al.*, 1991).²⁰⁾

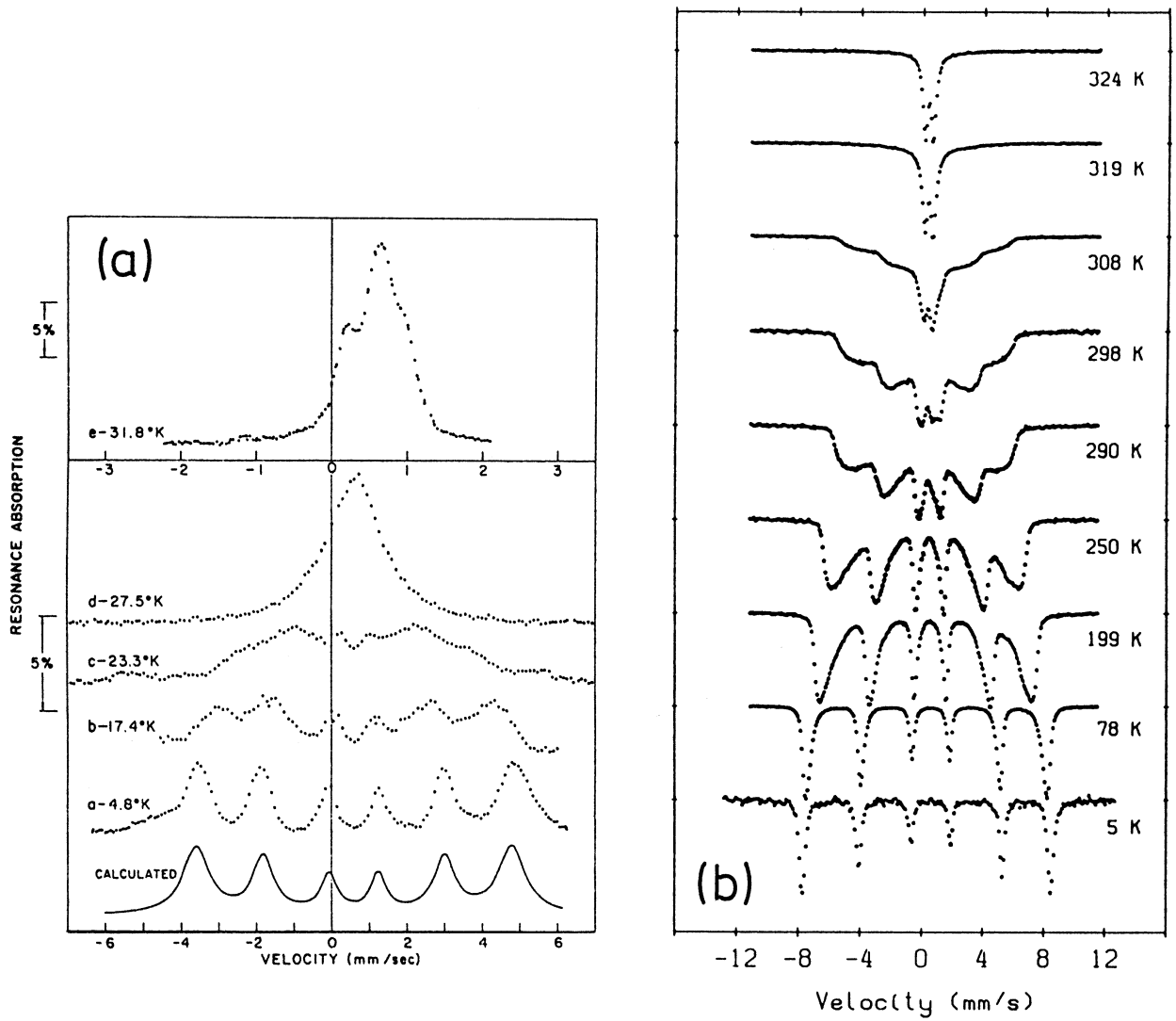


Fig. 2.6. Mössbauer spectra of (a) a spin-glass $\text{Au}_{93.3}\text{Fe}_{6.7}$ alloy (from Violet and Borg, 1966)¹⁵⁾ and of (b) goethite fine particles (from Koch *et al.*, 1986)²¹⁾ at various temperatures.

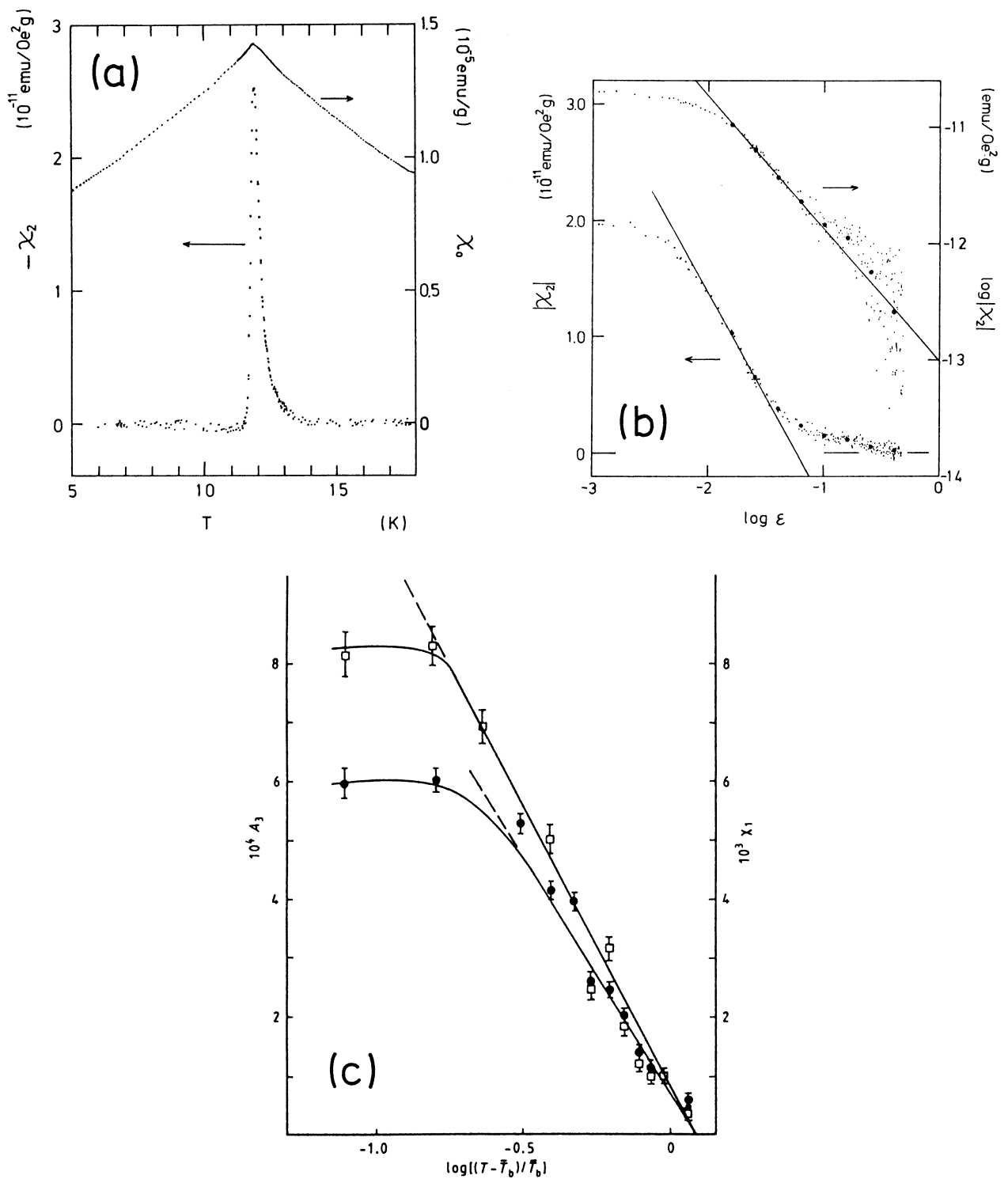


Fig. 2.7. Nonlinear susceptibility χ_2 of ((a) and (b)) a spin-glass $\text{Au}_{98.5}\text{Fe}_{1.5}$ alloy (from Taniguchi *et al.*, 1983)²⁸⁾ and of (c) Fe fine particles in an amorphous Al_2O_3 film (from Fiorani *et al.*, 1986).³³⁾

Section 3

Experimental Methods

3.1 Samples

The author prepared $\text{Cu}_{97}\text{Co}_3$ and $\text{Au}_{96}\text{Fe}_4$ alloys to be used as samples. The sample $\text{Cu}_{97}\text{Co}_3$ alloy was prepared as follows. Raw materials of copper (99.99 %) and cobalt (99.9 %) in a quartz glass crucible were melted in an electric furnace under argon atmosphere. The molten alloy was sucked into quartz tube and rapidly solidified into a rod by quenching in ice water. The quenched rod was cut into small pieces which were used as samples of $\text{Cu}_{97}\text{Co}_3$. The $\text{Cu}_{97}\text{Co}_3$ sample had the dimensions of $15.7 \times 1.8 \times 0.57 \text{ mm}^3$ and the weight of 0.143 g.

The sample $\text{Au}_{96}\text{Fe}_4$ alloy was prepared as follows. Gold (99.99 %) and iron (99.999 %) were melted in an arc furnace turning upside down for several times under argon atmosphere to obtain homogeneous alloy. The obtained alloy was cut into small pieces which were used as samples of $\text{Au}_{96}\text{Fe}_4$. The $\text{Au}_{96}\text{Fe}_4$ sample had the dimensions of $10.2 \times 2.7 \times 2.6 \text{ mm}^3$ and the weight of 1.51 g. Then the $\text{Au}_{96}\text{Fe}_4$ sample was homogenized by annealing at $900 \text{ }^\circ\text{C}$ for 2 days in vacuum followed by quenching in ice water.

Figure 3.1 shows the X-ray diffraction patterns of the $\text{Cu}_{97}\text{Co}_3$ and $\text{Au}_{96}\text{Fe}_4$ alloys. The $\text{Cu}_{97}\text{Co}_3$ alloy has the fcc structure and no peak corresponding to fcc or hcp cobalt precipitates has been detected. The lattice constant for $\text{Cu}_{97}\text{Co}_3$ is $3.609 \pm 0.005 \text{ \AA}$ which is slightly smaller than that of 3.615 \AA for pure fcc copper. This result suggests that cobalt atoms appreciably dissolved in the copper matrix. The $\text{Au}_{96}\text{Fe}_4$ alloy also has the fcc

structure and its lattice constant is 4.074 ± 0.004 Å which is slightly smaller than that of 4.079 Å for pure fcc gold.

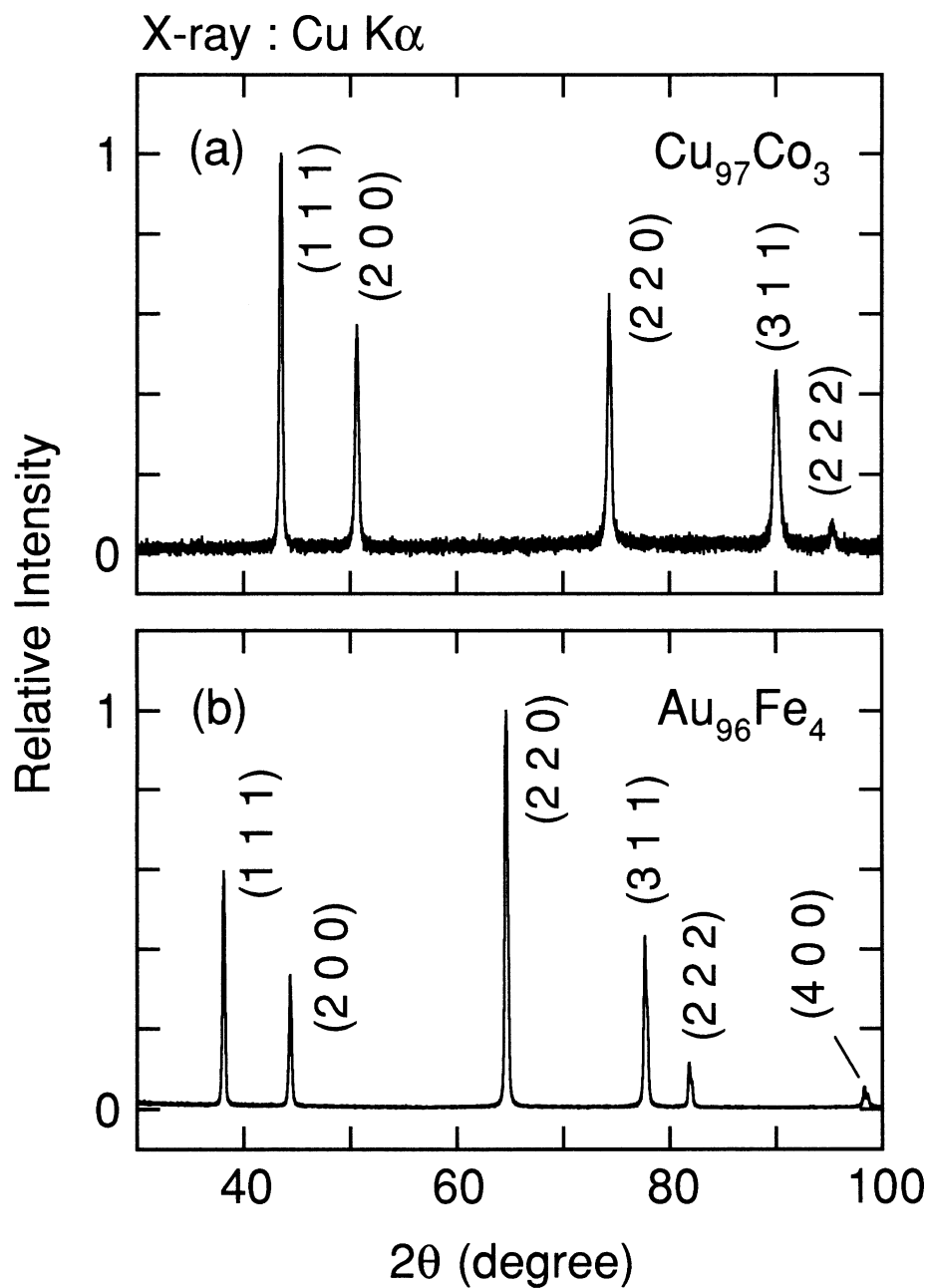


Fig. 3.1. X-ray diffraction patterns of (a) $\text{Cu}_{97}\text{Co}_3$ and (b) $\text{Au}_{96}\text{Fe}_4$ alloys.

3.2 Linear and nonlinear susceptibilities

The ac susceptibilities were measured with a Corson's type mutual inductance bridge.³⁵⁾ When the magnetization M has inversion symmetry concerned with the change in the sign of magnetic field H , then M is expressed as the odd power series of H for a demagnetizing state as³⁶⁾

$$M = \chi_0 H + \chi_2 H^3 + \chi_4 H^5 + \dots, \quad (3.1)$$

where H is an applied field, χ_0 is the linear susceptibility, χ_2, χ_4, \dots are the nonlinear susceptibilities. When an ac field, $H = h_0 \cos \omega t$, is applied, the nonlinear ac magnetic response, $m(t)$, contains the components with various frequencies, which consist of in-phase and out-of-phase components as $m_n = m'_n - im''_n$. Thus the magnetization $m(t)$ is given by

$$m(t) = \sum_{n=0}^{\infty} [m'_{2n} \cos(2n+1)\omega t - m''_{2n} \sin(2n+1)\omega t], \quad (3.2)$$

where

$$m'_0 = \chi'_0 h_0 + \frac{3}{4} \chi'_2 h_0^3 + \dots, \quad (3.3)$$

$$m''_0 = \chi''_0 h_0 + \frac{3}{4} \chi''_2 h_0^3 + \dots, \quad (3.4)$$

$$m'_2 = \frac{1}{4} \chi'_2 h_0^3 + \frac{5}{16} \chi'_4 h_0^5 + \dots, \quad (3.5)$$

$$m''_2 = \frac{1}{4} \chi''_2 h_0^3 + \frac{5}{16} \chi''_4 h_0^5 + \dots, \quad (3.6)$$

\vdots

An induced voltage in a secondary coil by the sample is given as

$$\begin{aligned} E &= -L^* \frac{dm(t)}{dt} \\ &= \omega L^* [m'_0 \sin \omega t + m''_0 \cos \omega t \\ &\quad + 3(m'_2 \sin 3\omega t + m''_2 \cos 3\omega t) + \dots] \end{aligned}$$

$$\begin{aligned}
&= \omega h_0 L^* [\chi_0^{t'} \sin \omega t + \chi_0^{t''} \cos \omega t \\
&\quad + \frac{3}{4} h_0^2 (\chi_2^{t'} \sin 3\omega t + \chi_2^{t''} \cos 3\omega t) + \dots], \quad (3.7)
\end{aligned}$$

where $L^* = L/n$, L is the mutual inductance between a secondary coil and an equivalent solenoid³⁷⁾ that has the same size of the sample and proportional to n , which is the number of turns in the equivalent solenoid per unit length, and

$$\chi_0^{t'} = \frac{m_0'}{h_0} = \chi_0' + \frac{3}{4} \chi_2' h_0^2 + \dots, \quad (3.8)$$

$$\chi_0^{t''} = \frac{m_0''}{h_0} = \chi_0'' + \frac{3}{4} \chi_2'' h_0^2 + \dots, \quad (3.9)$$

$$\frac{3}{4} \chi_2^{t'} h_0^2 = \frac{3m_2'}{h_0} = \frac{3}{4} \chi_2' h_0^2 + \frac{15}{16} \chi_4' h_0^4 + \dots, \quad (3.10)$$

$$\frac{3}{4} \chi_2^{t''} h_0^2 = \frac{3m_2''}{h_0} = \frac{3}{4} \chi_2'' h_0^2 + \frac{15}{16} \chi_4'' h_0^4 + \dots, \quad (3.11)$$

\vdots

When h_0 is small, we can put here $\chi_0' \approx \chi_0^{t'}$, $\chi_0'' \approx \chi_0^{t''}$, $\chi_2' \approx \chi_2^{t'}$, $\chi_2'' \approx \chi_2^{t''}$, \dots . These linear (χ_0' , χ_0'') and nonlinear (χ_2' , χ_2'' , \dots) susceptibilities could be measured simultaneously by detecting ω , 3ω , \dots components using several two-phase lock-in amplifiers. The magnitude of susceptibilities were calibrated by numerical calculations of the mutual inductance L^* .³⁷⁾

Figure 3.2 shows the schematic diagram of the measuring system for ac susceptibilities. Figures 3.3 and 3.4 show the circuit diagram of the mutual inductance bridge. During operation, an ac exciting voltage is applied from the function synthesizer (NF 1925) to the input jack J1 of the bridge, and the bridge supplies an ac current to the primary coil. The output signal of the secondary coil, which is delivered at the output jack J3 of the bridge, is detected by the two lock-in amplifiers (NF 5610B). The bridge also provides

a monitor signal for the primary current at the monitor jack J2. The digital frequency multiplier (which was made by H. Arisawa) makes two reference signals from the monitor signal for the lock-in amplifiers;³⁸⁾ one (the reference signal for χ_0) has a frequency of ν (equals to that of the monitor signal) and its phase is delayed for $\pi/2$ that of the monitor signal, and the other (the reference signal for χ_2) has a frequency of 3ν and in-phase with the reference signal for χ_0 .

Figure 3.5 schematically shows the coil configuration and the sample holder. The measuring coils were carefully designed and wound onto the glass bobbin using formal covered copper wire (0.1 ϕ for primary coil and 0.07 ϕ for secondary coil) with collodion to hold the winding in place. The dimensions and the number of turns in the coils are shown in Table 3.1. The sample holder was made of thin copper plate whose thickness was 0.3 mm. It was mounted on a copper tube which could be moved up- and downward. The sample was set on the sample holder using GE7031 varnish. The ac field was applied parallel to the longest dimension of the samples. After cooling to 4.2 K by putting helium exchange gas into a vacuum space, the temperature range up to room temperature was obtained by pumping the vacuum space with a diffusion pump and by heating with the heater wound onto the copper tube. The temperature was measured with a silicon-diode thermometer (PALM BEACH STD-108sp S/N 807) attached on the sample holder. This thermometer was calibrated with the standard silicon-diode thermometer (Lake Shore DT-470-LR-12 S/N D65600) in the temperature range between 4.2 K to 300 K.

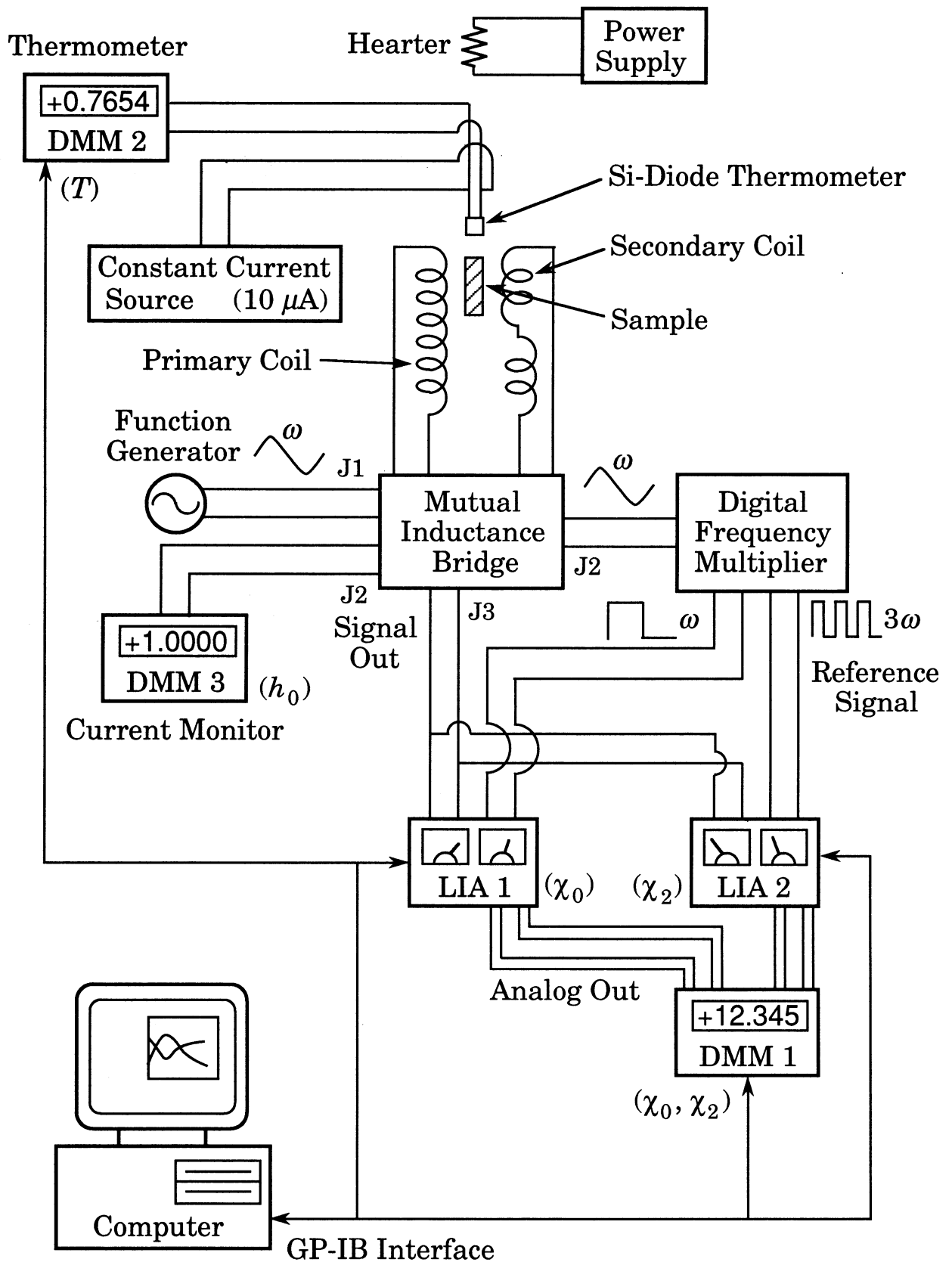


Fig. 3.2. Schematic diagram of the measuring system for ac susceptibilities.

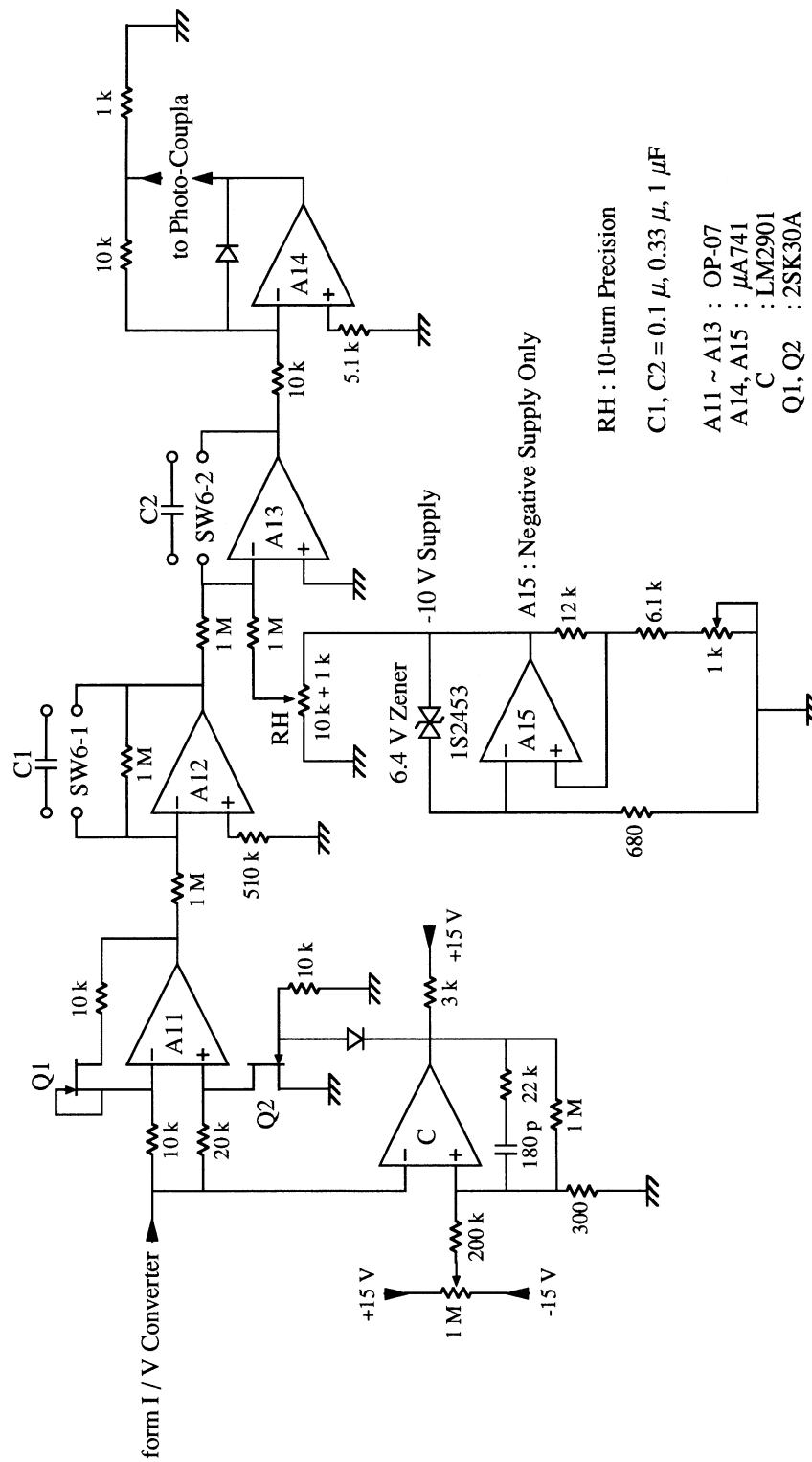


Fig. 3.4. Circuit diagram of the mutual inductance bridge (2).

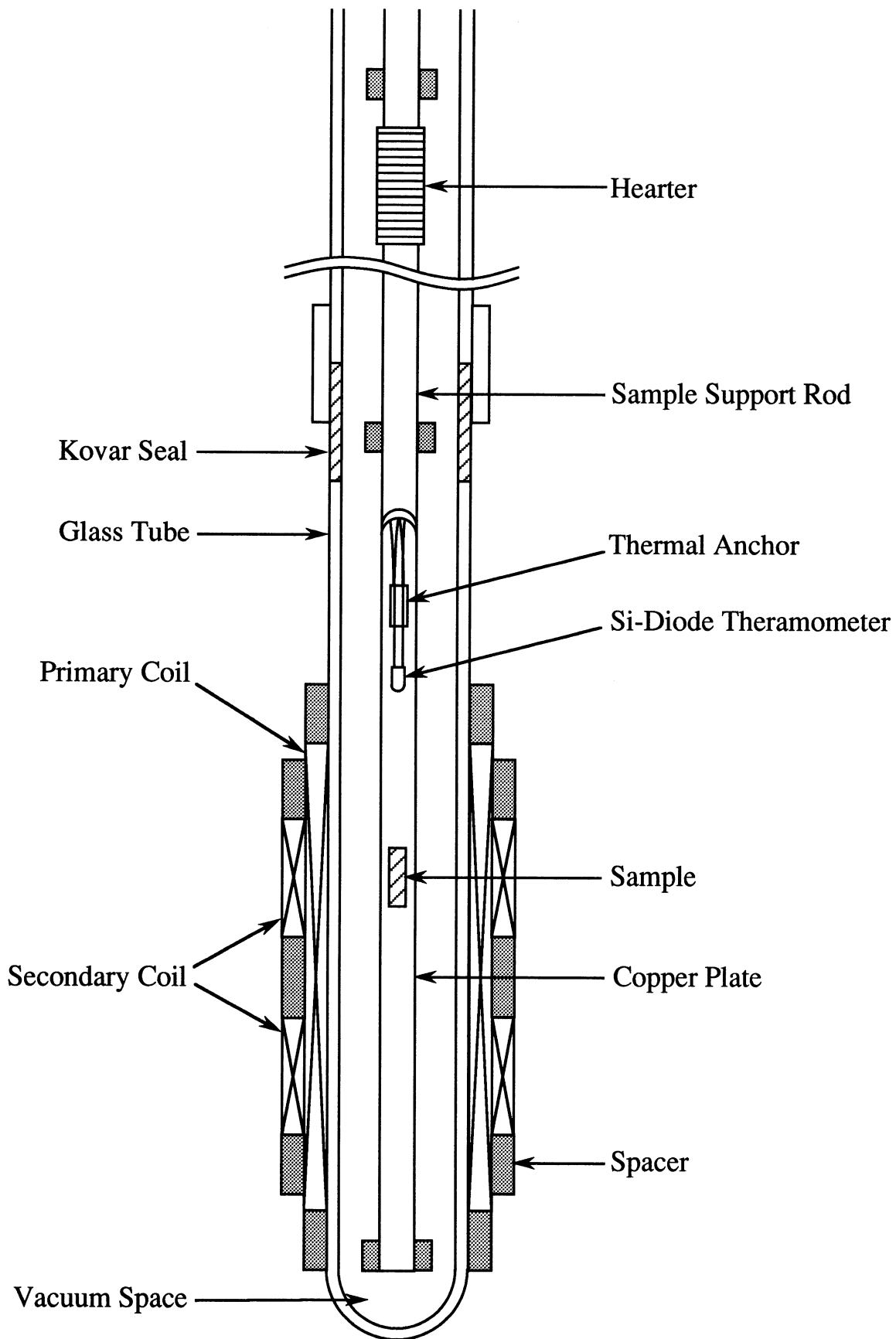


Fig. 3.5. Schematic cross section of the measuring coils.

Table 3.1. Dimensions and the number of turns in the measuring coils.

Coil	Length (mm)	Diameters		Number of turns
		Inner (mm)	Outer (mm)	
Primary	135.0	9.10	9.85	6488 (4 layers)
Secondary	35.0 ^{a)}	9.95	11.35	4206 ^{a)} (10 layers)

a) These values for each half of the secondary coil.

3.3 Dc magnetization

The dc magnetization was measured with an rf superconducting quantum interference device (rf-SQUID: QUANTUM DESIGN MPMS₂). The temperature dependence of the magnetization was measured as follows. First, the sample were cooled in a zero field from above 200 K. Then a magnetic field was applied and zero-field-cooled magnetization (ZFCM) was measured with increasing temperature from 6 K to 100 K. Subsequently, field-cooled-magnetization (FCM) was measured with decreasing temperature from 100 K to 6 K. The magnetization versus magnetic field isotherms were also measured in a field up to 10 kOe and in a temperature range from 6 to 300 K after zero-field cooling from above 200 K. The magnetic field was applied parallel to the longest dimension of the samples by a superconducting magnet operating in the persistent mode. The magnitude of magnetization was calibrated with pure palladium and pure nickel.

Section 4

Experimental Results

4.1 Linear and nonlinear susceptibilities

4.1.1 Temperature dependence

Figure 4.1 shows a typical temperature dependence of the in-phase linear susceptibility χ'_0 and the in-phase nonlinear susceptibility χ'_2 of $\text{Cu}_{97}\text{Co}_3$ alloy measured at the frequency $\nu = 80$ Hz with the ac field amplitude $h_0 = 30$ Oe. When the temperature increases, χ'_0 increases at lower temperatures, exhibiting a round maximum around 25 K, and then decreases gradually at higher temperatures. On the other hand, χ'_2 is nearly zero at 4.2K. With increasing temperature χ'_2 decreases first, exhibiting a minimum around 28 K, and then gradually approaches zero at higher temperatures. Figure 4.2 shows a example of the out-of-phase susceptibilities of $\text{Cu}_{97}\text{Co}_3$ alloy. The out-of-phase linear susceptibility χ''_0 exhibits a maximum around 17 K and becomes zero around 150 K. On the other hand, with increasing temperature the out-of-phase nonlinear susceptibility χ''_2 exhibits a minimum around 22 K and becomes zero around 150 K.

Figure 4.3 shows $(\chi'_0 - \chi_c)^{-1}$ of $\text{Cu}_{97}\text{Co}_3$ as a function of temperature. The constant term χ_c ($= (1.1 \pm 0.2) \times 10^{-5}$ emu/cm³) of χ'_0 was obtained by χ'_0 versus T^{-1} plot (Fig. 4.4). The paramagnetic Curie temperature of $\text{Cu}_{97}\text{Co}_3$ was determined to be $\Theta = -0.2 \pm 0.2$ K; χ'_0 obeys approximately the Curie law above 100 K. The effective number of Bohr magnetrons per cobalt atom is estimated as $p_{\text{eff}} = 65.6 \pm 0.5$. This value is very large and indicates the existence of precipitated ferromagnetic particles in the

Cu₉₇Co₃ alloy.

4.1.2 Frequency dependence

Figures 4.5 and 4.6 show the frequency dependence of the susceptibilities for Cu₉₇Co₃ alloy at $h_0=30$ Oe. With increasing the frequency all the peaks in the susceptibilities move to higher temperature. For χ'_0 , χ'_2 and χ''_2 , the height of the peaks decreases with increasing the frequency. On the other hand, the height of the positive peak in χ''_0 increases with increasing the frequency.

4.1.3 Comparison with Au-Fe alloy

In order to compare the results of Cu₉₇Co₃ and of Au₉₆Fe₄ alloy, the susceptibilities of both these alloys are shown in Figs. 4.7 and 4.8 as a function of temperature. The in-phase linear susceptibility χ'_0 of Au₉₆Fe₄ has a clear cusp at a well-defined transition temperature T_g ($= 20.3$ K), and χ'_2 has a very sharp negative peak at T_g . The out-of-phase linear susceptibility χ''_0 of Au₉₆Fe₄ has a sharp positive peak just below T_g , and χ''_2 , as well as χ'_2 , has a very sharp negative peak at T_g . The present result for Au₉₆Fe₄ also reproduces the features reported by Taniguchi and Miyako.²⁹⁾

Figure 4.9 shows $(\chi'_0 - \chi_c)^{-1}$ of Au₉₆Fe₄ as a function of temperature, where $\chi_c = (-8.7 \pm 0.5) \times 10^{-5}$ emu/cm³ (Fig. 4.10). The paramagnetic Curie temperature of Au₉₆Fe₄ was determined to be $\Theta = -1.5 \pm 0.5$ K; χ'_0 obeys approximately the Curie law above 50 K. The effective number of Bohr magnetons per iron atom is estimated as $p_{\text{eff}} = 6.8 \pm 0.2$.

The susceptibilities of the Cu₉₇Co₃ alloy exhibit the spin-glass-like be-

havior; χ'_0 and χ''_0 have a maximum, and χ'_2 and χ''_2 have a negative peak at low temperature. In particular, the temperature dependence of χ'_0 in $\text{Cu}_{97}\text{Co}_3$ is similar to that of the spin glass in Au-Fe alloys measured in large fields,³⁾ though χ'_0 of $\text{Cu}_{97}\text{Co}_3$ is two orders of magnitude larger than that of $\text{Au}_{96}\text{Fe}_4$. Furthermore, both χ'_0 of $\text{Cu}_{97}\text{Co}_3$ and of $\text{Au}_{96}\text{Fe}_4$ obey approximately the Curie law at high temperatures. However, the negative peak in χ'_2 of $\text{Cu}_{97}\text{Co}_3$ is very broad compared with that of the spin-glass $\text{Au}_{96}\text{Fe}_4$ alloy. In addition, χ'_2 of $\text{Cu}_{97}\text{Co}_3$ does not return to zero even at 280 K far from the negative peak while that of $\text{Au}_{96}\text{Fe}_4$ shows a sharp peak only in the vicinity of T_g : $T_g \pm 1$ K. It seems that the temperature dependence of χ'_2 of $\text{Cu}_{97}\text{Co}_3$ alloy is qualitatively different from that of $\text{Au}_{96}\text{Fe}_4$ alloy.

It is well known that in spin glasses, the temperature dependence of χ'_2 for temperatures just above T_g is dominated by the following power law divergence:^{22, 24)}

$$\chi'_2 = \Gamma t^{-\gamma}, \quad (4.1)$$

$$t \equiv \frac{T - T_g}{T_g}, \quad (4.2)$$

where t is the reduced temperature, γ is the critical exponent, Γ is the critical amplitude. In Au-Fe alloys, the values of γ between 1 to 2 have been reported.²⁷⁻²⁹⁾ Figure 4.11 shows log-log plot of $-\frac{3}{4}\chi'_2 h_0^2$ versus t for $\text{Au}_{96}\text{Fe}_4$. The value of T_g ($= 20.36$ K) were determined from the peak temperature of χ'_2 . The nonlinear susceptibility χ'_2 of $\text{Au}_{96}\text{Fe}_4$ well obeys the power law divergence (eq. (4.1)) just above T_g with a value of $\gamma = 1.39 \pm 0.20$.

Figure 4.12 shows the log-log plots of $-\frac{3}{4}\chi'_2 h_0^2$ versus temperature for $\text{Cu}_{97}\text{Co}_3$. Figure 4.12 indicates that over the high temperature range above

100 K, χ_2 of $\text{Cu}_{97}\text{Co}_3$ can be expressed well as power law of temperature:

$$\chi_2' = -CT^{-n}, \quad (4.3)$$

where C is a positive constant. From the slope of the straight line in Fig. 4.12, the author obtained $n = 3.17$. The values of n are nearly independent of the ac field amplitude and of the frequency in the present measuring conditions. Averaging all these values the author obtained $n = 3.15 \pm 0.20$; χ_2' of $\text{Cu}_{97}\text{Co}_3$ is nearly proportional to T^{-3} above 100 K.

It is clear that the temperature dependence of χ_2' of $\text{Cu}_{97}\text{Co}_3$ alloy is very different from that of $\text{Au}_{96}\text{Fe}_4$ alloy; χ_2' in the spin-glass $\text{Au}_{96}\text{Fe}_4$ alloy shows divergent behavior, while χ_2 in $\text{Cu}_{97}\text{Co}_3$ alloy does not. Furthermore, χ_2' of $\text{Cu}_{97}\text{Co}_3$ alloy is nearly proportional to T^{-3} at high temperatures.

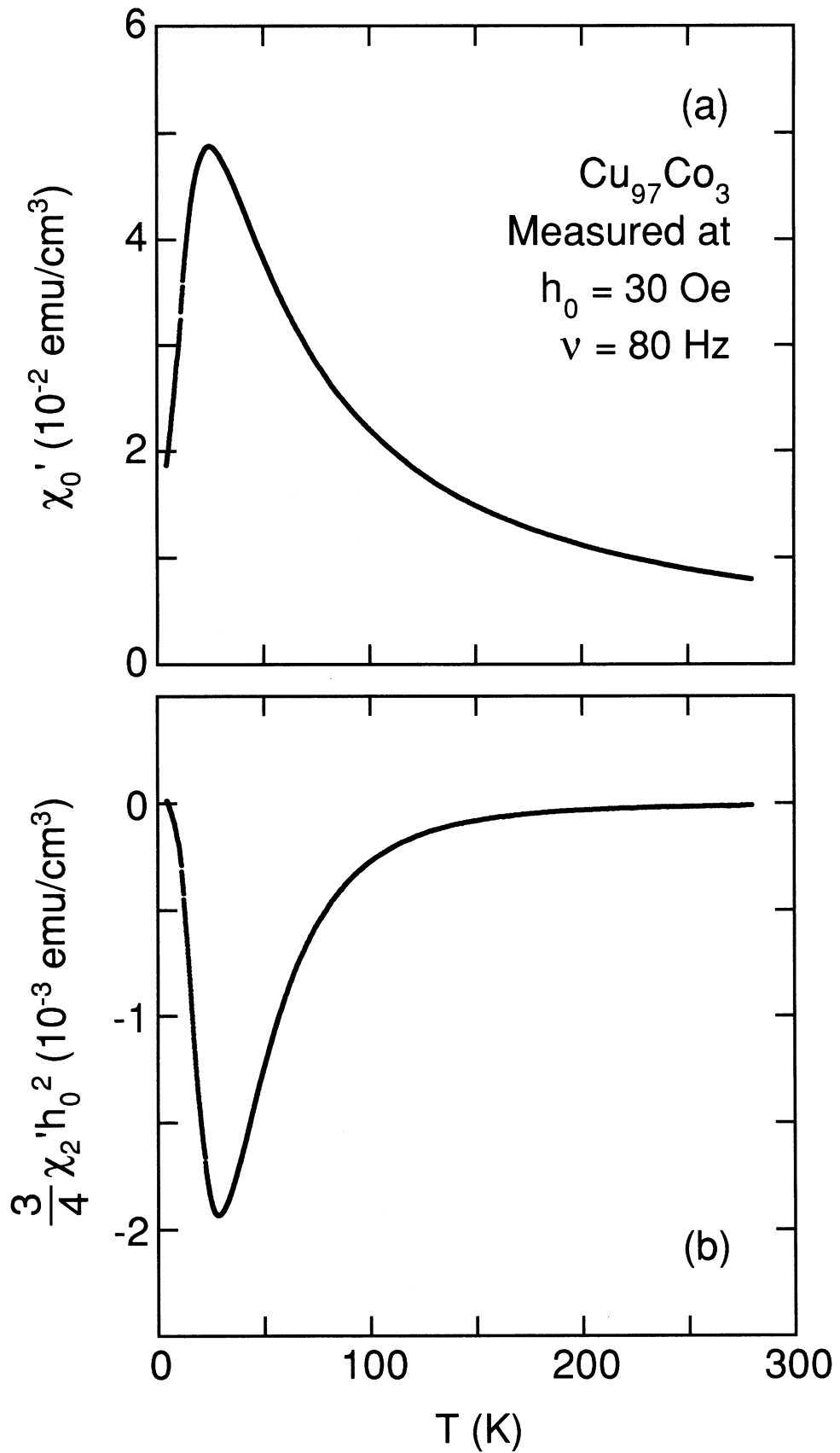


Fig. 4.1. Temperature dependence of (a) the in-phase linear (χ_0') and (b) nonlinear ($\frac{3}{4}\chi_2'h_0^2$) susceptibilities of $\text{Cu}_{97}\text{Co}_3$ alloy.

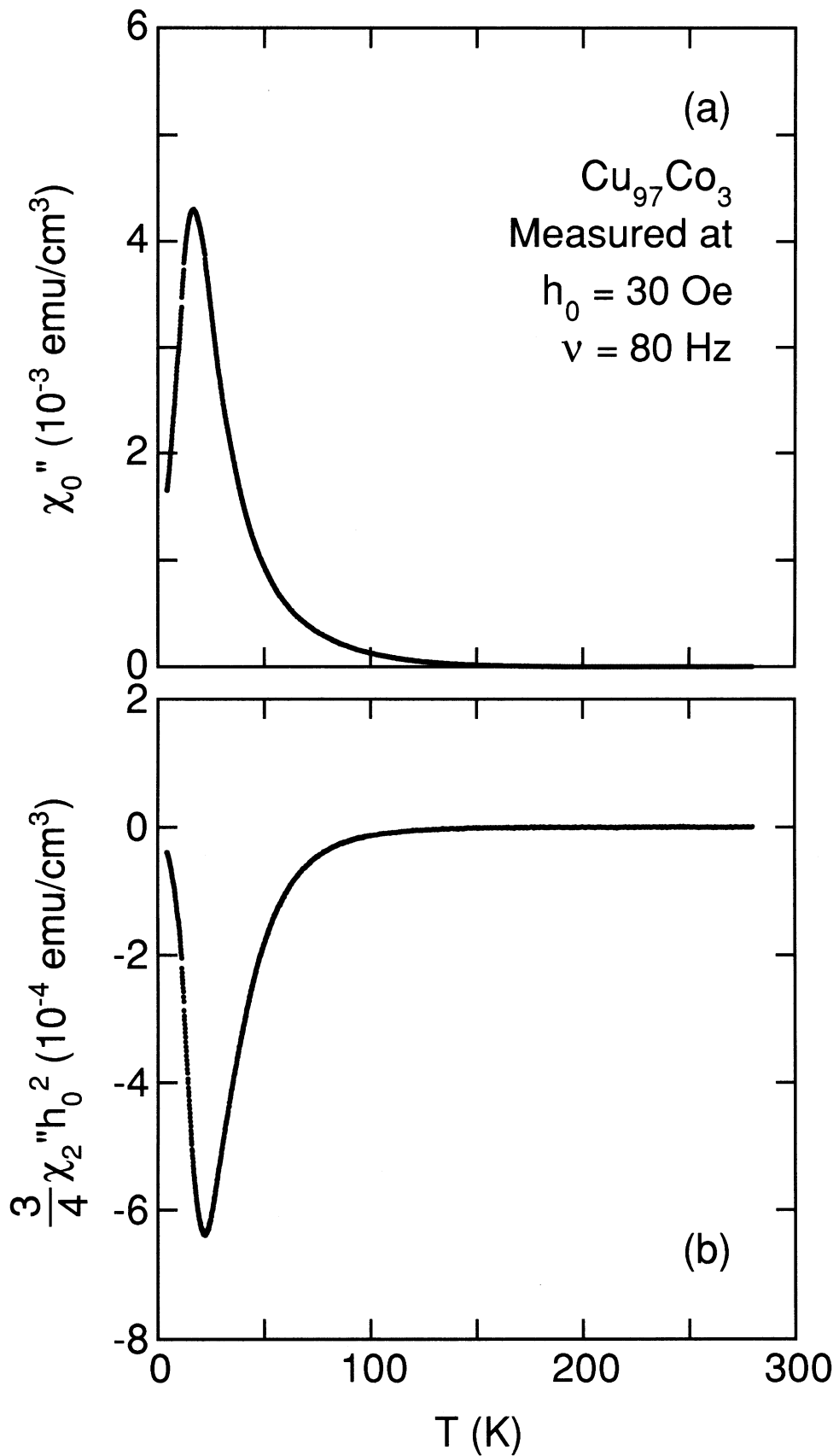


Fig. 4.2. Temperature dependence of (a) the out-of-phase linear (χ_0'') and (b) nonlinear ($\frac{3}{4}\chi_2''h_0^2$) susceptibilities of $\text{Cu}_{97}\text{Co}_3$ alloy.

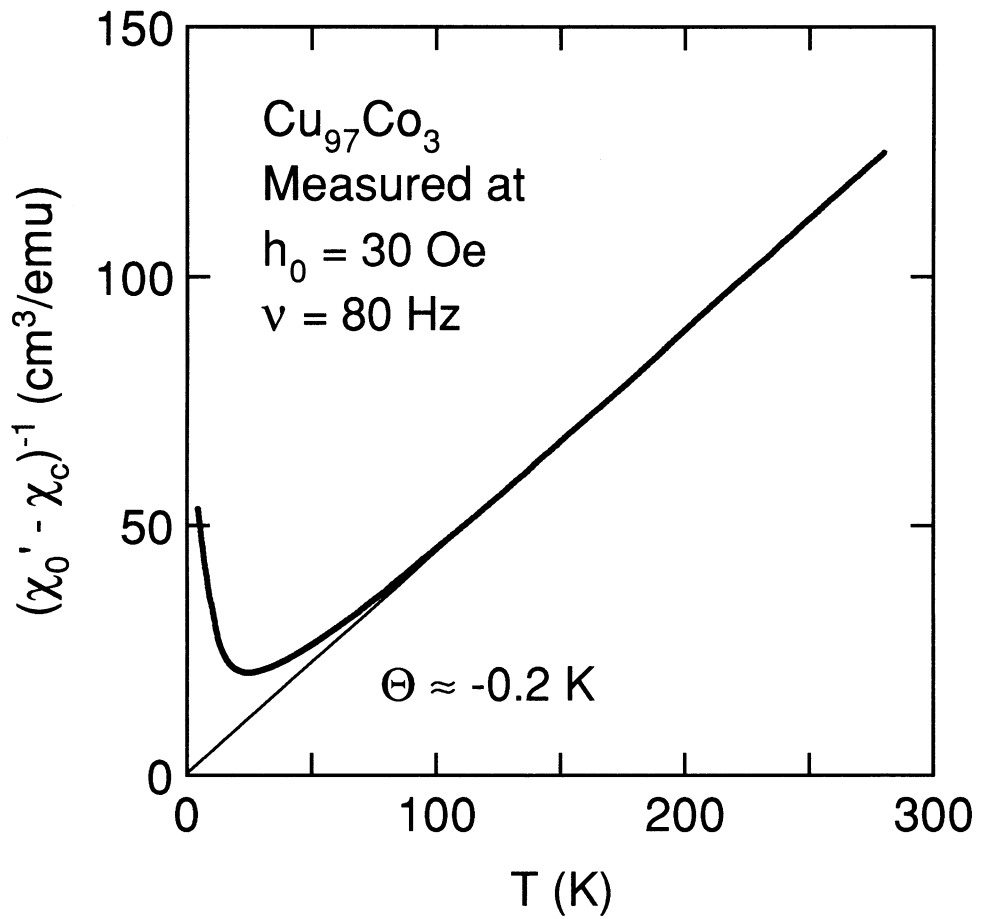


Fig. 4.3. Inverse of the in-phase susceptibility $(\chi_0' - \chi_c)^{-1}$ of $\text{Cu}_{97}\text{Co}_3$ alloy as a function of temperature.

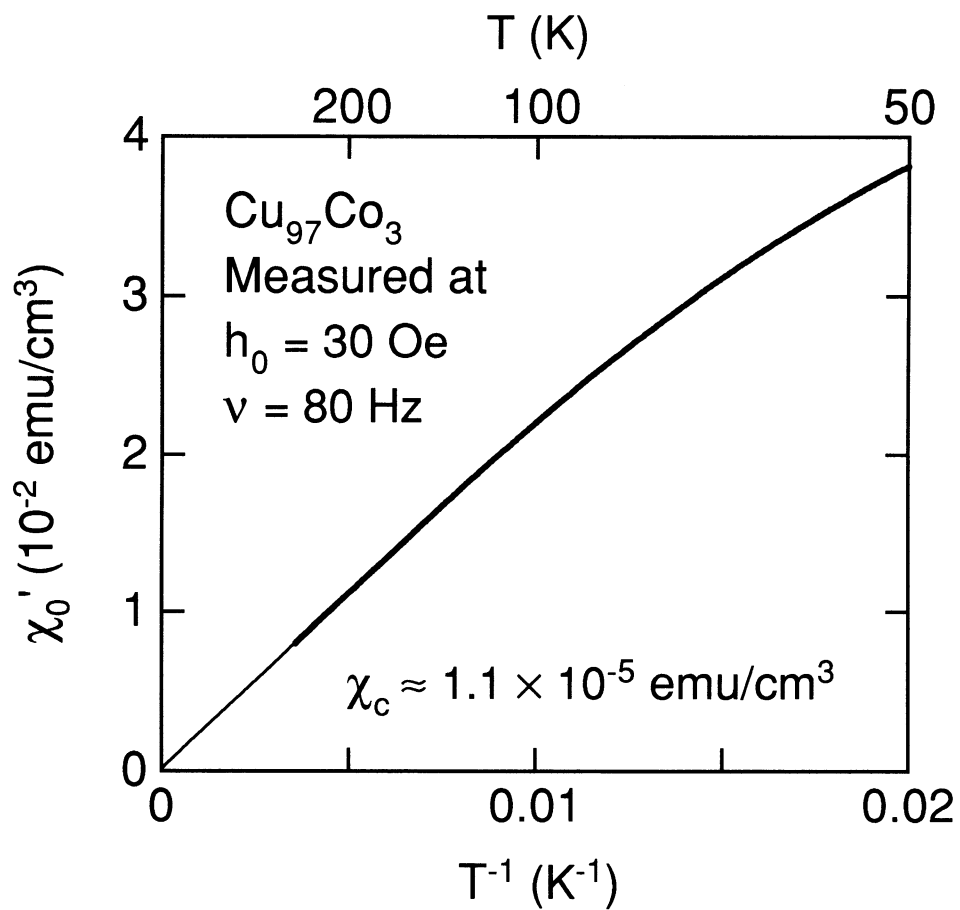


Fig. 4.4. In-phase susceptibility χ_0' of Cu $_{97}$ Co $_3$ alloy as a function of T^{-1} .

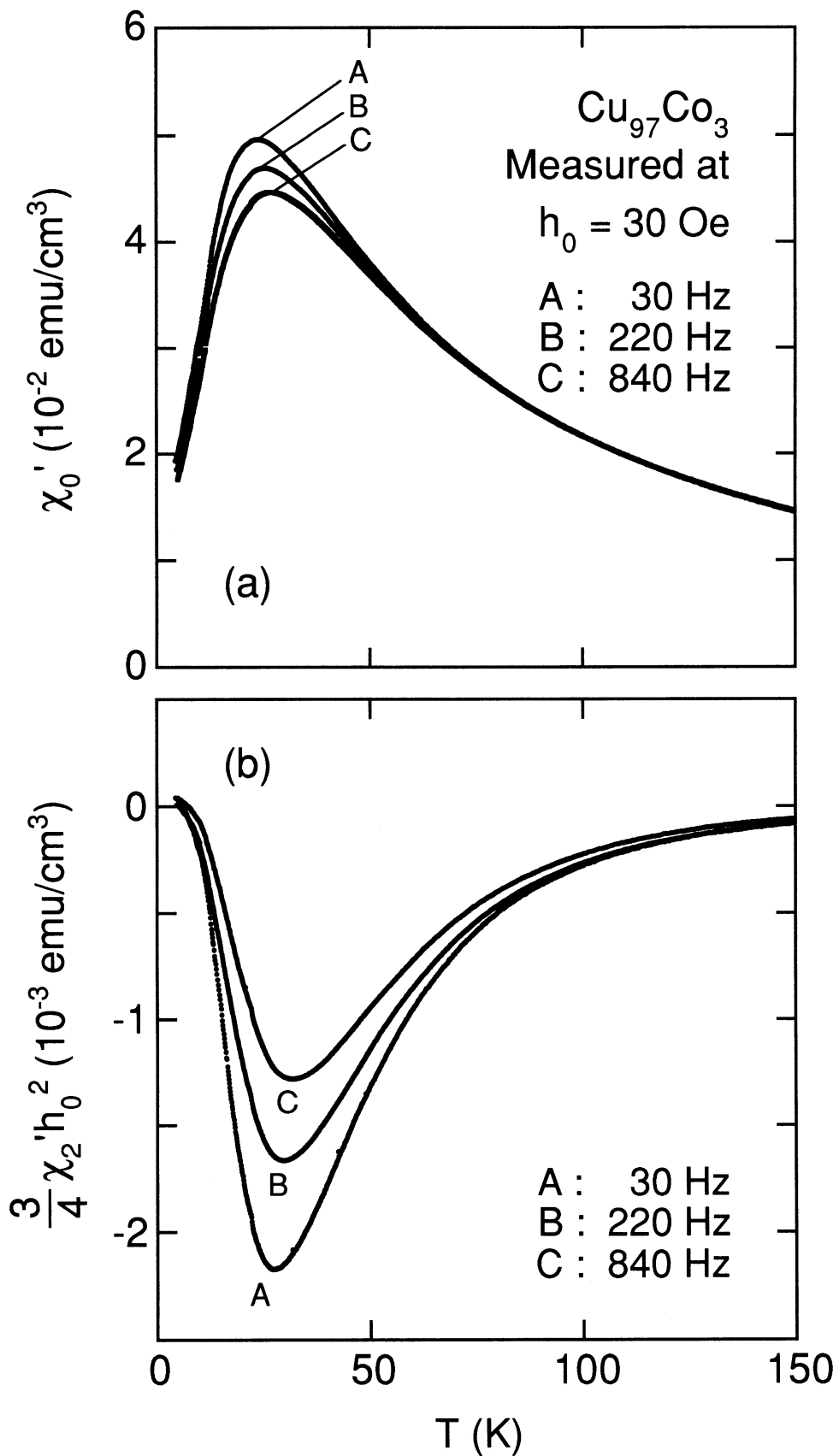


Fig. 4.5. Frequency dependence of (a) the in-phase linear (χ'_0) and (b) non-linear ($\frac{3}{4}\chi'_2 h_0^2$) susceptibilities of $\text{Cu}_{97}\text{Co}_3$ alloy.

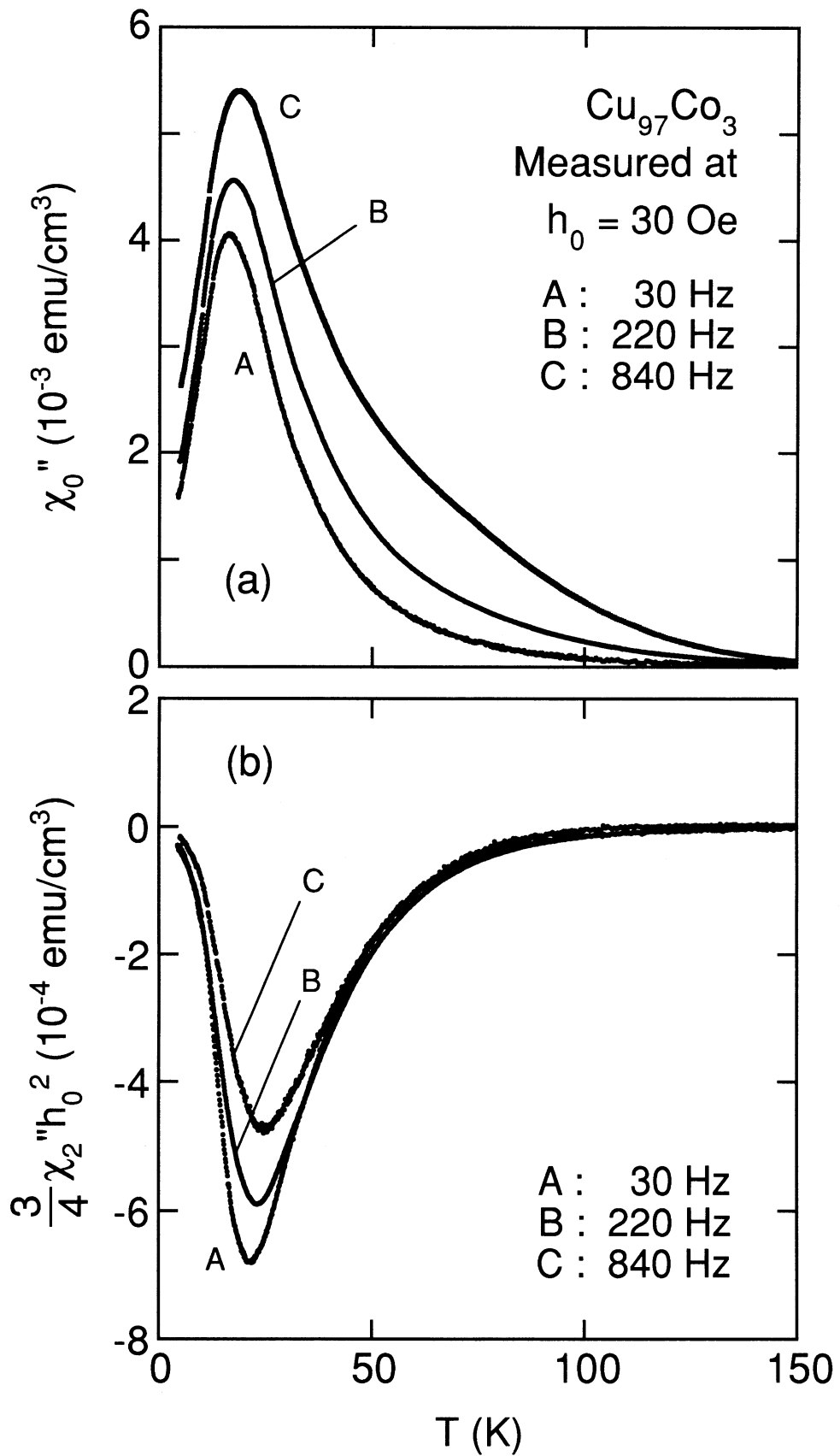


Fig. 4.6. Frequency dependence of (a) the in-phase linear (χ_0'') and (b) non-linear ($\frac{3}{4}\chi_2''h_0^2$) susceptibilities of Cu₉₇Co₃ alloy.

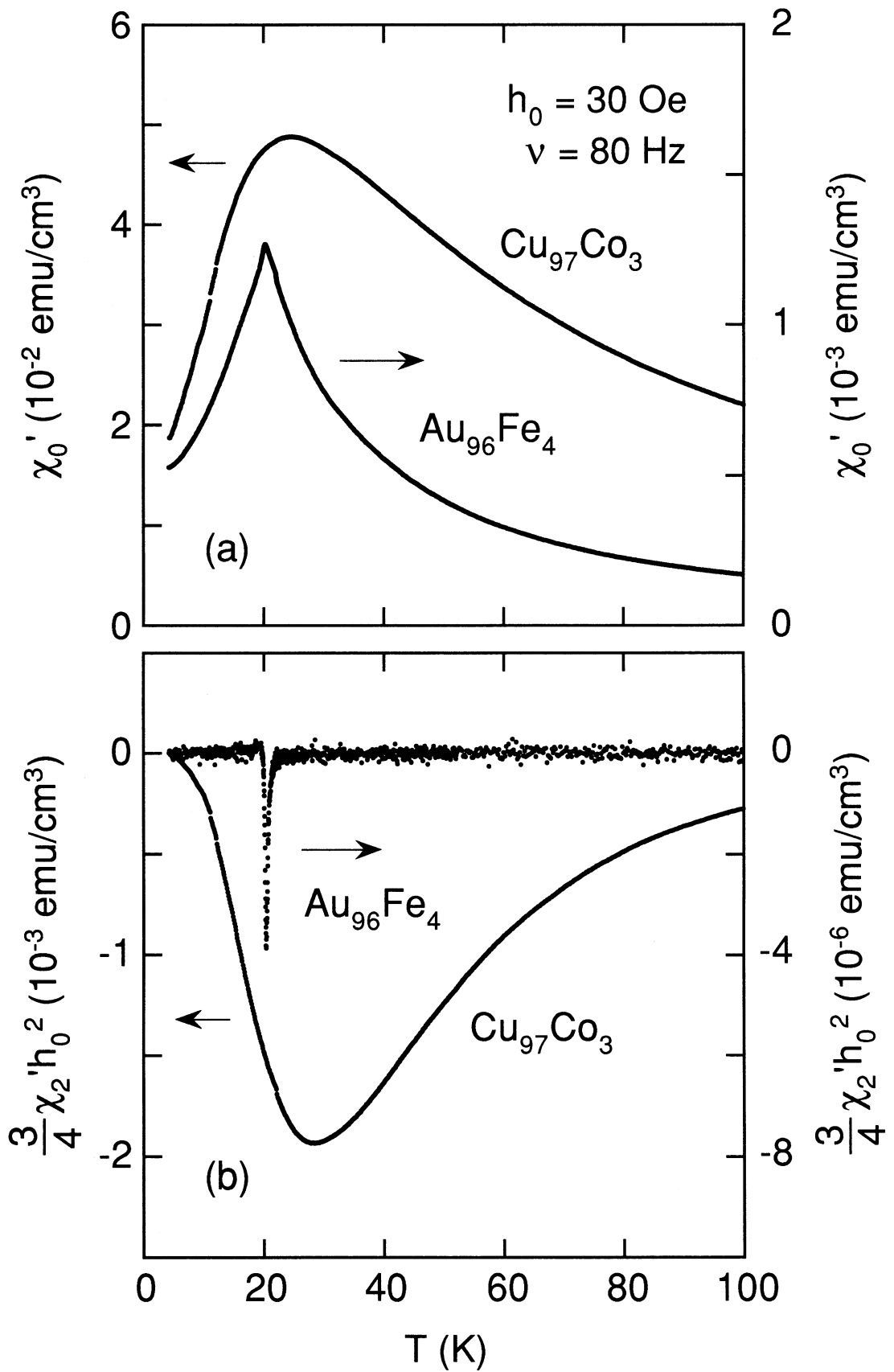


Fig. 4.7. (a) In-phase linear (χ_0') and (b) nonlinear ($\frac{3}{4}\chi_2'h_0^2$) susceptibilities of $\text{Cu}_{97}\text{Co}_3$ and $\text{Au}_{96}\text{Fe}_4$ as a function of temperature.

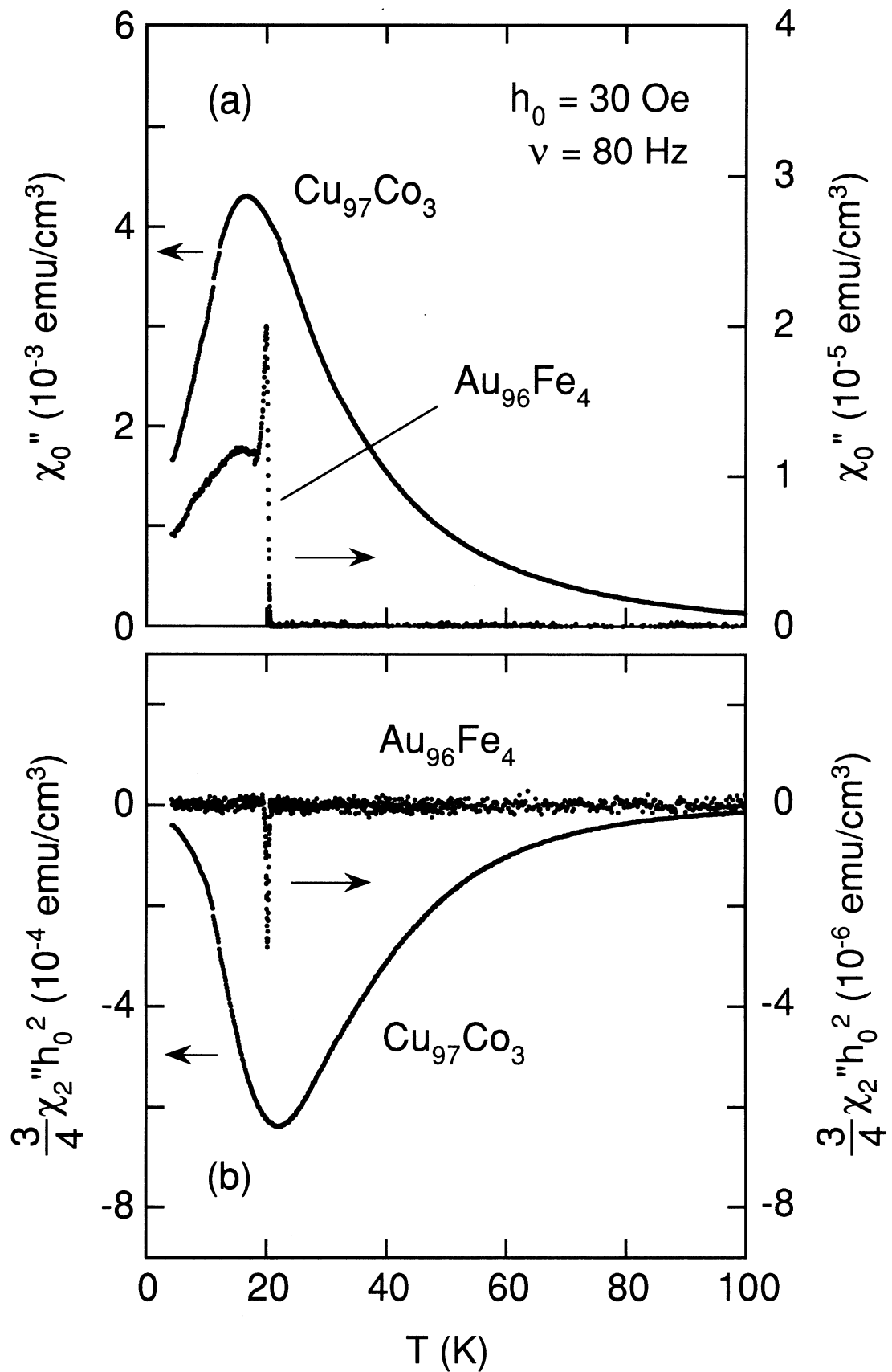


Fig. 4.8. (a) Out-of-phase linear (χ_0'') and (b) nonlinear ($\frac{3}{4}\chi_2''h_0^2$) susceptibilities of $\text{Cu}_{97}\text{Co}_3$ and $\text{Au}_{96}\text{Fe}_4$ as a function of temperature.

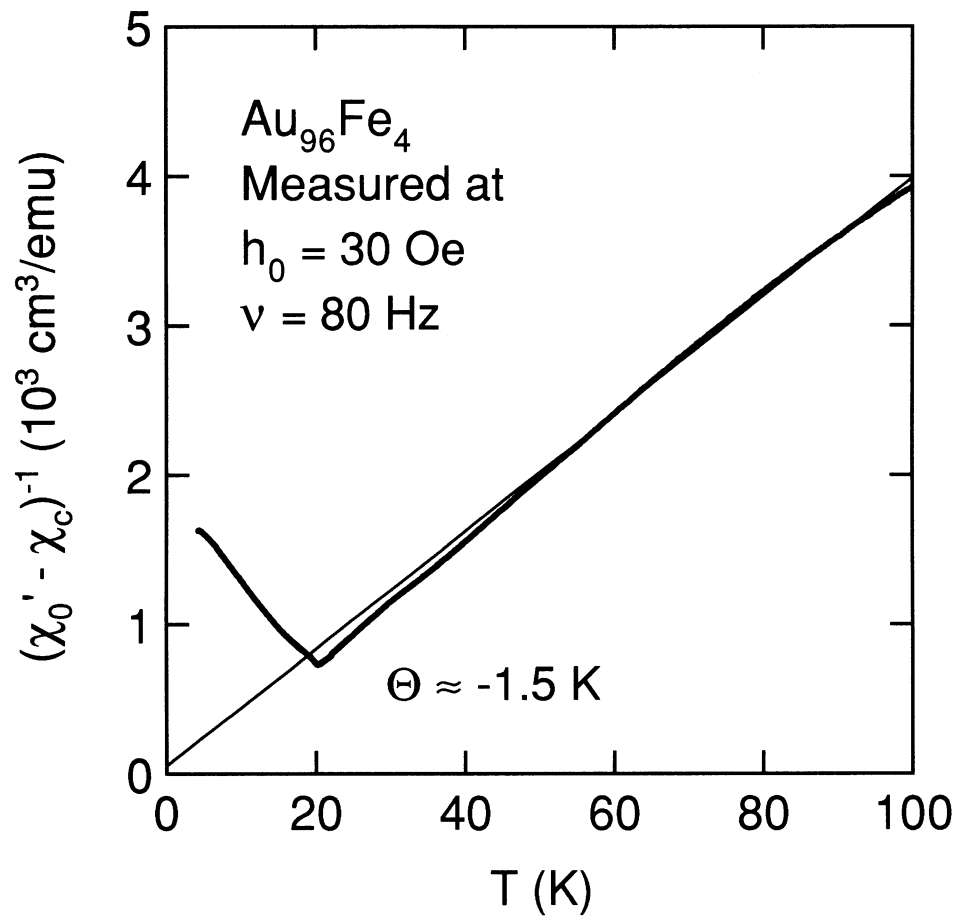


Fig. 4.9. Inverse of the in-phase susceptibility $(\chi_0' - \chi_c)^{-1}$ of $\text{Au}_{96}\text{Fe}_4$ alloy as a function of temperature.

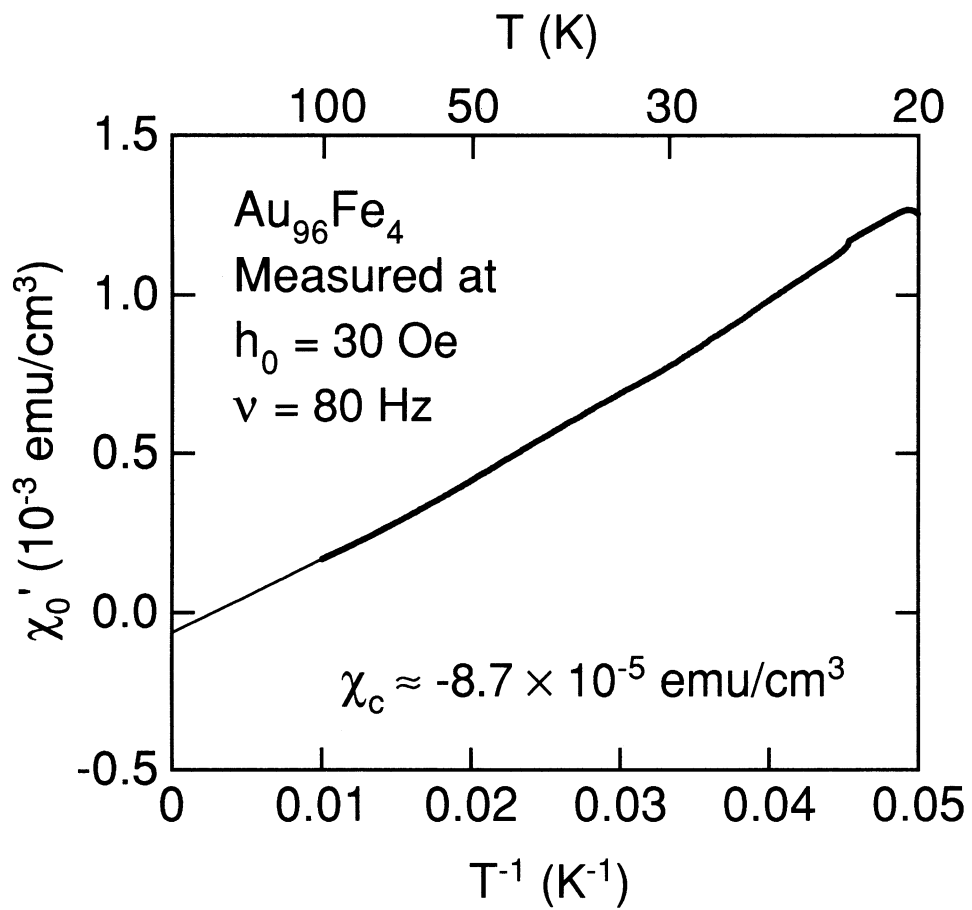


Fig. 4.10. In-phase susceptibility χ_0' of $\text{Au}_{96}\text{Fe}_4$ alloy as a function of T^{-1} .

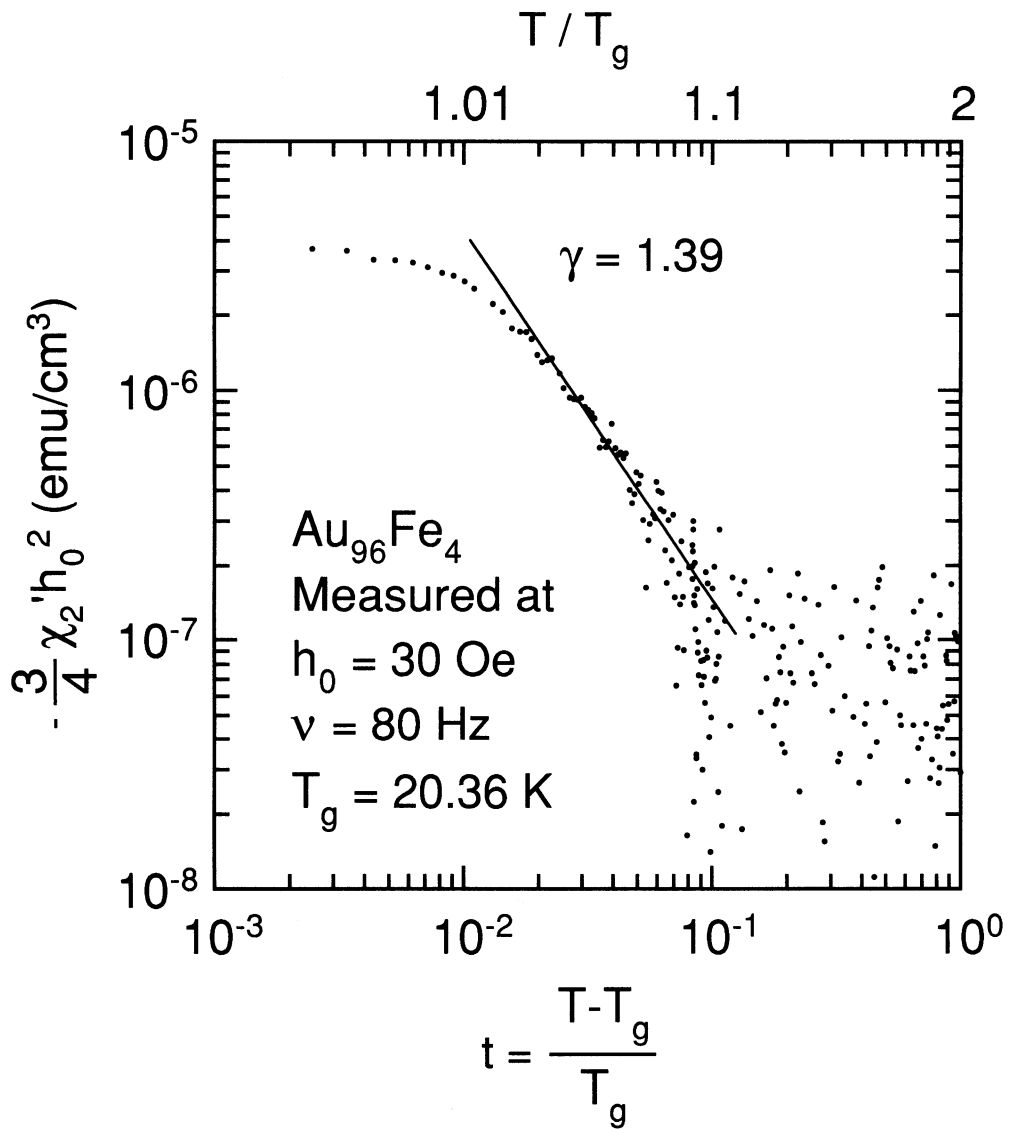


Fig. 4.11. Log-log plot $-\frac{3}{4}\chi_2'h_0^2$ versus the reduced temperature t of $\text{Au}_{96}\text{Fe}_4$ above T_g ($= 20.36 \text{ K}$). The value of T_g were determined from the peak temperature of χ_2' . The slope of the straight line gives a value for γ .

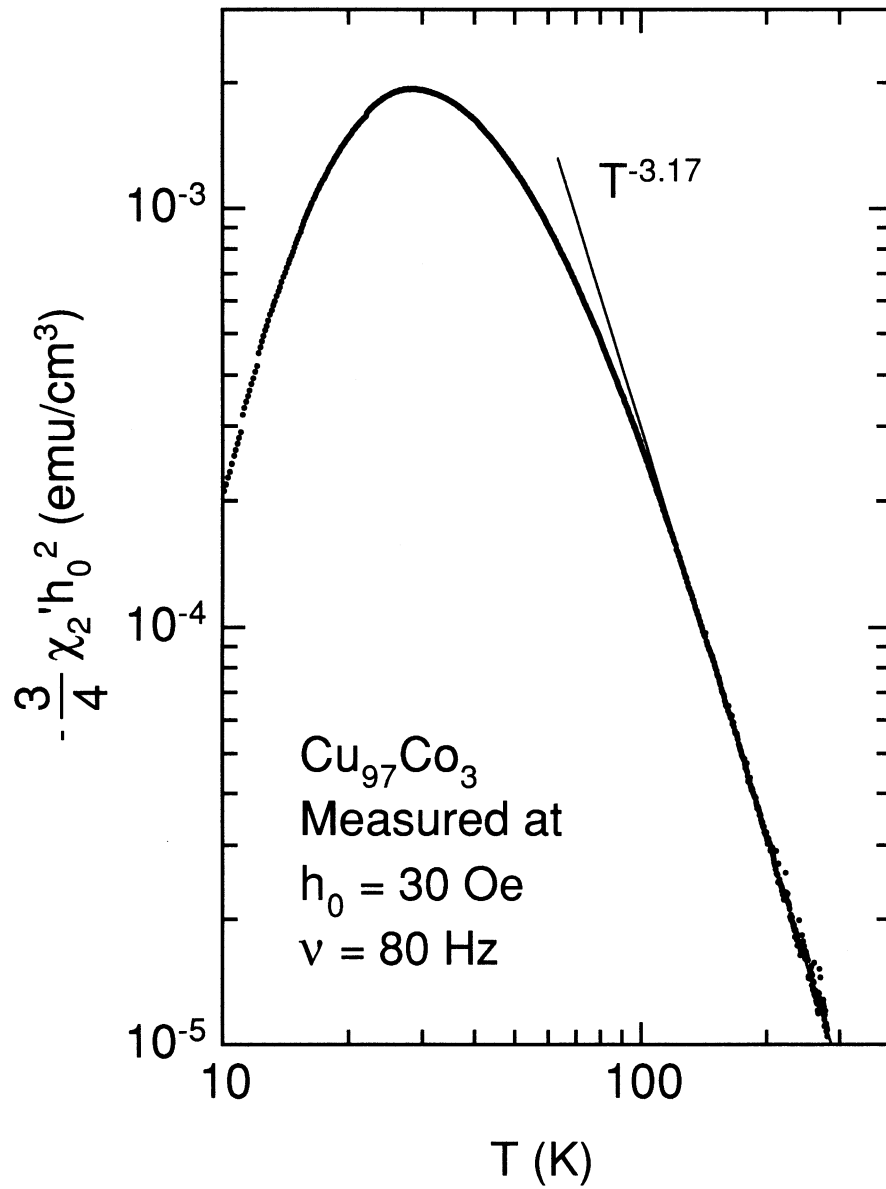


Fig. 4.12. Log-log plot of $-\frac{3}{4}\chi_2'h_0^2$ versus temperature for Cu₉₇Co₃. The straight line represents a fit to the data of the form $\chi_2 = -CT^{-n}$ above 100 K.

4.2 Field-cooled and zero-field-cooled magnetization

A typical temperature dependence of FCM/ H (M/H in a field-cooled process) and ZFCM/ H (M/H in a zero-field-cooled process) of $\text{Cu}_{97}\text{Co}_3$ and $\text{Au}_{96}\text{Fe}_4$ is shown in Fig. 4.13. The zero-field-cooled magnetization ZFCM of $\text{Cu}_{97}\text{Co}_3$ exhibits a spin-glass-like maximum at T_p (≈ 18 K) and that of $\text{Au}_{96}\text{Fe}_4$ has a cusp-like peak at T_g (≈ 20 K). The field-cooled magnetization FCM of $\text{Cu}_{97}\text{Co}_3$ is considerably larger than ZFCM at low temperatures. The magnetic field dependence of ZFCM/ H and FCM/ H for $\text{Cu}_{97}\text{Co}_3$ and $\text{Au}_{96}\text{Fe}_4$ is shown in Figs. 4.14 and 4.15, respectively. With increasing the magnetic field, ZFCM/ H and FCM/ H of $\text{Cu}_{97}\text{Co}_3$ considerably decrease and T_p shifts to lower, from 18 K for $H = 30$ Oe to 10 K for $H = 300$ Oe. On the other hand, ZFCM/ H of $\text{Au}_{96}\text{Fe}_4$ is slightly decreases only near T_g . The present results for $\text{Au}_{96}\text{Fe}_4$ also reproduces the features reported by Chamberlin *et al.* in spin-glass Ag-Mn alloys.^{39, 40)}

The magnetization of the $\text{Cu}_{97}\text{Co}_3$ alloy exhibits the spin-glass-like behavior. However, there are two significant different points from that of the spin-glass $\text{Au}_{96}\text{Fe}_4$ alloy to be noted:

- (1) The difference between FCM and ZFCM of $\text{Cu}_{97}\text{Co}_3$ obviously exists far above T_p while that of $\text{Au}_{96}\text{Fe}_4$ exists only below T_g .
- (2) The field-cooled magnetization FCM of $\text{Cu}_{97}\text{Co}_3$ increases monotonously with decreasing temperature. On the other hand, FCM of $\text{Au}_{96}\text{Fe}_4$ is nearly temperature independent at low temperatures with a constant value of $\approx 0.9 \text{ZFCM}_{\text{max}}$, where ZFCM_{max} is the maximum value of ZFCM.

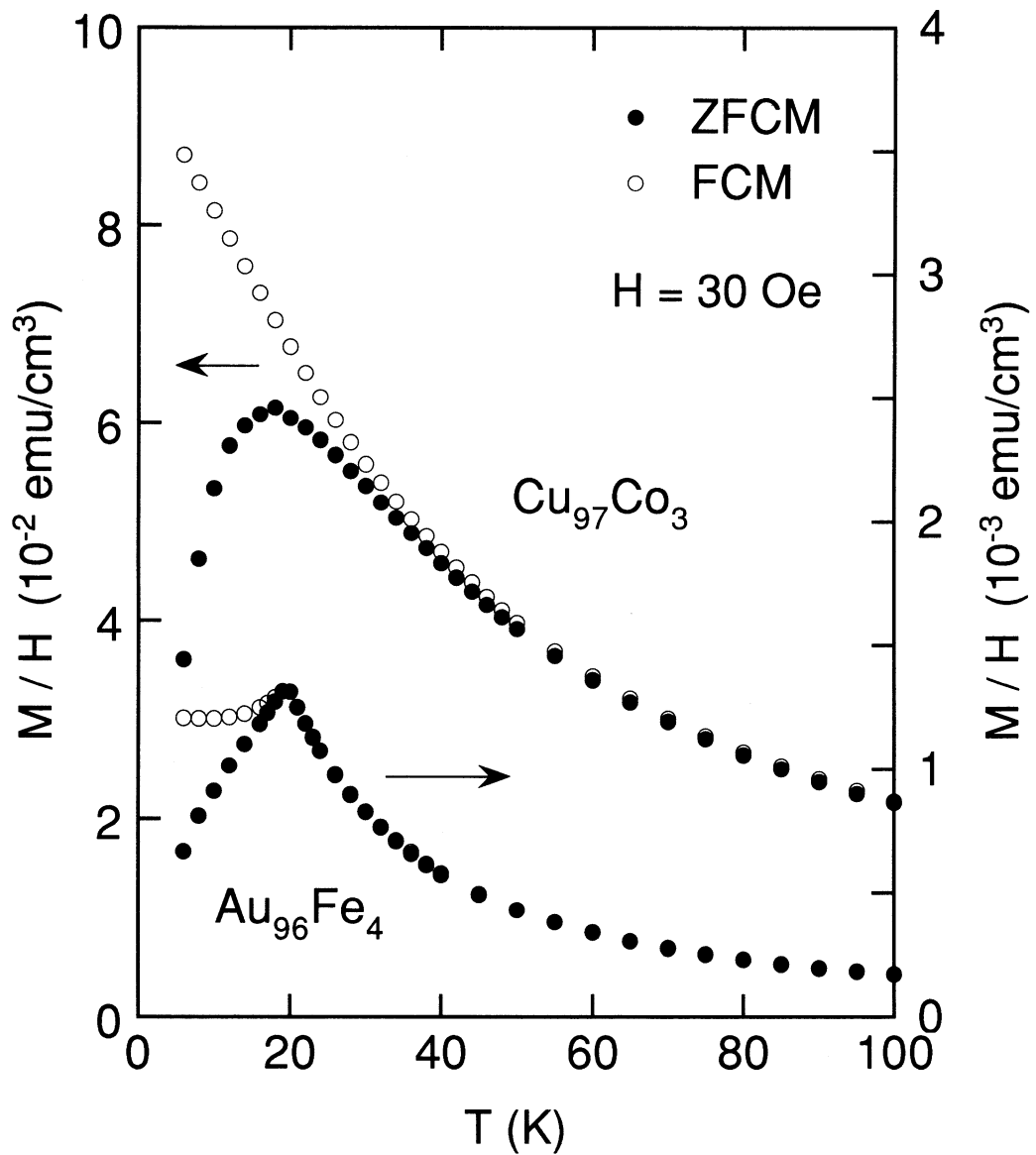


Fig. 4.13. Temperature dependence of the field-cooled (FCM/ H) and the zero-field-cooled (ZFCM/ H) magnetization/field for $\text{Cu}_{97}\text{Co}_3$ and $\text{Au}_{96}\text{Fe}_4$.

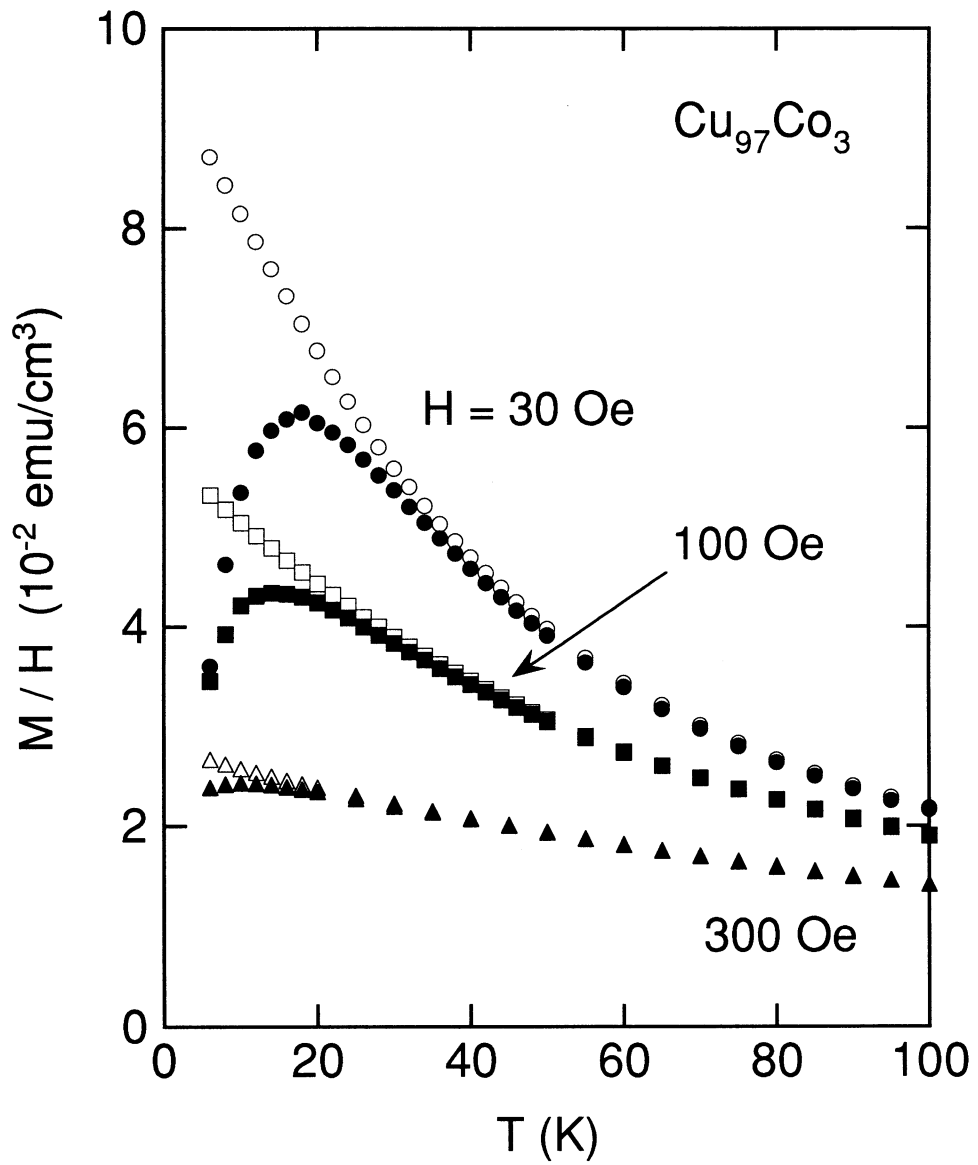


Fig. 4.14. Magnetic field dependence of FCM/ H (open symbols) and ZFCM/ H (closed symbols) of $\text{Cu}_{97}\text{Co}_3$ alloy.

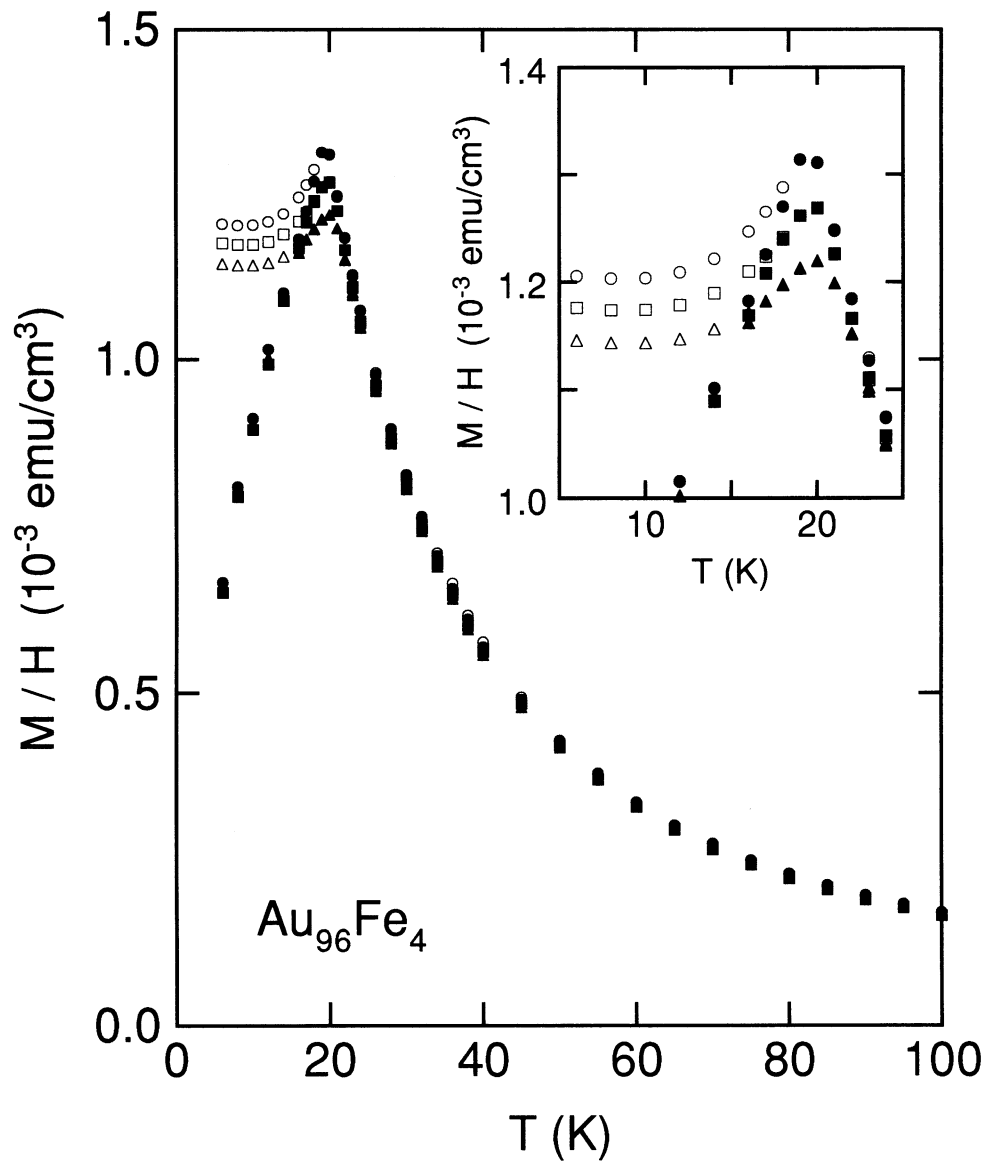


Fig. 4.15. Magnetic field dependence of FCM/ H (open symbols) and ZFCM/ H (closed symbols) of $\text{Au}_{96}\text{Fe}_4$ alloy. \circ , \bullet : 30 Oe, \square , \blacksquare : 100 Oe, \triangle , \blacktriangle : 300 Oe.

4.3 Magnetization curve

The magnetization curves of $\text{Cu}_{97}\text{Co}_3$ alloy at various temperatures are shown in Figs. 4.16–4.18. All the magnetization curves clearly show a tendency to saturate. The magnetization of $\text{Cu}_{97}\text{Co}_3$ shows no hysteresis above 50 K. Figure 4.19 shows the magnetization curves of $\text{Cu}_{97}\text{Co}_3$ as a function of H/T . The curves above 100 K coincide with one another. These results of the magnetization curves show that the $\text{Cu}_{97}\text{Co}_3$ alloy exhibits superparamagnetic behavior at high temperatures.

Figures 4.20–4.22 shows the magnetization curves of $\text{Au}_{96}\text{Fe}_4$ alloy at various temperatures. All the magnetization curves of $\text{Au}_{96}\text{Fe}_4$ do not show a tendency to saturate in contrast with those of $\text{Cu}_{97}\text{Co}_3$. Above 50 K, the magnetization of $\text{Au}_{96}\text{Fe}_4$ maintains a linear relationship with the magnetic field up to 10 kOe. The magnetization of $\text{Au}_{96}\text{Fe}_4$ shows no hysteresis above 20 K. Figure 4.23 shows the magnetization curves of $\text{Au}_{96}\text{Fe}_4$ as a function of H/T . Since the value of the temperature-independent susceptibility χ_c ($= -8.7 \times 10^{-5} \text{ emu/cm}^3$) is large, the author plotted $M - \chi_c H$ against H/T . The $M - \chi_c H$ curves above 20 K coincide with one another.

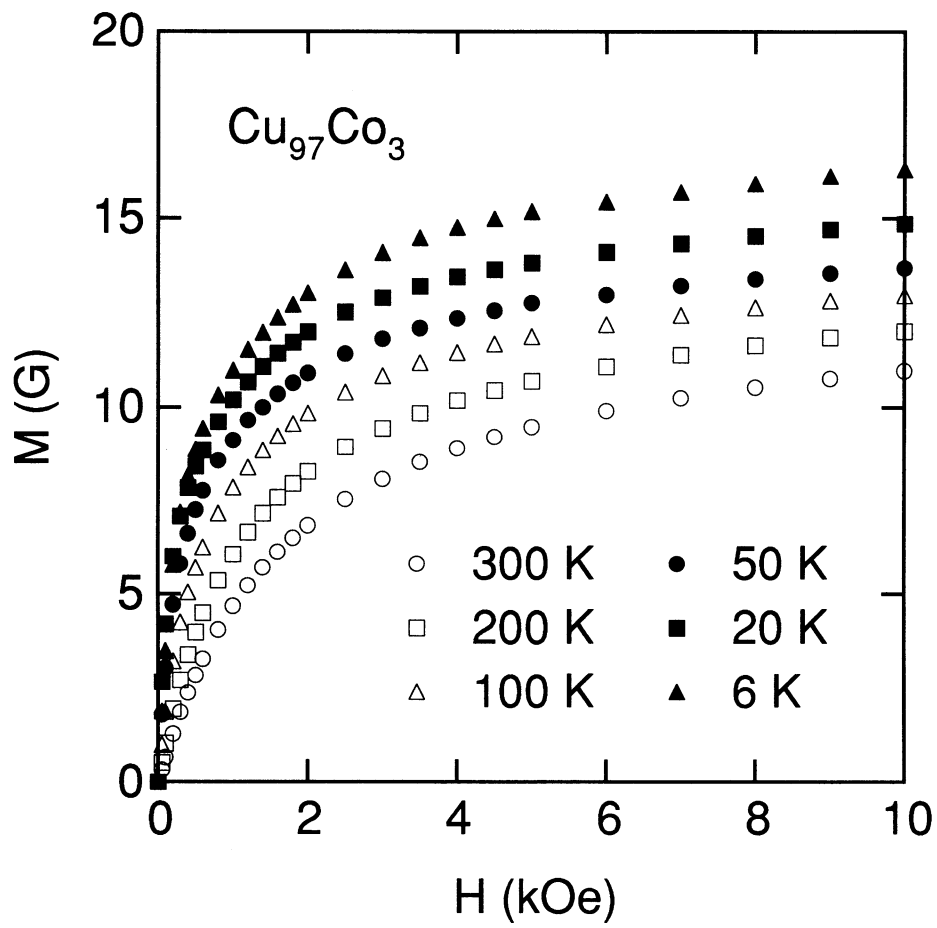


Fig. 4.16. Initial magnetization curves of $\text{Cu}_{97}\text{Co}_3$ alloy at various temperatures.

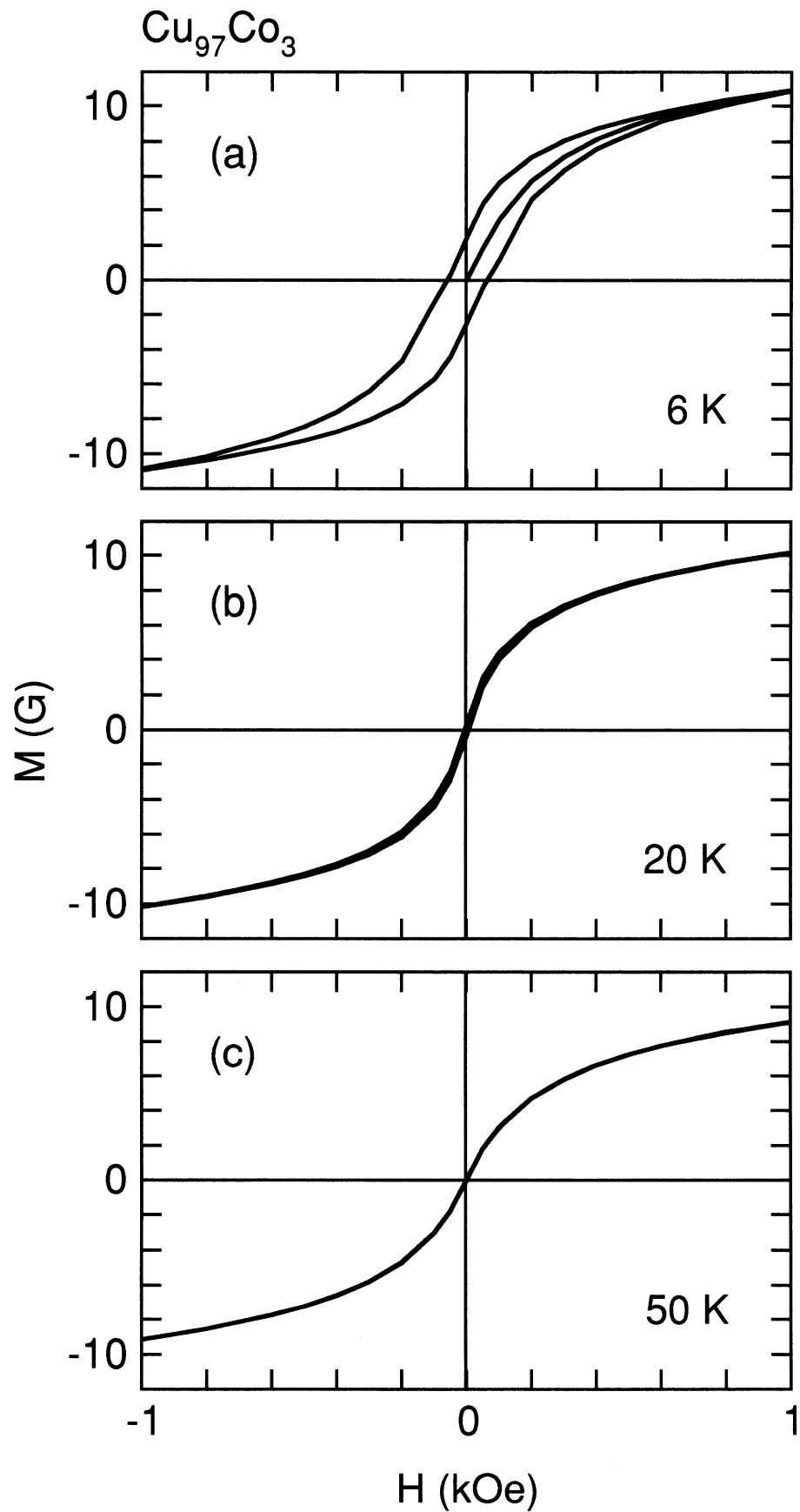


Fig. 4.17. Magnetization curves of $\text{Cu}_{97}\text{Co}_3$ alloy at (a) 6 K, (b) 20 K and (c) 50 K.

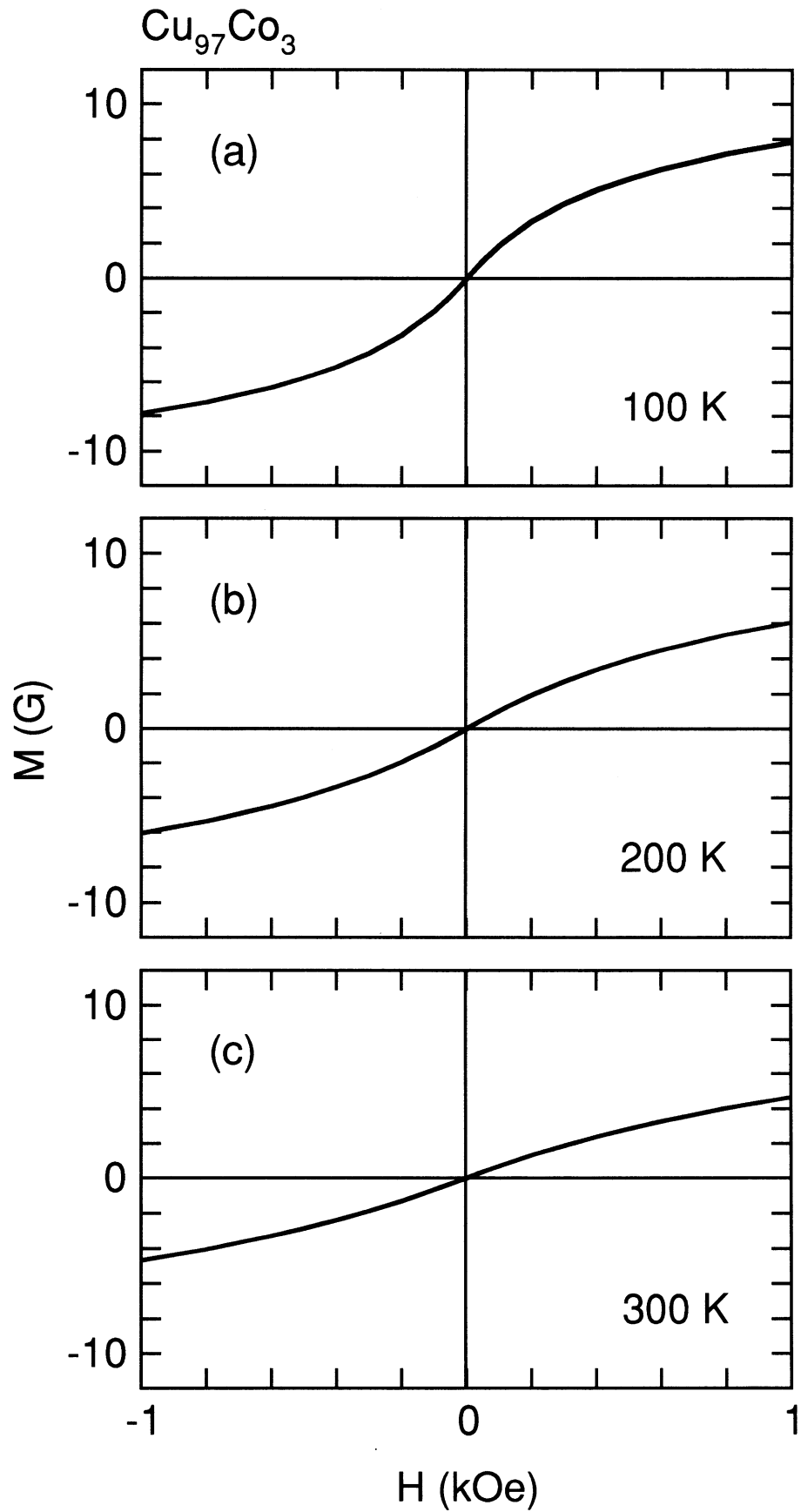


Fig. 4.18. Magnetization curves of $\text{Cu}_{97}\text{Co}_3$ alloy at (a) 100 K, (b) 200 K and (c) 300 K.

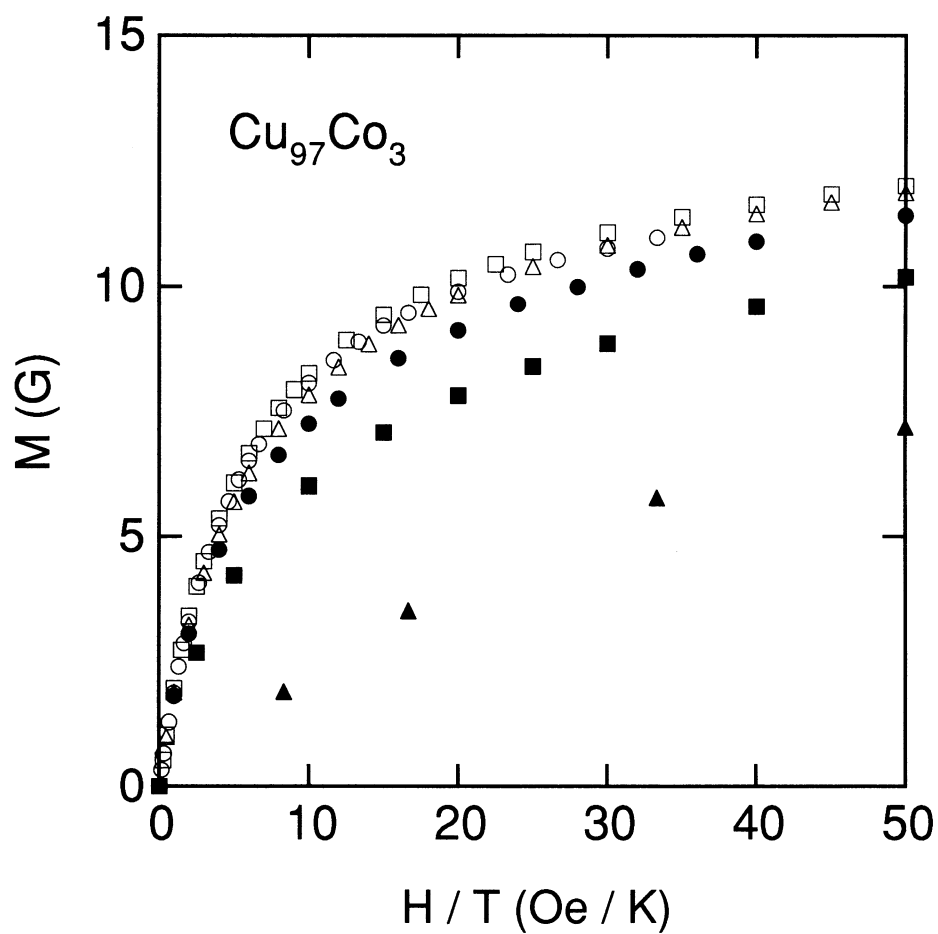


Fig. 4.19. Initial magnetization curves of $\text{Cu}_{97}\text{Co}_3$ alloy as a function of H/T . \circ : 300 K, \square : 200 K, \triangle : 100 K, \bullet : 50 K, \blacksquare : 20 K, \blacktriangle : 6 K.

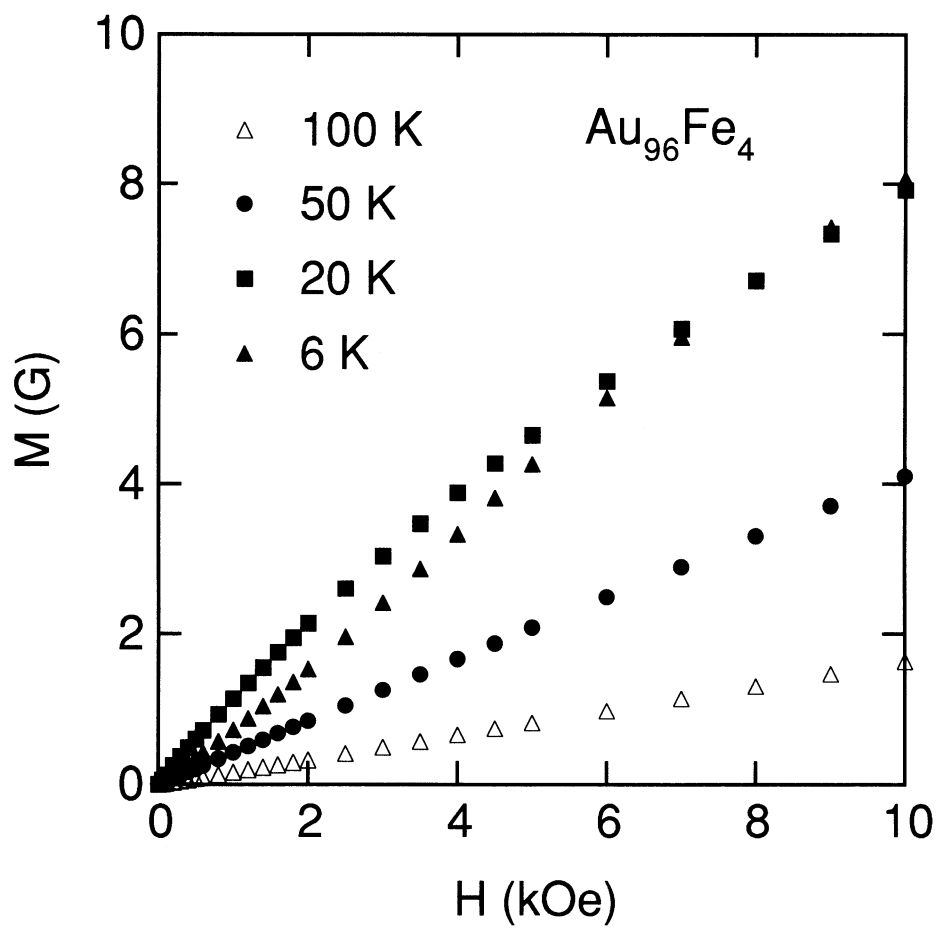


Fig. 4.20. Initial magnetization curves of $\text{Au}_{96}\text{Fe}_4$ alloy at various temperatures.

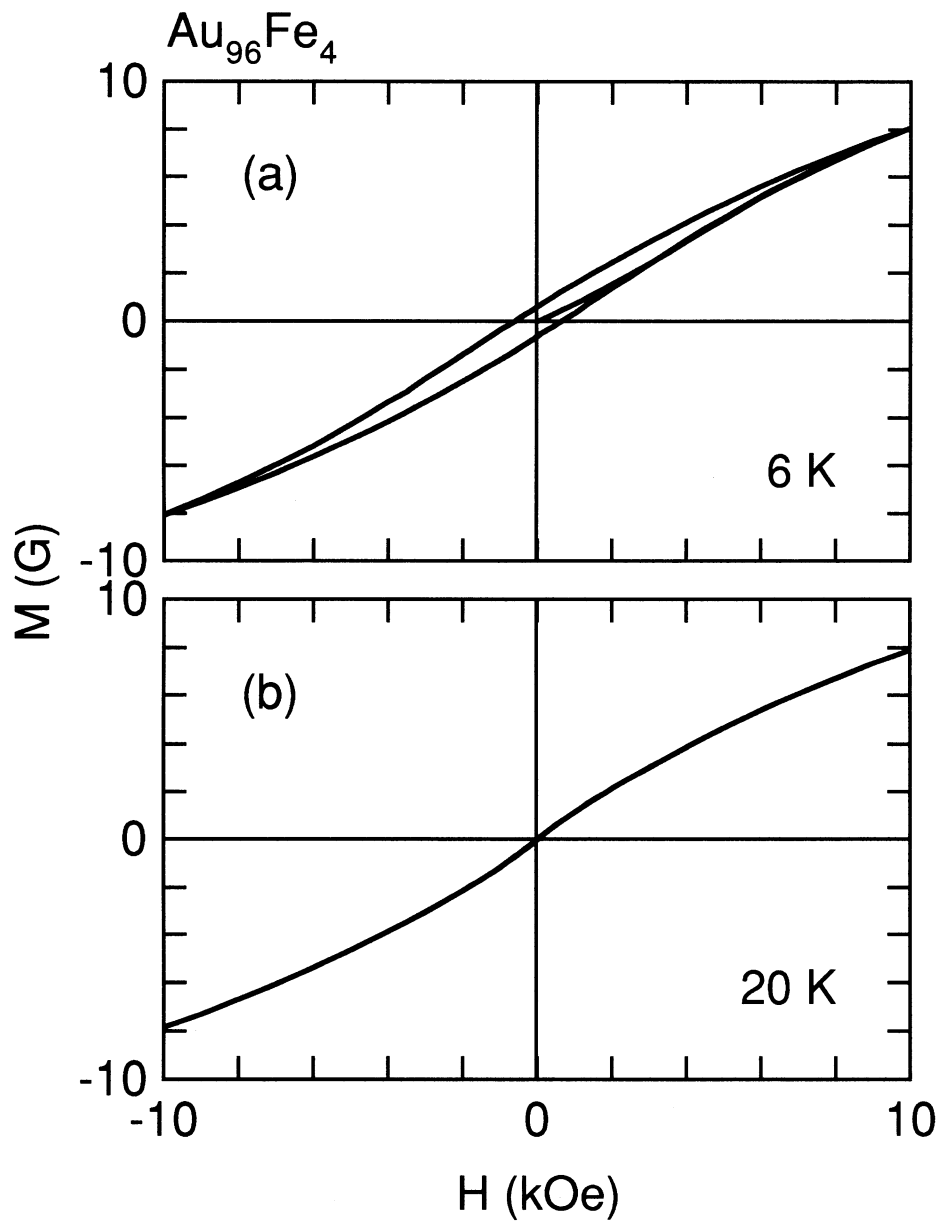


Fig. 4.21. Magnetization curves of $\text{Au}_{96}\text{Fe}_4$ alloy at (a) 6 K and (b) 20 K.

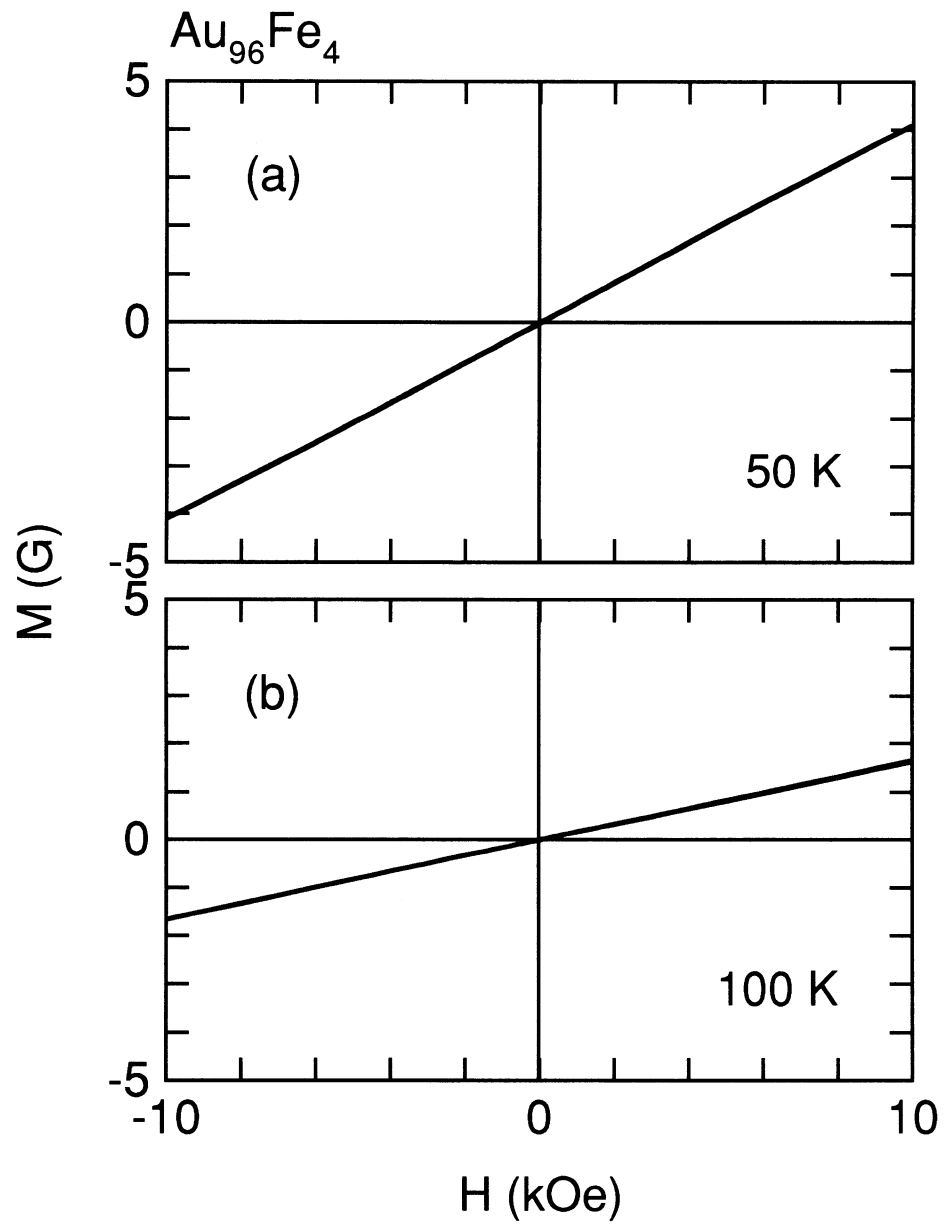


Fig. 4.22. Magnetization curves of $\text{Au}_{96}\text{Fe}_4$ alloy at (a) 50 K and (b) 100 K.

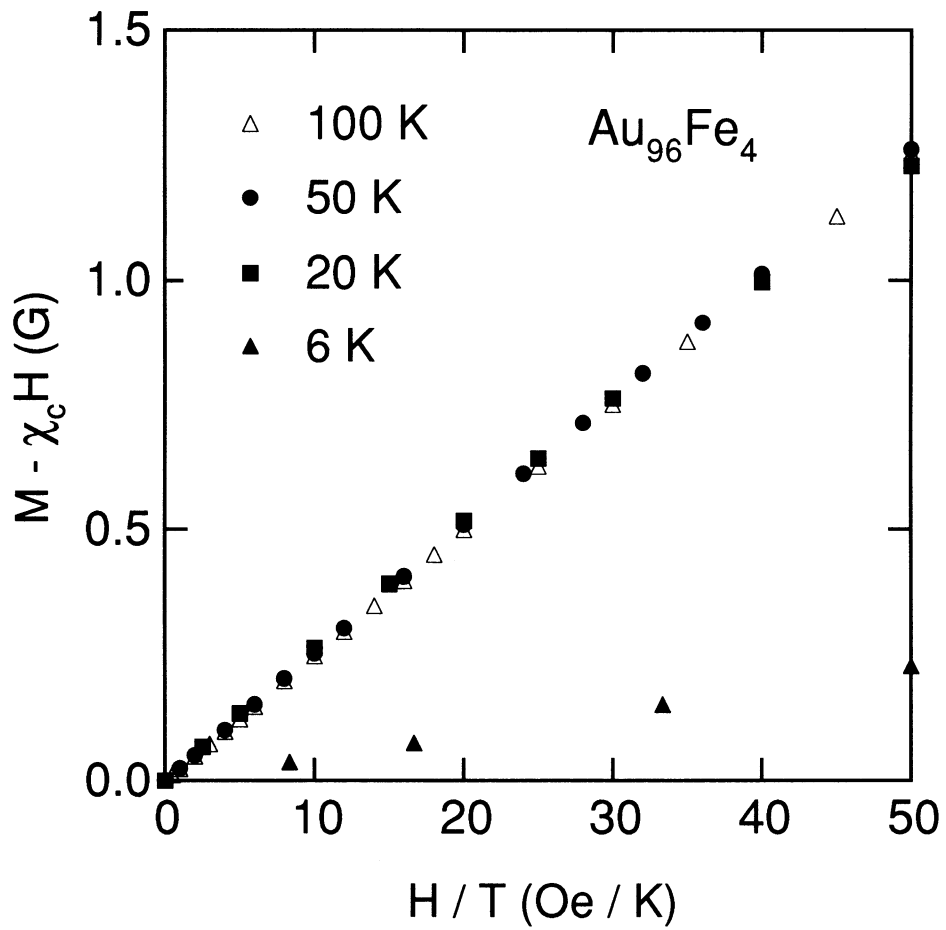


Fig. 4.23. Initial magnetization curves of $\text{Au}_{96}\text{Fe}_4$ alloy as a function of H/T .

It should be noted that the vertical axis denotes $M - \chi_c H$.

Section 5

Data Analysis

5.1 Superparamagnetic blocking model

5.1.1 Assumption

As described in Section 4.1.3, the temperature dependence of the non-linear susceptibility χ'_2 of $\text{Cu}_{97}\text{Co}_3$ alloy is qualitatively different from that of spin-glass $\text{Au}_{96}\text{Fe}_4$ alloy; χ'_2 of $\text{Cu}_{97}\text{Co}_3$ does not diverge at any temperature and is proportional to T^{-3} at high temperatures, while that of $\text{Au}_{96}\text{Fe}_4$ diverges at the transition temperature T_g . This result indicates that the origin of the magnetic properties of $\text{Cu}_{97}\text{Co}_3$ and $\text{Au}_{96}\text{Fe}_4$ is different, though the behavior of χ_0 , ZFCM and FCM of $\text{Cu}_{97}\text{Co}_3$ is similar those of $\text{Au}_{96}\text{Fe}_4$. In this section, to study the origin of the magnetic properties of fine particles, the author analyzes the results of $\text{Cu}_{97}\text{Co}_3$ alloy based on the superparamagnetic blocking model with special emphasis on χ_0 and χ_2 . For simplicity, the author has assumed as follows:

- (1) There are no interactions between the cobalt particles.
- (2) The particles consist of a single magnetic domain.
- (3) The saturation magnetization M_s of the particle is independent of temperature because the Curie temperature of each cobalt particle is very high (≈ 1400 K).
- (4) The magnetic anisotropy of the particles is uniaxial and all particles have a same uniaxial anisotropy constant K_u .
- (5) The anisotropy axes of the particles are randomly oriented.

5.1.2 Linear and nonlinear susceptibilities

A magnetic response of noninteracting single-domain particles will follow the Néel^{41, 42)} relaxation process characterized by a relaxation time given by

$$\tau = \tau_0 \exp\left(\frac{\Delta E_a}{k_B T}\right), \quad (5.1)$$

where τ_0 is the order of 10^{-10} sec,⁴¹⁻⁴⁴⁾ $\Delta E_a (=K_u V$, where V is the particle volume) is the height of the energy barrier due to anisotropy, k_B is the Boltzmann constant and T is the absolute temperature. It is well known that noninteracting single-domain particles exhibit superparamagnetic behavior at high temperatures.⁴⁵⁾ On the other hand, at low temperatures, the particle moment cannot achieve thermal equilibrium in the time of a measurement. Then the particle moment is blocked in the direction of the anisotropy axis. The blocking temperature T_b at which the blocking of the moment occurs is given by setting τ equals to the measurement time τ_m ($=\omega^{-1}$ is chosen for a typical ac measurement, where $\omega = 2\pi\nu$ is the angular frequency) as¹⁶⁾

$$T_b = \frac{K_u V}{k_B \ln\left(\frac{\tau_m}{\tau_0}\right)}. \quad (5.2)$$

1. Static susceptibilities

Above T_b , if all particles have a same volume V , then the total magnetization M_V^{sp} for particles is given by⁴⁵⁾

$$\begin{aligned} M_V^{\text{sp}} &= \varepsilon M_s L\left(\frac{M_s V H}{k_B T}\right) \\ &= \varepsilon M_s \left[\frac{M_s V H}{3k_B T} - \frac{1}{45} \left(\frac{M_s V H}{k_B T}\right)^3 + \dots \right], \end{aligned} \quad (5.3)$$

where

$$L(x) = \coth x - \frac{1}{x} \quad (5.4)$$

is the Langevin function, ε is the volume fraction occupied by ferromagnetic particles. The superparamagnetic linear ($\chi_{V_0}^{\text{sp}}$) and nonlinear ($\chi_{V_2}^{\text{sp}}$) susceptibilities are given by the first and the second terms of eq. (5.3) as

$$\chi_{V_0}^{\text{sp}} = \frac{\varepsilon M_s^2 V}{3k_B T}, \quad (5.5)$$

$$\chi_{V_2}^{\text{sp}} = -\frac{\varepsilon M_s}{45} \left(\frac{M_s V}{k_B T} \right)^3, \quad (5.6)$$

respectively. The linear susceptibility $\chi_{V_0}^{\text{sp}}$ obeys the Curie law, and $\chi_{V_2}^{\text{sp}}$ is negative and proportional to T^{-3} .

Below T_b , the linear susceptibility $\chi_{V_0}^{\text{bl}}$ in the blocked state is given by^{6, 46)}

$$\chi_{V_0}^{\text{bl}} = \frac{\varepsilon M_s^2}{3K_u}. \quad (5.7)$$

It should be noted that the value of $\chi_{V_0}^{\text{bl}}$ is very small:

$$\frac{\chi_{V_0}^{\text{bl}}}{\chi_{V_0}^{\text{sp}}(T_b)} = \ln \left(\frac{\tau_m}{\tau_0} \right) \approx \frac{1}{17}, \quad \text{at } \tau_0 = 10^{-10} \text{ sec, } \nu = 80 \text{ Hz.} \quad (5.8)$$

The author has neglected the nonlinear susceptibility $\chi_{V_2}^{\text{bl}}$ in this analysis. The broken lines in Fig. 5.1 shows schematic behavior of χ_{V_0} and χ_{V_2} as a function of T/T_b . It must be noted that χ_2 for fine particles does not diverge at any temperature.

In general, there is a distribution in the volumes of precipitated particles. Then the total susceptibilities are given as

$$\chi_0 = \frac{\varepsilon M_s^2}{3k_B T} \int_0^{V_m(T)} V f(V) dV + \frac{\varepsilon M_s^2}{3K_u} \int_{V_m(T)}^{\infty} f(V) dV, \quad (5.9)$$

$$\chi_2 = -\frac{\varepsilon M_s}{45} \left(\frac{M_s}{k_B T} \right)^3 \int_0^{V_m(T)} V^3 f(V) dV, \quad (5.10)$$

where $f(V)$ the distribution function of particle volume and

$$V_m(T) = \frac{k_B T}{K_u} \ln \left(\frac{\tau_m}{\tau_0} \right) \quad (5.11)$$

is the maximum particle volume exhibiting the superparamagnetic behavior at the temperature T .

2. Complex susceptibilities

In order to calculate the complex susceptibilities $\chi_{V_n}^*$ ($= \chi'_{V_n} - i\chi''_{V_n}$), the author used following formations. The temperature dependence of the complex linear susceptibility $\chi_{V_0}^*$ ($= \chi'_{V_0} - i\chi''_{V_0}$) for particles is given by Gittleman *et al.*¹⁶⁾ as

$$\chi_{V_0}^* = \frac{\chi_{V_0}^{\text{sp}} + i\omega\tau\chi_{V_0}^{\text{bl}}}{1 + i\omega\tau}, \quad (5.12)$$

whose in-phase and out-of-phase components are given by

$$\chi'_{V_0} = \frac{\chi_{V_0}^{\text{sp}} + \omega^2\tau^2\chi_{V_0}^{\text{bl}}}{1 + \omega^2\tau^2}, \quad (5.13)$$

$$\chi''_{V_0} = \omega\tau \frac{\chi_{V_0}^{\text{sp}} - \chi_{V_0}^{\text{bl}}}{1 + \omega^2\tau^2}, \quad (5.14)$$

respectively. Recently, Kimura and Hayakawa⁴⁷⁾ calculated the nonlinear dielectric relaxation spectra on the basis of a simple model for freely rotatable dipoles. Since superparamagnetic particles are regraded as freely rotatable dipoles, this model can be applied to superparamagnetic particles. In this model, the complex nonlinear susceptibility $\chi_{V_2}^*$ ($= \chi'_{V_2} - i\chi''_{V_2}$) given as⁴⁷⁾

$$\chi_{V_2}^* = \frac{\chi_{V_2}^{\text{sp}}}{(1 + i\omega\tau)(1 + 3i\omega\tau)\left(1 + \frac{2}{3}i\omega\tau\right)}, \quad (5.15)$$

whose in-phase and out-of-phase components are given by

$$\chi'_{V_2} = \frac{\chi_{V_2}^{\text{sp}} \left(1 - \frac{17}{3}\omega^2\tau^2\right)}{(1 + \omega^2\tau^2)(1 + 9\omega^2\tau^2)\left(1 + \frac{4}{9}\omega^2\tau^2\right)}, \quad (5.16)$$

$$\chi''_{V_2} = \frac{\omega\tau\chi_{V_2}^{\text{sp}} \left(\frac{14}{3} - 2\omega^2\tau^2\right)}{(1 + \omega^2\tau^2)(1 + 9\omega^2\tau^2)\left(1 + \frac{4}{9}\omega^2\tau^2\right)}, \quad (5.17)$$

respectively.

Figure 5.1 shows schematic behavior of χ'_{V0} , χ'_{V2} (solid lines), χ''_{V0} , χ''_{V2} (dotted lines) as a function of T/T_b . When temperature is much higher than T_b , then χ'_{Vn} equals χ_{Vn}^{sp} ($n = 0, 2$); χ'_{V0} obeys the Curie law, χ'_{V2} is negative and proportional to T^{-3} . Below T_b , then χ'_{V0} and χ'_{V2} nearly equal to χ_{V0}^{bl} and zero, respectively. On the other hand, χ''_{V0} and χ''_{V2} are observed in the vicinity of T_b .

When the particle volume has a distribution, the total complex susceptibilities given as

$$\chi_n^* = \int_0^\infty \chi_{Vn}^* f(V) dV \quad (n = 0, 2). \quad (5.18)$$

5.1.3 Field-cooled and zero-field-cooled magnetization

In order to calculate the magnetization in rather large magnetic fields, the author used the model as follows. The energy barrier ΔE_a in a dc magnetic field H is given by^{43, 48)}

$$\Delta E_a = K_u V \left(1 - \frac{H}{H_K}\right)^2, \quad (5.19)$$

where

$$H_K = \frac{2K_u}{M_s} \quad (5.20)$$

is the anisotropy field. The blocking temperature T_b in a dc magnetic field is given as⁴⁸⁾

$$T_b(H) = \frac{K_u V}{k_B \ln\left(\frac{\tau_m}{\tau_0}\right)} \left(1 - \frac{H}{H_K}\right)^2, \quad (5.21)$$

where $\tau_m = 100$ sec is usually chosen for a typical dc measurement.

Above T_b , if all particles have a same volume V , the magnetization M_V^{sp} of superparamagnetic particles is given by the Langevin function as eq.

(5.3). Below T_b , the magnetization $\text{ZFCM}_V^{\text{bl}}$ and FCM_V^{bl} are given by^{6, 46, 48)}

$$\text{ZFCM}_V^{\text{bl}} = \frac{\varepsilon M_s^2 H}{3K_u}, \quad (5.22)$$

$$\text{FCM}_V^{\text{bl}} = M_V^{\text{sp}}(T_b) = \varepsilon M_s L \left(\frac{M_s V H}{k_B T_b(H)} \right). \quad (5.23)$$

It should be noted that $\text{ZFCM}_V^{\text{bl}}$ is much smaller than $M_V^{\text{sp}}(T_b)$ ($= \text{FCM}_V^{\text{bl}}$) as eq. (5.8). When the particle volume has a distribution, the total magnetization given as

$$\text{ZFCM} = \int_0^{V_m(T)} M_V^{\text{sp}} f(V) dV + \int_{V_m(T)}^{\infty} \text{ZFCM}_V^{\text{bl}} f(V) dV, \quad (5.24)$$

$$\text{FCM} = \int_0^{V_m(T)} M_V^{\text{sp}} f(V) dV + \int_{V_m(T)}^{\infty} \text{FCM}_V^{\text{bl}} f(V) dV, \quad (5.25)$$

where

$$V_m(T) = \frac{k_B T}{K_u \left(1 - \frac{H}{H_K}\right)^2} \ln \left(\frac{\tau_m}{\tau_0} \right). \quad (5.26)$$

Figure 5.2 shows schematic behavior of ZFCM_V (solid lines) and FCM_V (dotted lines) as a function of $T/T_b(H=0)$ at various magnetic fields.

5.1.4 Magnetization curve at high temperatures

It is difficult to calculate the magnetization curves for ferromagnetic fine particles below T_b . Here, the author considers the magnetization curves only at high temperatures where all particles exhibit superparamagnetic behavior. As described in Section 5.1.2, if there is no distribution in the volumes of particles, then the total magnetization M_V^{sp} for particles is given by the Langevin function as eq. (5.3) above T_b . When the particle volume has a distribution, the total magnetization M^{sp} at high temperatures given by

$$M^{\text{sp}} = \varepsilon M_s \int_0^{\infty} L \left(\frac{M_s V H}{k_B T} \right) f(V) dV. \quad (5.27)$$

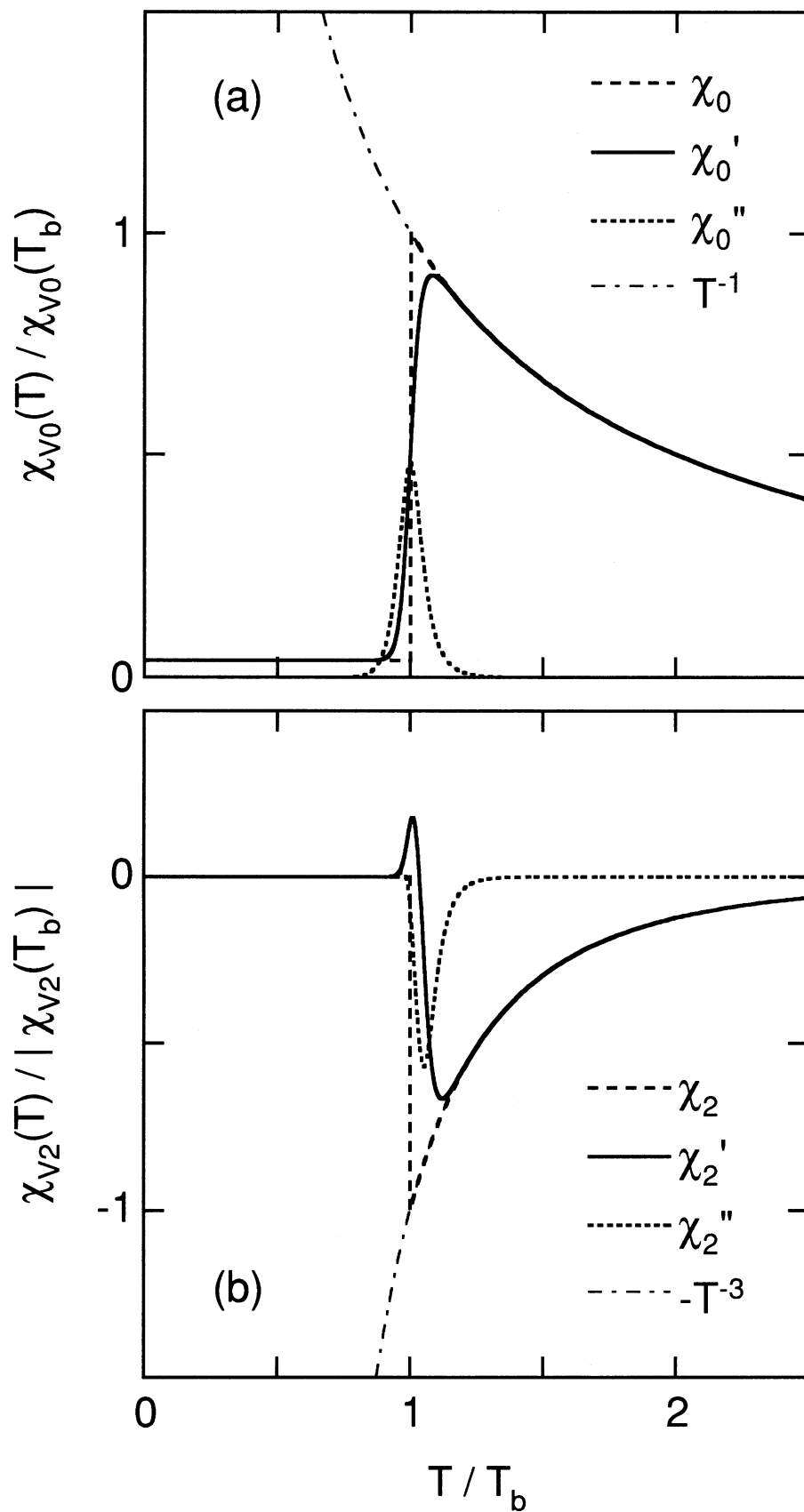


Fig. 5.1. Schematic behavior of (a) the linear susceptibility χ_{V0} and (b) the nonlinear susceptibility χ_{V2} as a function of T/T_b .

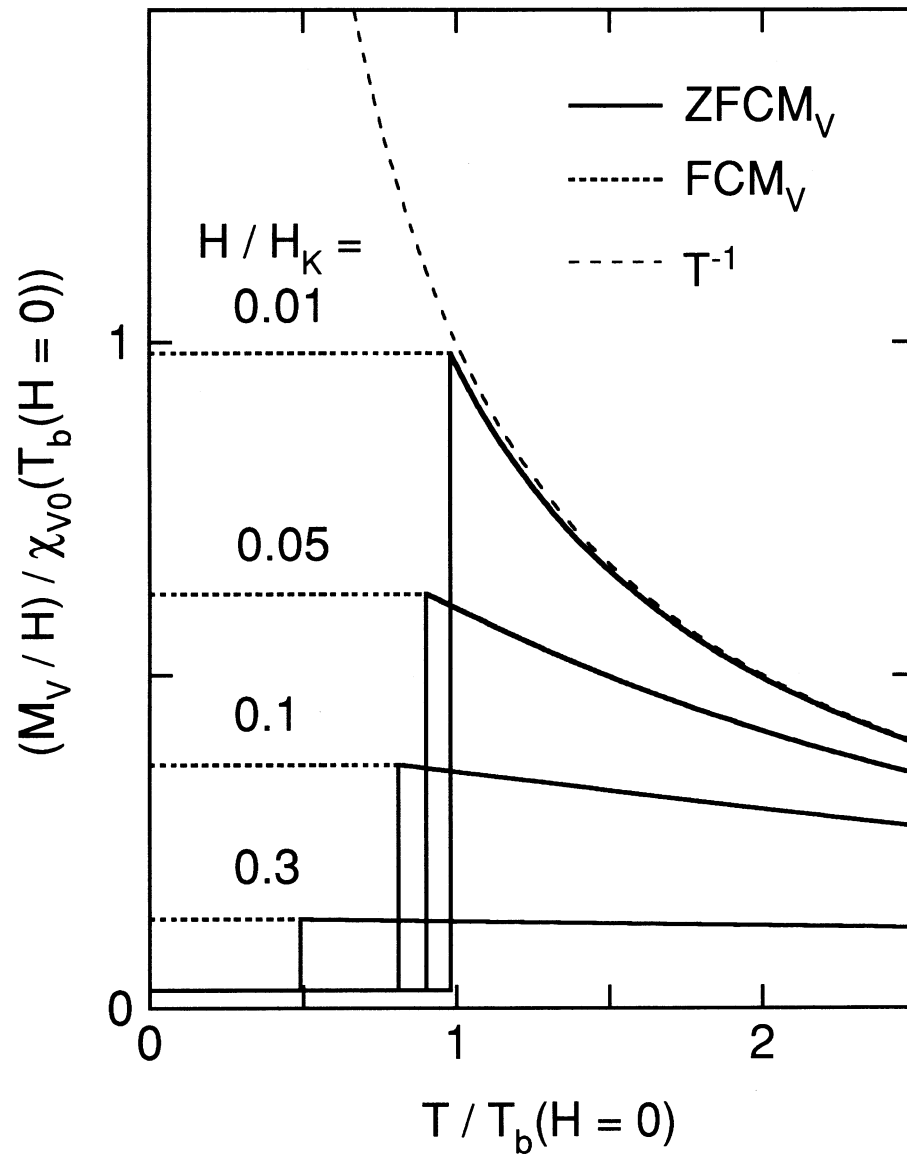


Fig. 5.2. Schematic behavior of the field-cooled (FCM_V) and zero-field-cooled ($ZFCM_V$) magnetization as a function of $T/T_b(H = 0)$ at various magnetic fields.

5.2 Analysis for Cu-Co alloy

5.2.1 Characteristic relaxation time

From eq. (5.2), the frequency dependence of blocking temperature T_b is given as

$$\ln(\tau_m) = \ln(\tau_0) + \frac{K_u V}{k_B T_b}. \quad (5.28)$$

Since the temperature T_p where the susceptibilities exhibit a peak is proportional to the mean blocking temperature $\langle T_b \rangle$,¹⁶⁾ the frequency dependence of T_p is the same as that of T_b . Thus we are able to determine the characteristic relaxation time τ_0 from the frequency dependence of T_p . Figure 5.3 shows $\log(\tau_m)$ versus T_p^{-1} plot for each susceptibility component. This plot gives the straight lines that lead to an intercept to the $\log(\tau_m)$ axis equal to $\log(\tau_0)$. From Fig. 5.3, the author estimated $\tau_0 = 1.6 \times 10^{-14}$ sec. This value is rather smaller than the theoretical value (the order of 10^{-10} sec).⁴¹⁻⁴⁴⁾ Dormann *et al.*^{49, 50)} reported that the relaxation time τ of iron particles dispersed in an amorphous Al_2O_3 matrix does not obey eq. (5.1) due to dipole interaction between particles. However, in the low frequency as the present experiments, τ can be approximated using eq. (5.1) though the value of τ_0 is smaller than the theoretical value.

5.2.2 Volume distribution function

Since χ'_{V0} falls abruptly near T_b with decreasing temperature, it can be regarded as

$$\chi'_{V0} = \begin{cases} \chi_{V0}^{\text{sp}} & \text{for } T \geq T_b \\ 0 & \text{for } T < T_b. \end{cases} \quad (5.29)$$

Then the total linear susceptibility χ'_0 is given by

$$\chi'_0 = \frac{\varepsilon M_s^2 \langle V \rangle}{3k_B T} \int_0^{V_m(T)/\langle V \rangle} V_r f(V_r) dV_r, \quad (5.30)$$

where $\langle V \rangle$ is the mean volume of particles, $V_r = V/\langle V \rangle$ is the reduced volume, $f(V_r)$ is the distribution function of V_r . Since the blocking temperature T_b is proportional to the particle volume, eq. (5.30) can be written as

$$\frac{3k_B}{a^2 \varepsilon M_s^2 \langle V \rangle} \chi'_0 T = \int_0^T T_b f(aT_b) dT_b, \quad (5.31)$$

where

$$V_r = aT_b \quad (5.32)$$

and

$$a = \frac{k_B}{K_u \langle V \rangle} \ln \left(\frac{\tau_m}{\tau_0} \right). \quad (5.33)$$

Equation (5.31) can be inverted to give^{6, 51)}

$$\frac{3k_B}{a^2 \varepsilon M_s^2 \langle V \rangle} \frac{d}{dT} (\chi'_0 T) = T_b f(aT_b) = \frac{V_r}{a} f(V_r). \quad (5.34)$$

Therefore $f(V_r)$ is given as

$$V_r f(V_r) = \frac{3K_u}{\varepsilon M_s^2 \ln \left(\frac{\tau_m}{\tau_0} \right)} \frac{d}{dT} (\chi'_0 T). \quad (5.35)$$

Figure 5.4 shows $d(\chi'_0 T)/dT$ as a function of temperature. The solid curve in Fig. 5.4 shows $V_r f(V_r)$ as a function of T_b , which was calculated using a log-normal distribution function (Fig. 5.5)

$$f(V_r) = \frac{1}{\sqrt{2\pi}\sigma V_r} \exp \left[-\frac{(\ln V_r)^2}{2\sigma^2} \right]. \quad (5.36)$$

The blocking temperature T_b is given by eq. (5.2) as

$$T_b = V_r \langle T_b \rangle, \quad (5.37)$$

where

$$\langle T_b \rangle = \frac{K_u \langle V \rangle}{k_B \ln \left(\frac{\tau_m}{\tau_0} \right)} \quad (5.38)$$

is the mean blocking temperature. The author was able to fit $V_r f(V_r)$ to $d(\chi'_0 T)/dT$ very well using the two adjustable parameters: $\langle T_b \rangle$ ($= 14.0$ K) and the standard deviation σ ($= 0.72$).

5.2.3 Mean particle volume and volume fraction

Above 100 K, the measured χ'_0 and χ'_2 are proportional to T^{-1} and T^{-3} , respectively. This means that almost all particles exhibit superparamagnetic behavior above 100 K. In this temperature range, in-phase total susceptibilities $\chi_0^{\text{ht}'}$ and $\chi_2^{\text{ht}'}$ are given by

$$\chi_0^{\text{ht}'} = \frac{\varepsilon M_s^2 \langle V \rangle}{3k_B T} \int_0^\infty V_r f(V_r) dV_r, \quad (5.39)$$

$$\chi_2^{\text{ht}'} = -\frac{\varepsilon M_s}{45} \left(\frac{M_s \langle V \rangle}{k_B T} \right)^3 \int_0^\infty V_r^3 f(V_r) dV_r. \quad (5.40)$$

From eqs. (5.39) and (5.40), the mean volume $\langle V \rangle$ can be written by

$$\langle V \rangle = \frac{k_B T}{M_s} \sqrt{-\frac{15\chi_2^{\text{ht}'}}{\chi_0^{\text{ht}'}} \frac{\int_0^\infty V_r f(V_r) dV_r}{\int_0^\infty V_r^3 f(V_r) dV_r}}. \quad (5.41)$$

If the particle volume distribution is given as the log-normal distribution function (eq. (5.36)), then

$$\int_0^\infty V_r^n f(V_r) dV_r = \exp\left(\frac{n^2 \sigma^2}{2}\right), \quad (5.42)$$

thus

$$\langle V \rangle = \frac{k_B T}{M_s \exp(2\sigma^2)} \sqrt{-\frac{15\chi_2^{\text{ht}'}}{\chi_0^{\text{ht}'}}}. \quad (5.43)$$

The volume fraction ε of particles can be evaluated from the experimental value of χ'_0 or χ'_2 at high temperatures using eq. (5.39) or eq. (5.40) as

$$\begin{aligned}\varepsilon &= \frac{3k_{\text{B}}T\chi_0^{\text{ht}'}}{M_{\text{s}}^2\langle V\rangle\int_0^\infty V_{\text{r}}f(V_{\text{r}})dV_{\text{r}}} = -\frac{45k_{\text{B}}^3T^3\chi_2^{\text{ht}'}}{M_{\text{s}}^4\langle V\rangle^3\int_0^\infty V_{\text{r}}^3f(V_{\text{r}})dV_{\text{r}}} \\ &= \frac{3k_{\text{B}}T\chi_0^{\text{ht}'}}{M_{\text{s}}^2\langle V\rangle}\exp\left(-\frac{\sigma^2}{2}\right) = -\frac{45k_{\text{B}}^3T^3\chi_2^{\text{ht}'}}{M_{\text{s}}^4\langle V\rangle^3}\exp\left(-\frac{9}{2}\sigma^2\right).\end{aligned}\quad (5.44)$$

From the experimental data of the susceptibilities above 100 K and the saturation magnetization M_{s} ($= 1.46 \text{ kG}$)⁵²⁾ for bulk fcc cobalt, the author obtained $\langle V\rangle = 5.6 \times 10^{-20} \text{ cm}^3$ and $\varepsilon = 0.60 \%$. The mean particle diameter has been determined to be 47.5 Å assuming the particle shape is sphere. The value of ε indicates that atomic percentage of the cobalt atoms of the precipitated fcc cobalt particles in the $\text{Cu}_{97}\text{Co}_3$ is about 20 %. This result is also supported by the value of the lattice constant (see, Section 3.1). Isolated cobalt atoms probably exhibit constant paramagnetism.⁵³⁾ The value of the temperature-independent susceptibility of the matrix, which is constituted of copper and isolated cobalt atoms, is estimated to be $0.72 \times 10^{-5} \text{ emu/cm}^3$. Here, the earlier observed data of the susceptibility per copper atom ($\chi_{\text{Cu}} = -9.1 \times 10^{-30} \text{ emu/Cu atom}$)⁵⁴⁾ and the susceptibility per cobalt atom in Cu-Co alloy ($\chi_{\text{Co}} = 4.0 \times 10^{-27} \text{ emu/Co atom}$)⁵³⁾ were used. The estimated value of the temperature-independent susceptibility is consistent with the observed value ($1.1 \times 10^{-5} \text{ emu/cm}^3$) in Section 4.1.1.

5.2.4 Anisotropy constant

The uniaxial anisotropy constant of particles can be determined from eq. (5.38) as

$$K_{\text{u}} = \frac{k_{\text{B}}\langle T_{\text{b}}\rangle}{\langle V\rangle} \ln\left(\frac{\tau_{\text{m}}}{\tau_0}\right).\quad (5.45)$$

From eq. (5.45), the author obtained $K_u = 8.8 \times 10^5 \text{ erg/cm}^3$ using the values of $\langle V \rangle$ and $\langle T_b \rangle$ obtained above. Bulk fcc cobalt has a cubic anisotropy and its anisotropy constants are $K_1 \approx -1.2 \times 10^6 \text{ erg/cm}^3$ and $K_2 \approx K_1/4$.^{55, 56)} In this case, since the anisotropy energy barrier given by $\Delta E_a \approx |K_1|V/12$, the effective uniaxial anisotropy constant is given as $K_u \approx |K_1|/12 \approx 1.0 \times 10^5 \text{ erg/cm}^3$. Thus the crystalline anisotropy cannot explain the large barrier in cobalt fine particles. Similar results are reported in some fine-particle systems.^{16, 49, 57)} Other source of anisotropy is, for example, shape anisotropy. If the particle shape is prolate ellipsoid, the uniaxial shape anisotropy constant can be written as⁴⁶⁾

$$K_u = \frac{M_s^2}{2}(N_b - N_a), \quad (5.46)$$

where N_a and N_b are the demagnetization factor along the longer a -axis and the shorter b -axis of the ellipsoid, which are given by⁵⁸⁾

$$N_a = \frac{4\pi}{m^2 - 1} \left[\frac{m}{\sqrt{m^2 - 1}} \ln(m + \sqrt{m^2 - 1}) - 1 \right], \quad (5.47)$$

$$N_b = 2\pi - \frac{N_a}{2}, \quad (5.48)$$

where

$$m = \frac{a}{b} \quad (5.49)$$

is the dimensional ratio. The dimensional ratio $m \approx 1.18$ is required to account for the observed value of K_u . This value of m is consistent with the earlier observed value ($m \approx 1.3$) for $\text{Cu}_{99}\text{Co}_1$ single crystal by small-angle neutron scattering.⁵⁹⁾

The obtained values of the parameters for $\text{Cu}_{97}\text{Co}_3$ alloy are summarized in Table 5.1.

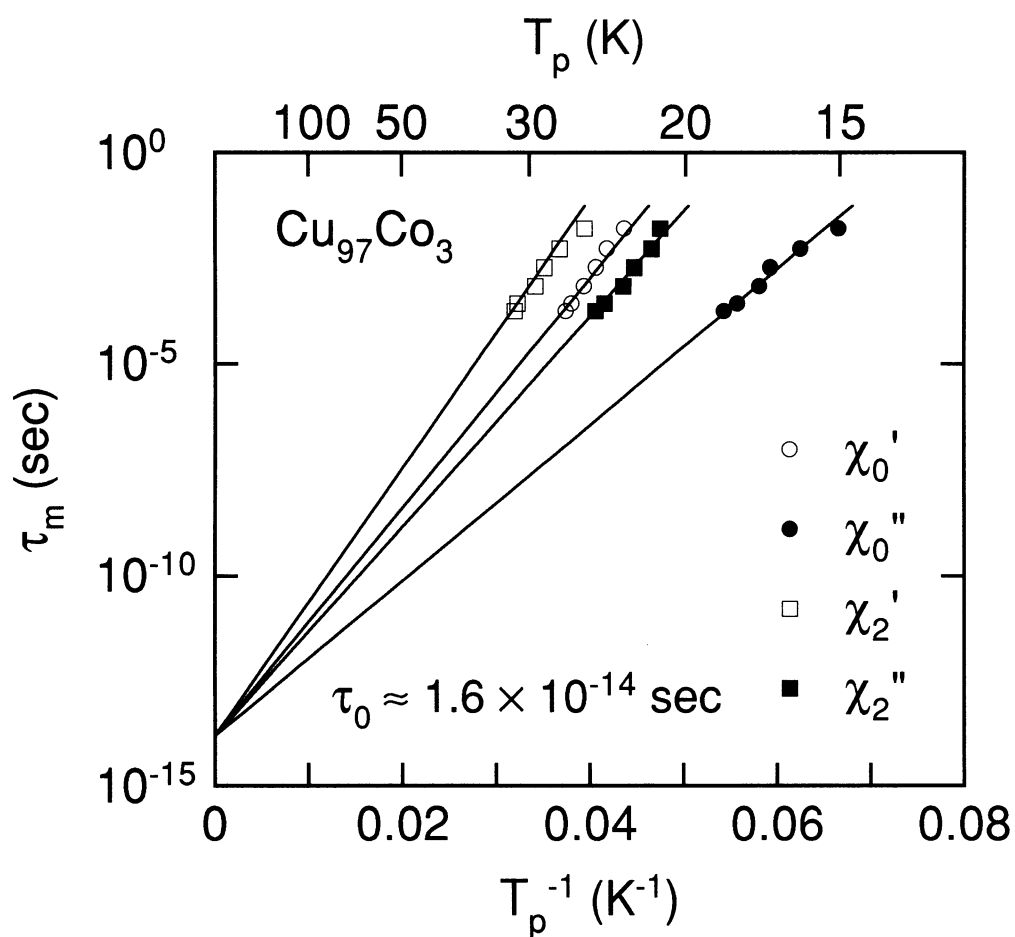


Fig. 5.3. $\text{Log}(\tau_m)$ versus T_p^{-1} plot for each susceptibility components of $\text{Cu}_{97}\text{Co}_3$ at $h_0 = 30$ Oe. The straight lines lead to an intercept to the τ_m axis equal to τ_0 .

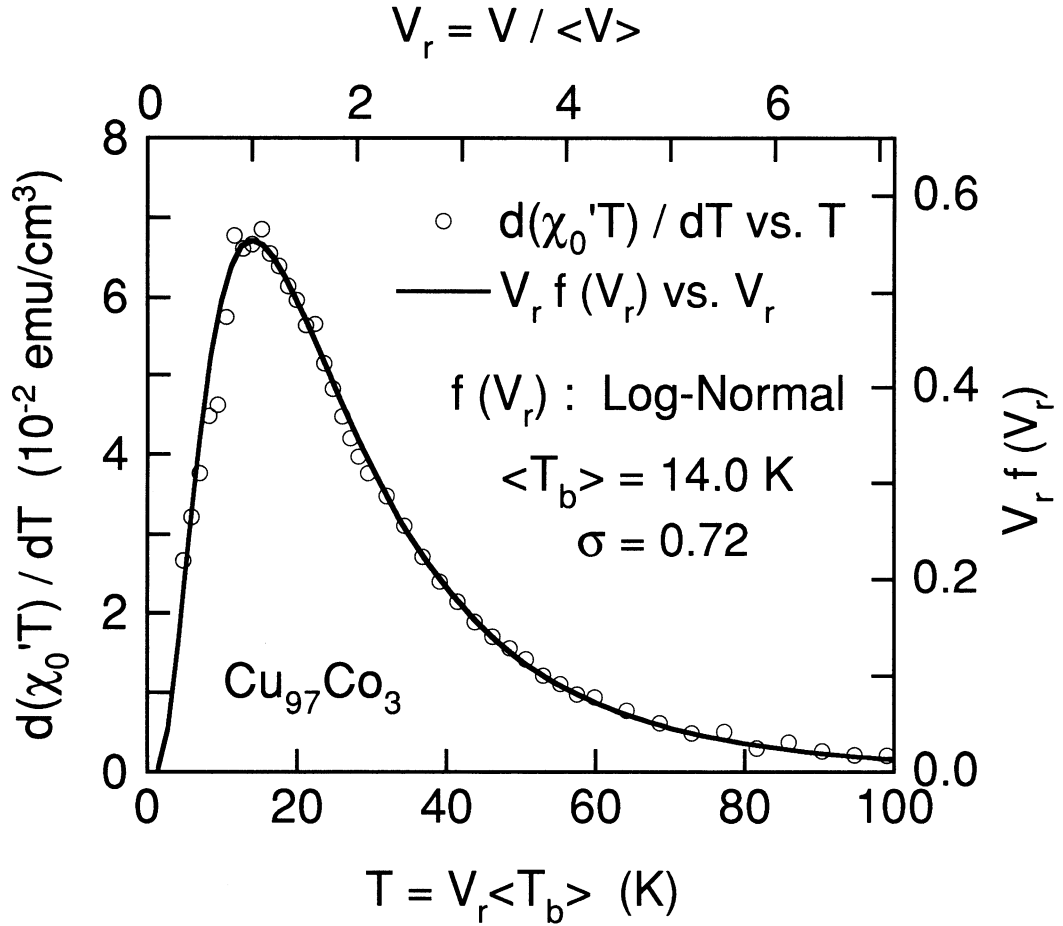


Fig. 5.4. $d(\chi_0'T)/dT$ versus T plot (open circles) for $\text{Cu}_{97}\text{Co}_3$ at $h_0 = 30$ Oe and at $\nu = 80$ Hz. The solid curve shows $V_r f(V_r)$ as a function of T_b ($= V_r \langle T_b \rangle$) calculated using the log-normal distribution function (eq. (5.36)).

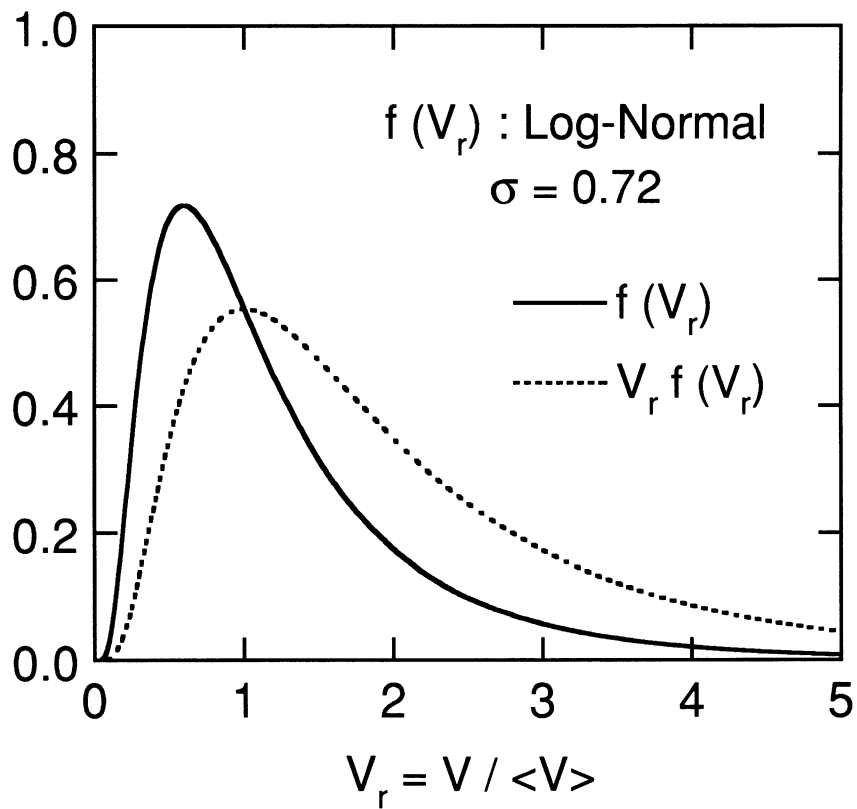


Fig. 5.5. Log-normal distribution function $f(V_r)$ (eq. (5.36)) and $V_r f(V_r)$ as a function of the reduced volume V_r .

Table 5.1. Summary of the obtained values of the parameters for $\text{Cu}_{97}\text{Co}_3$ alloy.

Characteristic relaxation time τ_0	1.6×10^{-14} sec
Mean particle volume $\langle V \rangle$	5.6×10^{-20} cm ³
(Mean particle diameter $\langle D \rangle$)	47.5 Å
Volume distribution function $f(V_r)$	Log-normal (eq. (5.36))
Standard deviation σ of $f(V_r)$	0.72
Volume fraction ε	0.60 %
Uniaxial anisotropy constant K_u	8.8×10^5 erg/cm ³
Saturation magnetization M_s	1.46 kG ^{a)}

a) The author used the value for bulk fcc cobalt.⁵²⁾

5.3 Analysis for Au-Fe alloy

In order to compare with the results of $\text{Cu}_{97}\text{Co}_3$ and of $\text{Au}_{96}\text{Fe}_4$ alloy, the analysis for $\text{Au}_{96}\text{Fe}_4$ based on the simplified blocking model has been performed. Figure 5.6 shows $d(\chi'_0 T)/dT$ versus T plot for $\text{Au}_{96}\text{Fe}_4$. The solid curve in Fig. 5.6 shows $V_r f(V_r)$ as a function of T_b , which was calculated using a rectangular distribution function (Fig. 5.7)

$$f(V_r) = \begin{cases} \frac{1}{2} & \text{for } V_r \leq 2 \\ 0 & \text{for } V_r > 2. \end{cases} \quad (5.50)$$

Since the value of $\chi''_{0\text{max}}/\chi'_{0\text{max}}$ (where $\chi'_{0\text{max}}$ and $\chi''_{0\text{max}}$ are the maximum values of χ'_0 and χ''_0 , respectively) depends on the value of τ_0 as Fig. 5.8, the value of τ_0 for was estimated from the value of $\chi''_{0\text{max}}/\chi'_{0\text{max}}$ for $\text{Au}_{96}\text{Fe}_4$. The mean particle volume $\langle V \rangle$ was determined from $|\chi'_2{}^{\text{max}}|T^3$ (where $|\chi'_2{}^{\text{max}}|$ is the maximum value of $|\chi'_2|$) and $\chi'_0 T$ above 50 K (where χ'_0 obeys the Curie law) for $\text{Au}_{96}\text{Fe}_4$.

The obtained values of the parameters for $\text{Au}_{96}\text{Fe}_4$ are summarized in Table 5.2.

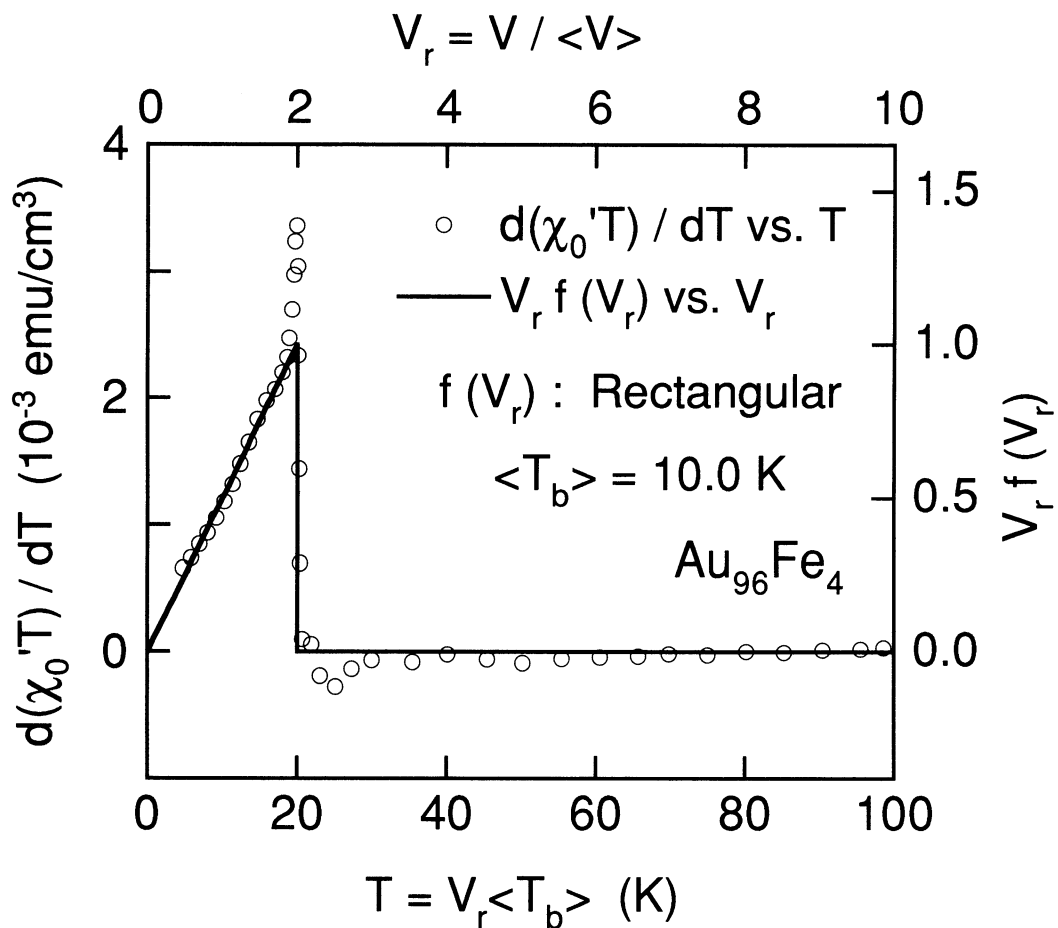


Fig. 5.6. $d(\chi_0'T)/dT$ versus T plot (open circles) for $\text{Au}_{96}\text{Fe}_4$ at $h_0 = 30$ Oe and at $\nu = 80$ Hz. The solid curve shows $V_r f(V_r)$ as a function of T_b ($= V_r \langle T_b \rangle$) calculated using the rectangular distribution function (eq. (5.50)).

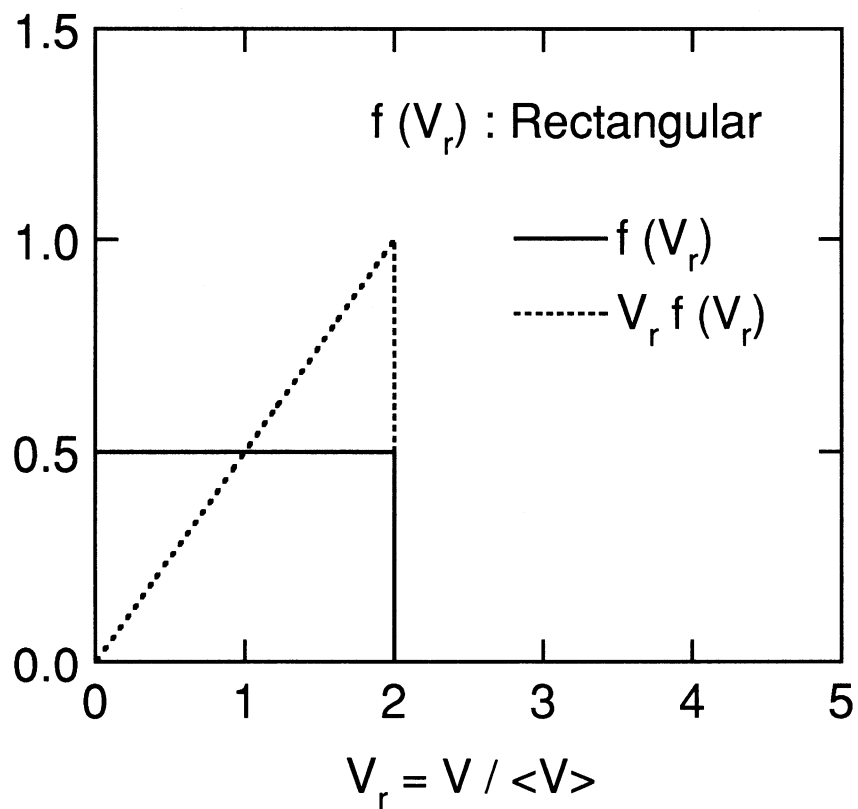


Fig. 5.7. Rectangular distribution function $f(V_r)$ (eq. (5.50)) and $V_r f(V_r)$ as a function of the reduced volume V_r .

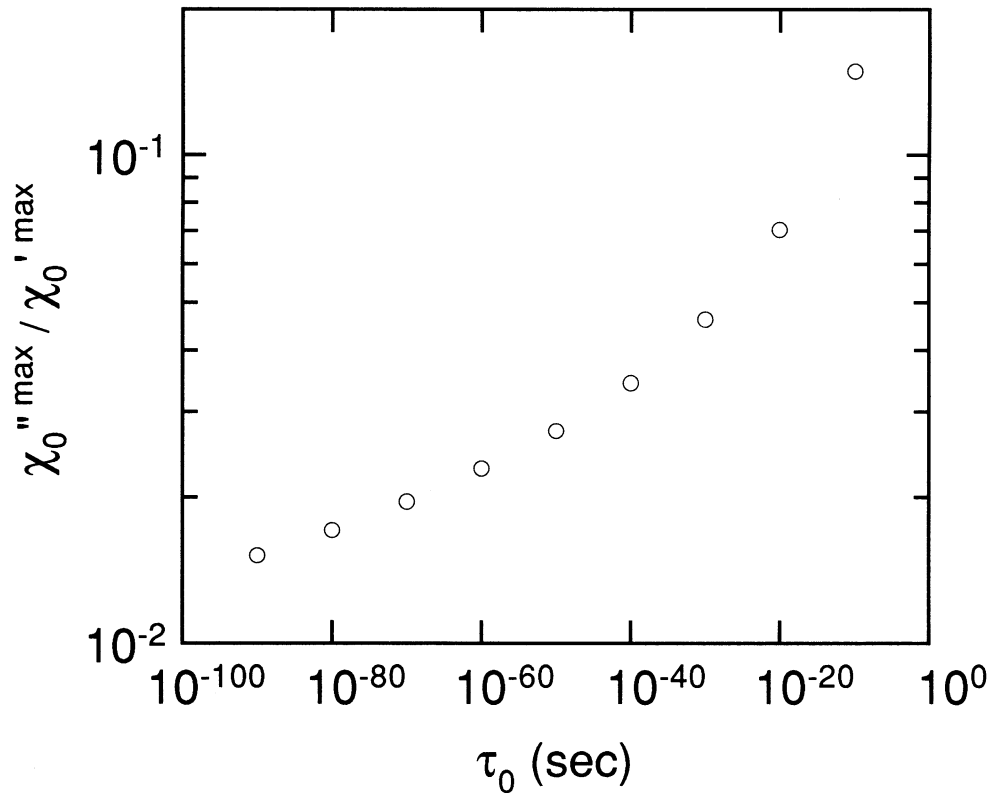


Fig. 5.8. Example of τ_0 dependence of $\chi_0''_{max} / \chi_0'_{max}$.

Table 5.2. Summary of the obtained values of the parameters for Au₉₆Fe₄ alloy.

Characteristic relaxation time τ_0	1.0×10^{-80} sec
Mean particle volume $\langle V \rangle$	9.7×10^{-21} cm ³
(Mean particle diameter $\langle D \rangle$)	26.5 Å)
Volume distribution function $f(V_r)$	Rectangular (eq. (5.50))
Volume fraction ε	3.3×10^{-2} %
Uniaxial anisotropy constant K_u	2.6×10^7 erg/cm ³
Saturation magnetization M_s	1.77 kG ^{a)}

a) The author used the value for bulk bcc iron.⁶⁰⁾

Section 6

Discussion

6.1 Linear and nonlinear susceptibilities

6.1.1 Temperature dependence

Figure 6.1 shows a representative of the calculated result of χ'_0 and χ'_2 based on the superparamagnetic blocking model described in Section 5.1.2 (eq. (5.18)) using the parameters determined in Section 5.2. All the temperature range, the calculated curve for χ'_0 is in good agreement with the experimental data for $\text{Cu}_{97}\text{Co}_3$. The temperature dependence of χ'_2 of $\text{Cu}_{97}\text{Co}_3$ is also explained by the blocking model using the volume distribution function determined from χ'_0 , except for the slight difference in the temperature at which the minimum occurs. For the out-of-phase components of the susceptibilities, as well as the in-phase susceptibilities, the blocking model reproduces the features of χ''_0 and χ''_2 of $\text{Cu}_{97}\text{Co}_3$ (Fig. 6.2).

In order to compare with the results of $\text{Cu}_{97}\text{Co}_3$ and of $\text{Au}_{96}\text{Fe}_4$ alloy, the analysis for $\text{Au}_{96}\text{Fe}_4$ based on the simplified blocking model has been performed. The calculated results for $\text{Au}_{96}\text{Fe}_4$ based on the blocking model are shown in Figs. 6.3 and 6.4. The clear cusp in χ'_0 of $\text{Au}_{96}\text{Fe}_4$ can be also explained by the blocking model with the rectangular volume distribution function (eq. (5.50)). However, it is clear that the blocking model cannot explain the divergent behavior of χ'_2 in $\text{Au}_{96}\text{Fe}_4$. In addition, the characteristic relaxation time $\tau_0 \approx 10^{-80}$ sec is required to account for the ratio of χ''_0^{max} to χ'_0^{max} . This τ_0 value has no physical meaning. It is clear that the blocking model cannot explain the divergent behavior of χ'_2 in spin glasses;

the origin of the divergent behavior of χ'_2 in spin glasses is the frustrated interaction between spins,²²⁻²⁴⁾ while the broad peak of χ_2 in fine-particle systems can be explained by the summation of the nonlinear term of the Langevin function over the particle volume distribution.

It seems that at low temperatures, calculated results for χ'_2 and χ''_2 deviate from the experimental data of $\text{Cu}_{97}\text{Co}_3$. The difference between the observed and the calculated results for χ_2 may be caused by the oversimplification of the blocking model. The causes of the difference are listed as follows. (1) Influence of interaction between the particles: As described in Section 5.2.1, the obtained value of τ_0 is rather smaller than the theoretical value. According to Dormann *et al.*,^{49, 50)} this is due to dipole interaction between the particles. They proposed a model which shows the height the anisotropy energy barrier of particles is affected by the dipole interaction, *i.e.*, the blocking temperature is affected by the interaction. (2) Distribution of the anisotropy constant K_u : As described in Section 5.2.4, the obtained value of K_u cannot be explained by the crystalline anisotropy. Therefore other source of anisotropy (*e.g.*, shape anisotropy) is important. This also suggests K_u probably have a distribution. In addition, as mentioned above, it is necessary to consider the contribution of the interaction on the height of the anisotropy energy barrier.

To describe completely the behavior of χ_0 and χ_2 , it is necessary to consider the influence of the interaction between the particles and of the distribution of K_u . However, the temperature dependence of χ_2 is rather well explained not only qualitatively but also quantitatively by the blocking model with no interaction between the particles and the distribution of K_u .

This result makes a contrast with that of spin glasses; the divergent behavior of χ_2 in spin glasses is described theoretically with the frustrated interaction between spins.²²⁻²⁴⁾

6.1.2 Frequency dependence

The calculated result of the susceptibilities for $\text{Cu}_{97}\text{Co}_3$ at various frequencies are shown in Figs. 6.5 and 6.6. For χ'_0 , χ'_2 and χ''_2 , the reduction and the shift of the peaks with increasing frequency are well explained by the superparamagnetic blocking model. On the other hand, the change of the peak height in χ''_0 is considerably smaller than that was observed by the experiment. The enhancement of the observed χ''_0 over the wide temperature range might be caused by eddy current. In this model, the inference of the eddy current is not considered. The frequency dependence of the susceptibilities is also well described by the simplified superparamagnetic blocking model.

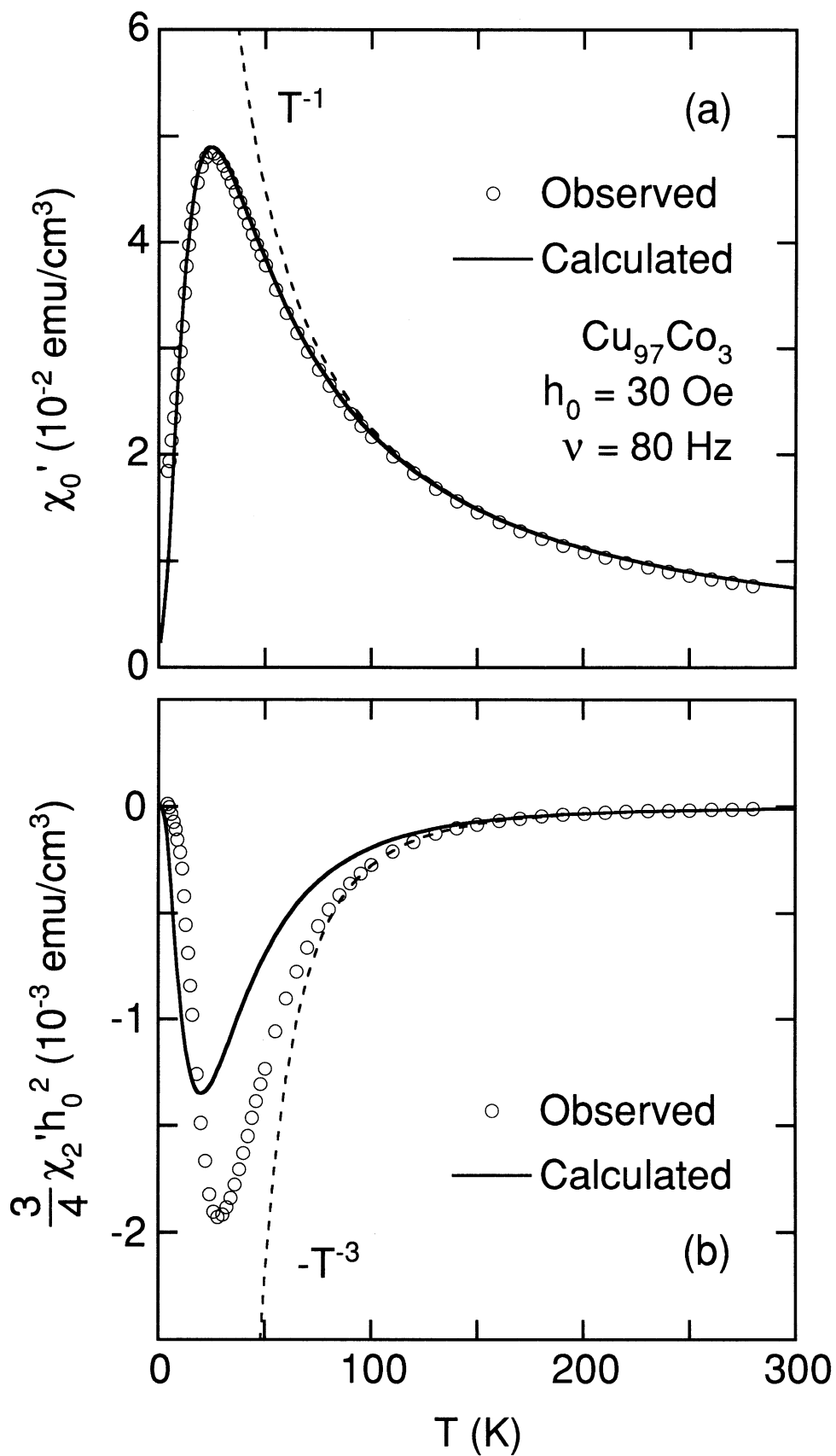


Fig. 6.1. Temperature dependence of (a) χ_0' and (b) $\frac{3}{4}\chi_2'h_0^2$ calculated for $\text{Cu}_{97}\text{Co}_3$ by the superparamagnetic blocking model. The open circles show parts of the experimental data of $\text{Cu}_{97}\text{Co}_3$.

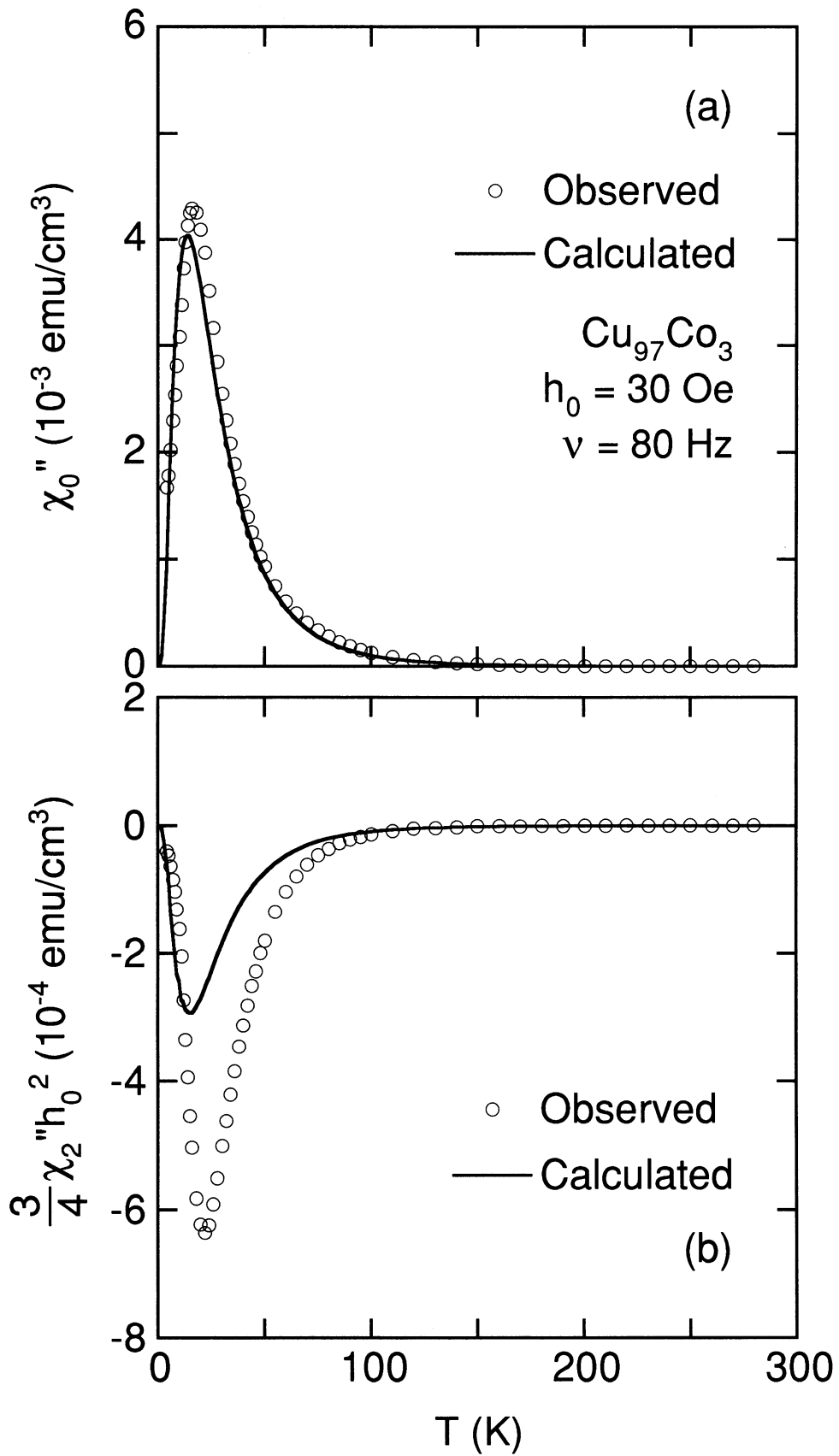


Fig. 6.2. Temperature dependence of (a) χ_0'' and (b) $\frac{3}{4}\chi_2''h_0^2$ calculated for $\text{Cu}_{97}\text{Co}_3$ by the superparamagnetic blocking model. The open circles show parts of the experimental data of $\text{Cu}_{97}\text{Co}_3$.

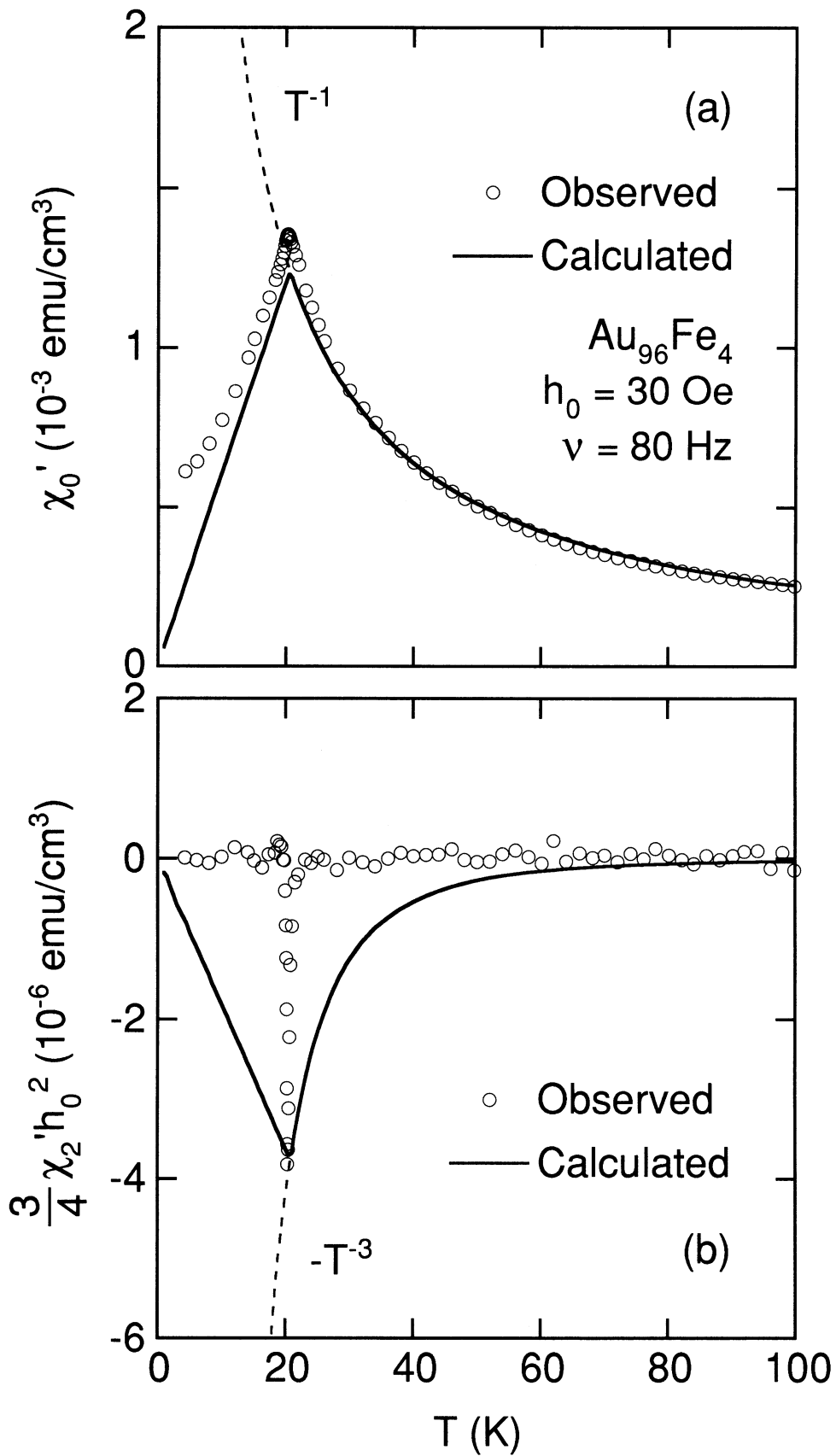


Fig. 6.3. Temperature dependence of (a) χ_0' and (b) $\frac{3}{4}\chi_2'h_0^2$ calculated for $\text{Au}_{96}\text{Fe}_4$ by the superparamagnetic blocking model. The open circles show parts of the experimental data of $\chi_0' - \chi_c$ and χ_2' for $\text{Au}_{96}\text{Fe}_4$.

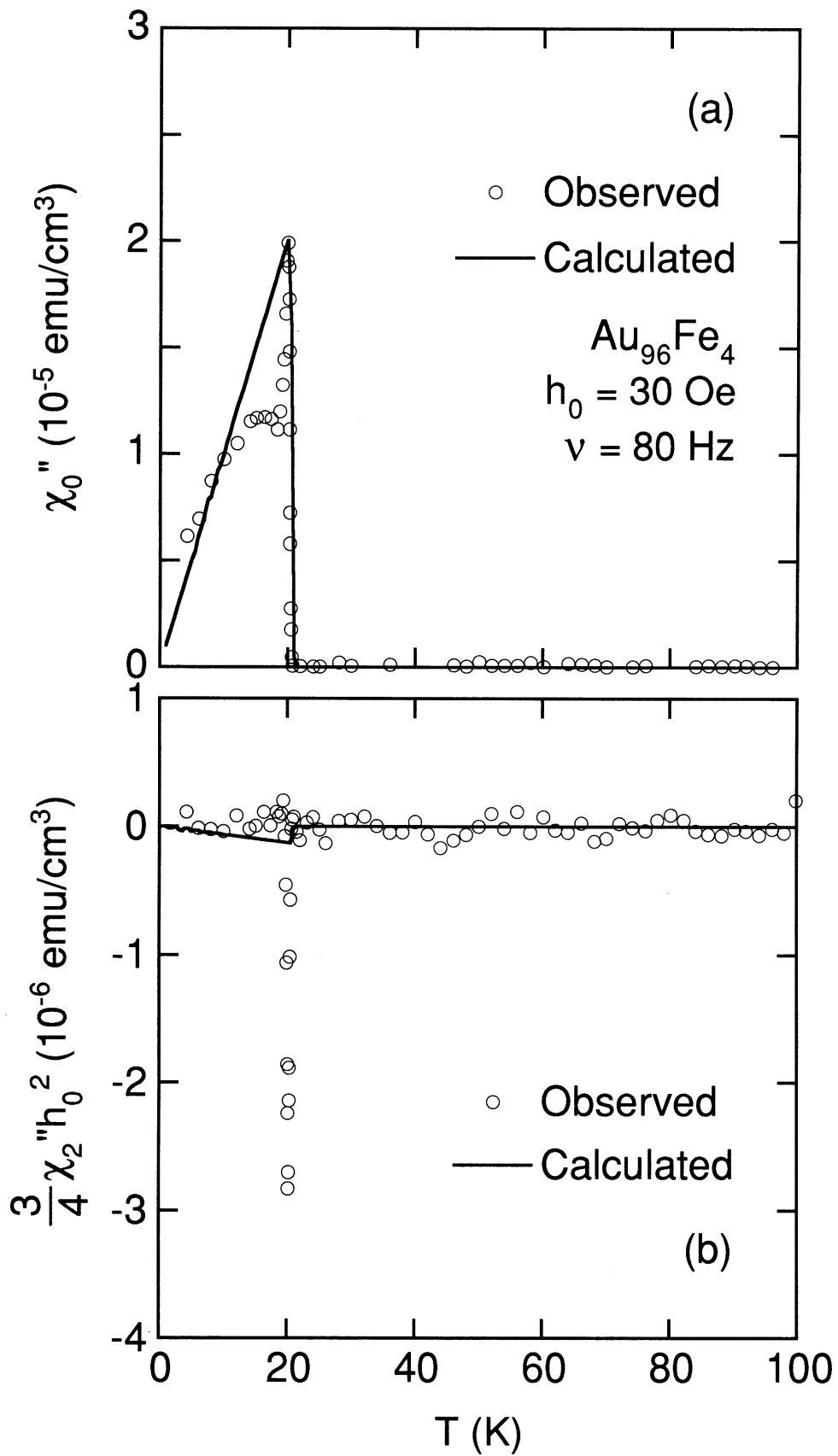


Fig. 6.4. Temperature dependence of (a) χ_0'' and (b) $\frac{3}{4}\chi_2''h_0^2$ calculated for $\text{Au}_{96}\text{Fe}_4$ by the superparamagnetic blocking model. The open circles show parts of the experimental data of $\text{Au}_{96}\text{Fe}_4$.

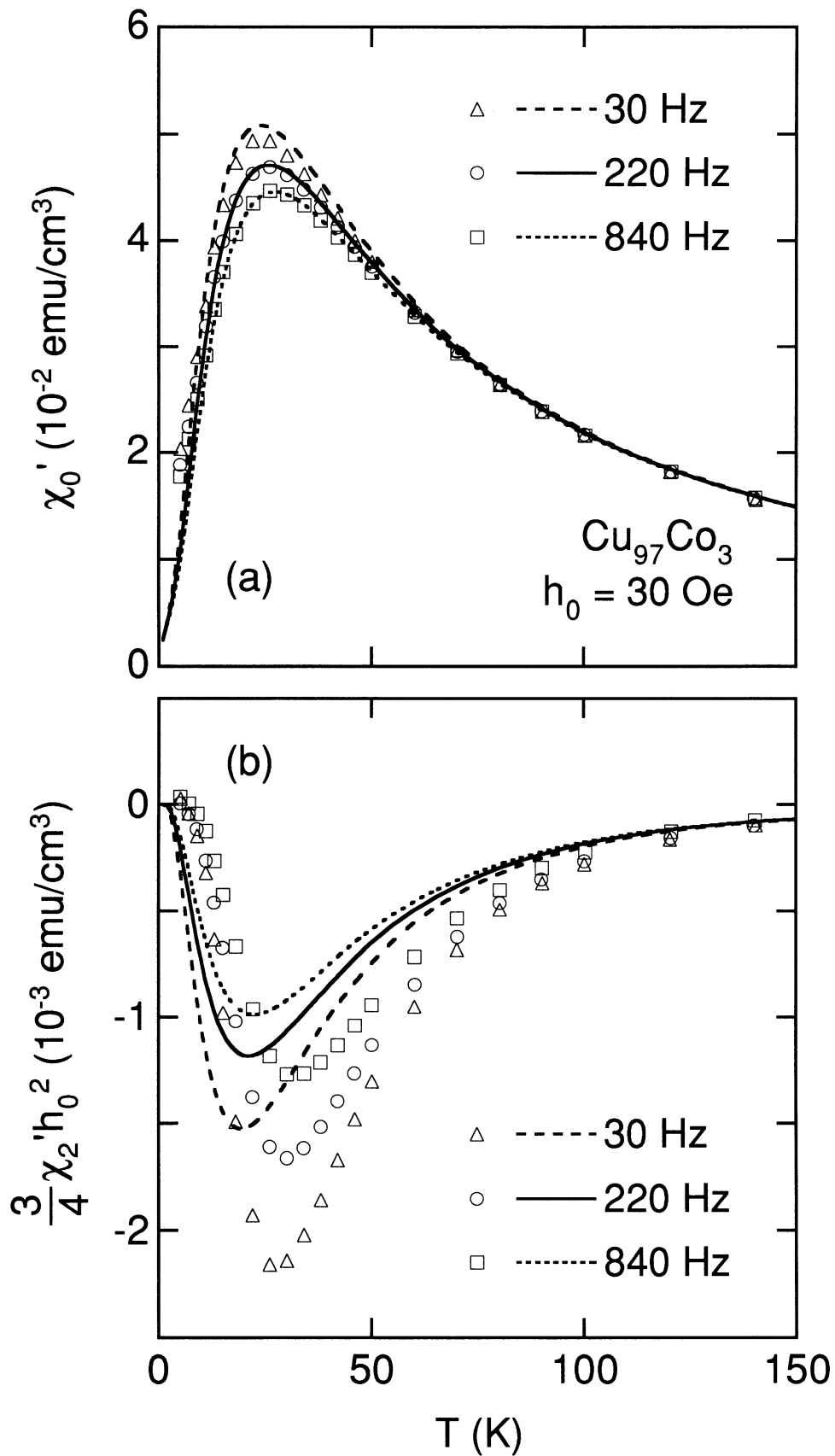


Fig. 6.5. Frequency dependence of (a) χ_0' and (b) $\frac{3}{4}\chi_2'h_0^2$ calculated by the superparamagnetic blocking model. The open symbols show parts of the experimental data of $\text{Cu}_{97}\text{Co}_3$.

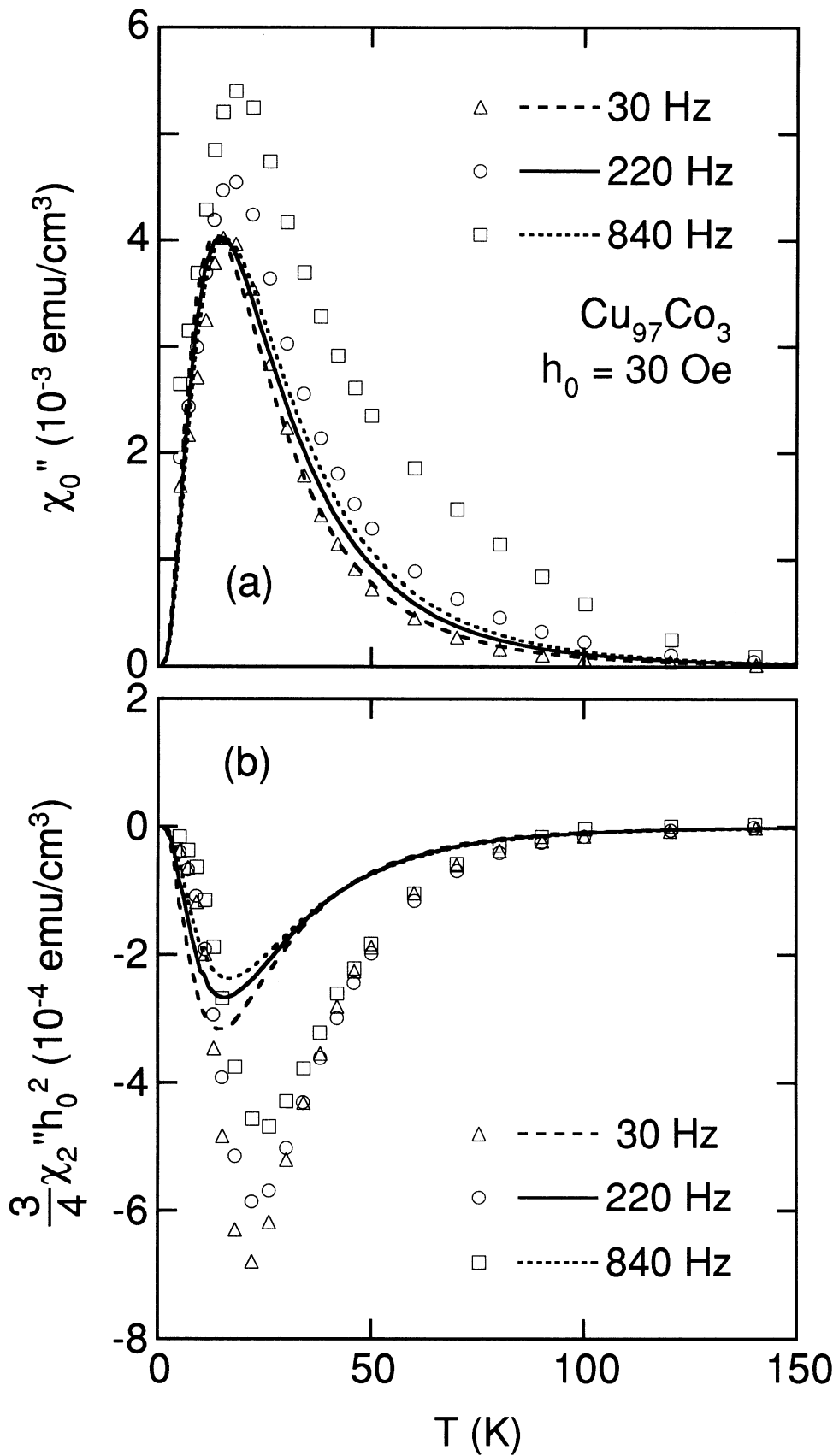


Fig. 6.6. Frequency dependence of (a) χ_0'' and (b) $\frac{3}{4}\chi_2''h_0^2$ calculated by the superparamagnetic blocking model. The open symbols show parts of the experimental data of $\text{Cu}_{97}\text{Co}_3$.

6.2 Field-cooled and zero-field-cooled magnetization

Figure 6.7 shows the calculated result of FCM and ZFCM for $\text{Cu}_{97}\text{Co}_3$ based on the superparamagnetic blocking model (eqs. (5.24) and (5.25)) using the parameters determined from the susceptibilities data in Section 5.2. The calculated curves reproduce the features of the magnetization, but there is the slight difference at low temperatures. However, as shown in Fig. 6.8, the author was able to fit the calculated results to the experimental data of ZFCM very well using the two adjustable parameters: ε ($= 0.57\%$) and σ ($= 0.76$). It should be noted that these values close to those determined from the susceptibilities data. The blocking model reproduces the following characteristic features; FCM of $\text{Cu}_{97}\text{Co}_3$ increases monotonously with decreasing temperature and becomes larger than ZFCM far above T_p . Such features reflect the distribution of the blocking temperature, *i.e.*, the distribution of the particle volume. The temperature at which the irreversibility appears corresponds to the maximum of the blocking temperature. The field-cooled-magnetization increases with decreasing temperature until all particles are blocked.

On the other hand, for $\text{Au}_{96}\text{Fe}_4$, the clear cusp in ZFCM can be also explained by the blocking model with the rectangular volume distribution function (Fig. 6.9). The difference between FCM and ZFCM appears only below T_g because T_g corresponds to the maximum blocking temperature when $f(V_r)$ is given by the rectangular distribution function.¹⁶⁾ However, the calculated result for FCM shows monotonous increasing with decreasing temperature, while the observed FCM in $\text{Au}_{96}\text{Fe}_4$ is nearly independent of temperature below T_g . This temperature-independent behavior of FCM

indicates the particle volumes have no distribution. However, it is clear that the temperature dependence of ZFCM cannot be explained by the blocking model with no particle volume distribution (Fig. 6.10). Thus, it is concluded that the blocking model cannot explain the behavior of FCM and ZFCM of $\text{Au}_{96}\text{Fe}_4$.

It must be noted that the characteristic features of FCM in fine particles (FCM increases monotonously with decreasing temperature and becomes larger than ZFCM far above T_p) are not always observed. As described above, when $f(V_r)$ is given by the rectangular distribution function, the irreversibility of the magnetization appears only below T_p . Furthermore, if the particle volumes have a narrow distribution, then FCM exhibits temperature-independent behavior at low temperatures.^{34, 61)} Therefore, the most important physical quantity, which shows the difference between the spin-glass transition and the progressive freezing of the particle moments, is the nonlinear susceptibility χ_2 .

The calculated values of FCM for $\text{Cu}_{97}\text{Co}_3$ is larger than the observed values at low temperatures (Figs. 6.7 and 6.8). This may be caused by the cooling rate dependence of T_b . Chantrell and Wohlfarth⁴⁸⁾ showed that the blocking temperature T_b depends on the cooling rate dT/dt of the sample; T_b increases with increasing $|dT/dt|$, *i.e.*, FCM at low temperatures decreases with increasing $|dT/dt|$. In this analysis, the author has neglected the cooling rate dependence of T_b because the value of $|dT/dt|$ could not be certain; the temperature was decreased stepwise in the present FCM measurements. To describe exactly the temperature dependence of FCM, it is necessary to consider the cooling rate dependence of T_b .

The calculated result of ZFCM and FCM for $\text{Cu}_{97}\text{Co}_3$ at various magnetic fields are shown in Fig. 6.11. The blocking model also reproduces the magnetic field dependence of ZFCM and FCM of $\text{Cu}_{97}\text{Co}_3$, except for the shift of T_p with increasing field. This is also due to the oversimplification of the blocking model. It is difficult to obtain the complete expression of $T_b(H)$ and of ZFCM_V below T_b . In this analysis, the expression of $T_b(H)$ when the magnetic field H is applied parallel to the easy axis,⁴⁸⁾ and the expression of ZFCM_V when H is small^{6, 46, 48)} were used.

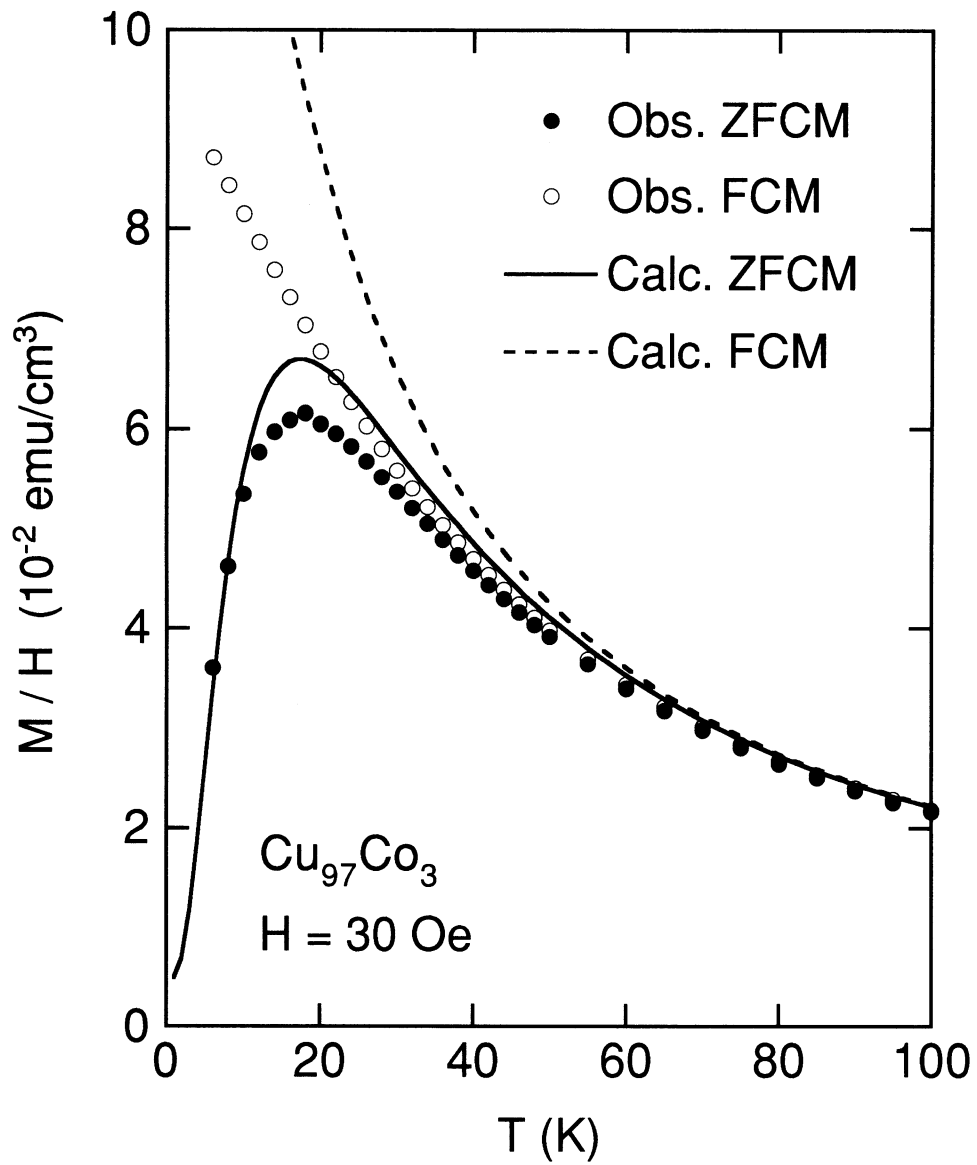


Fig. 6.7. Temperature dependence of FCM/ H and ZFCM/ H calculated for $\text{Cu}_{97}\text{Co}_3$ by the superparamagnetic blocking model using the parameters determined from the susceptibilities data. The circles show the experimental data of $\text{Cu}_{97}\text{Co}_3$.

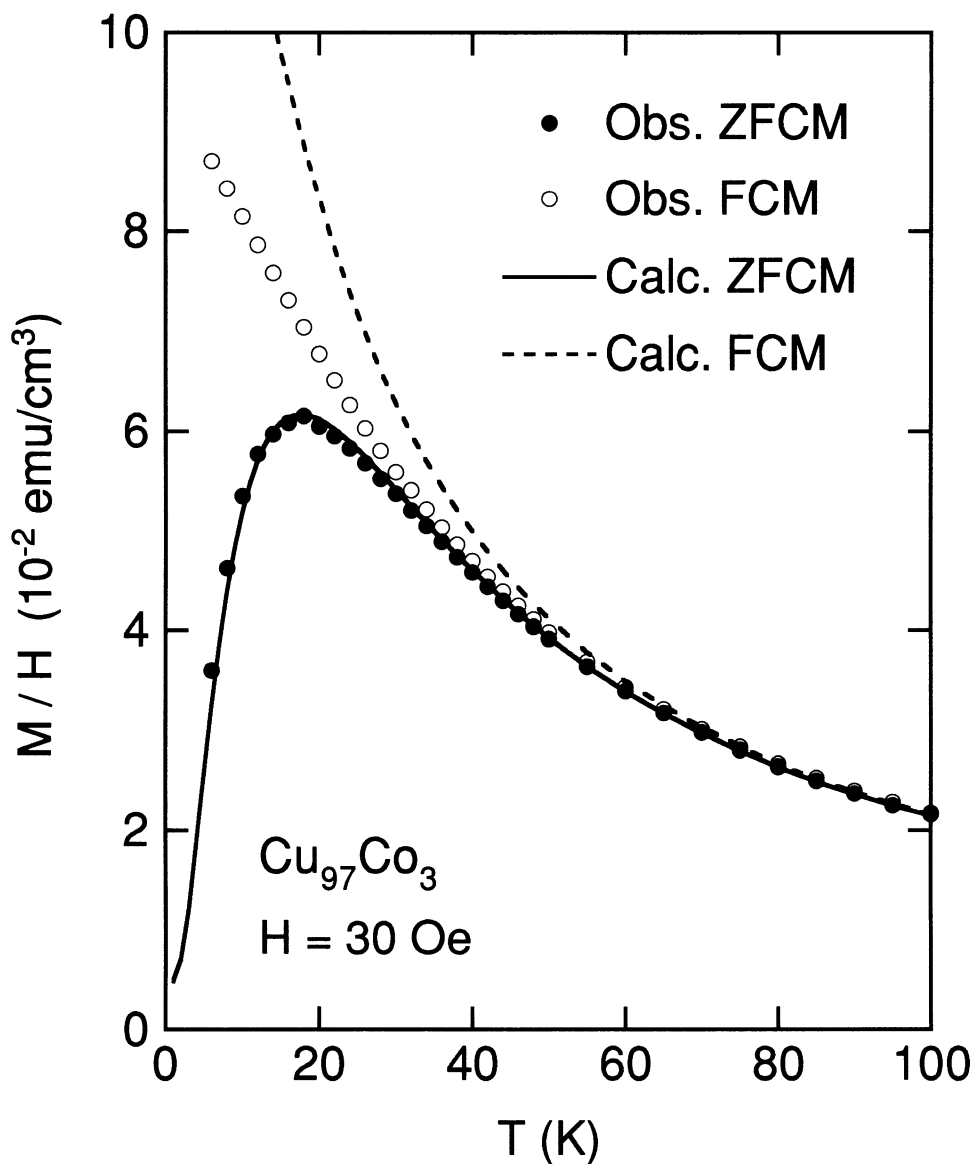


Fig. 6.8. Temperature dependence of FCM/ H and ZFCM/ H calculated for $\text{Cu}_{97}\text{Co}_3$ by the superparamagnetic blocking model using the parameters determined from the ZFCM data. The circles show the experimental data of $\text{Cu}_{97}\text{Co}_3$.

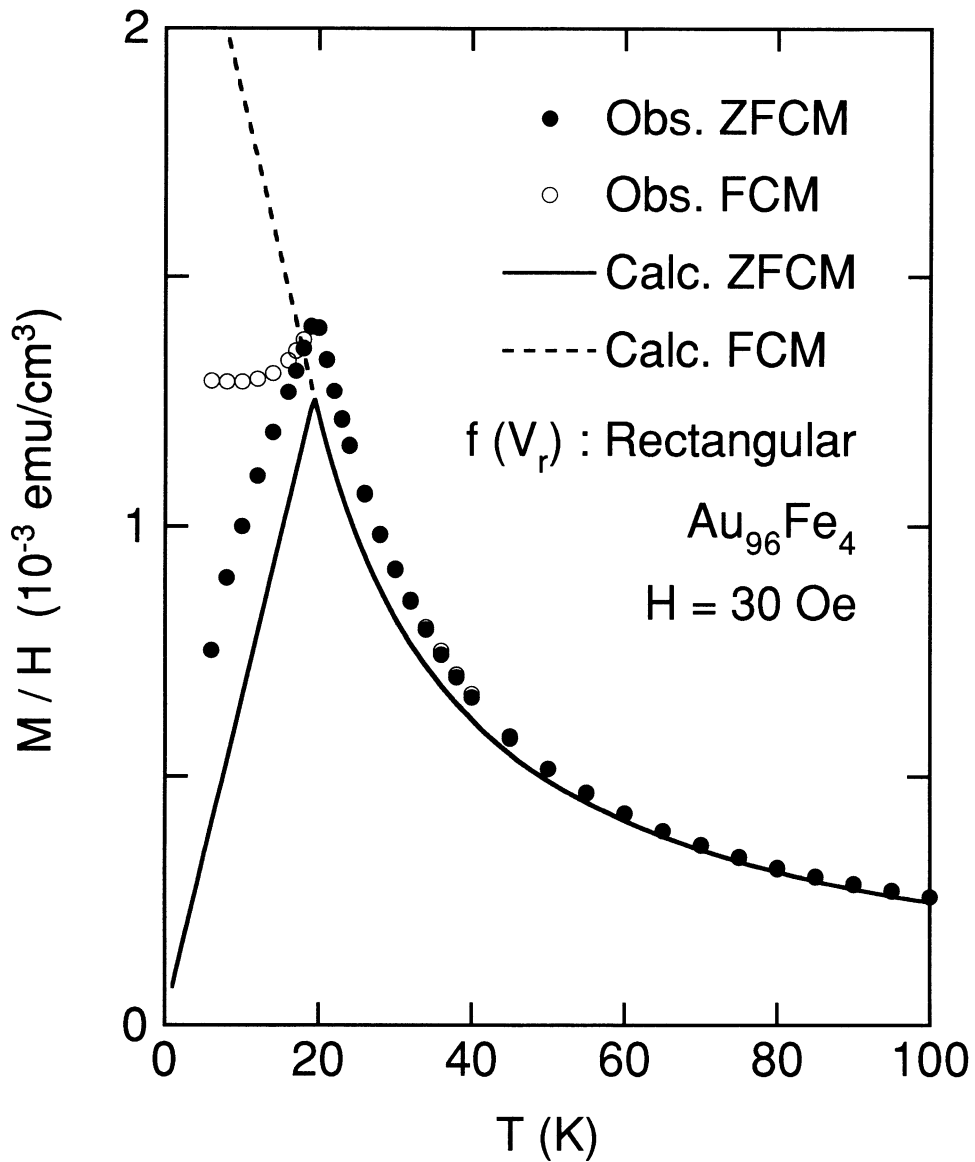


Fig. 6.9. Temperature dependence of FCM/H and ZFCM/H calculated for $\text{Au}_{96}\text{Fe}_4$ by the superparamagnetic blocking model with the rectangular volume distribution function. The circles show the experimental data of $\text{FCM}/H - \chi_c$ and $\text{ZFCM}/H - \chi_c$ for $\text{Au}_{96}\text{Fe}_4$.

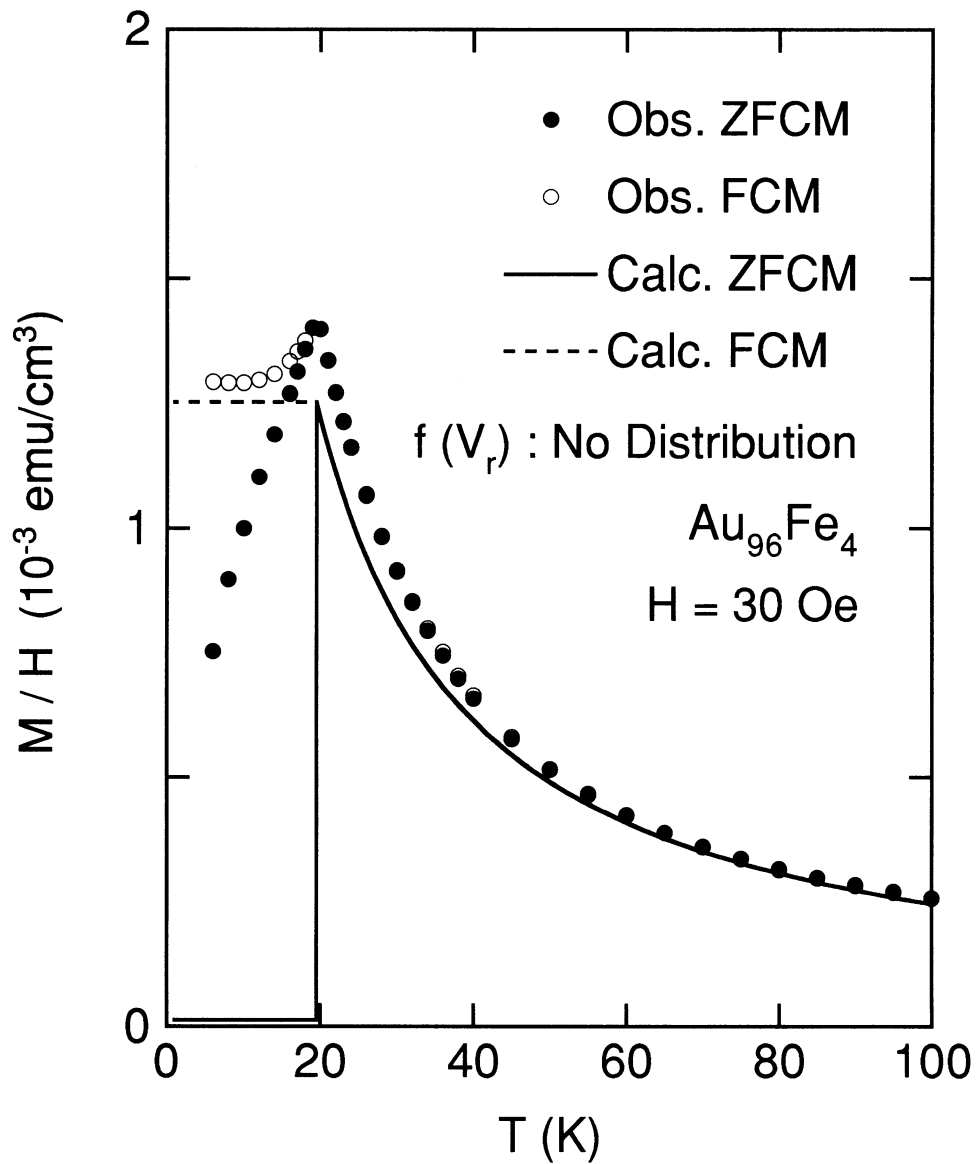


Fig. 6.10. Temperature dependence of FCM/ H and ZFCM/ H calculated for $Au_{96}Fe_4$ by the superparamagnetic blocking model with no particle volume distribution. The circles show the experimental data of FCM/ $H - \chi_c$ and ZFCM/ $H - \chi_c$ for $Au_{96}Fe_4$.

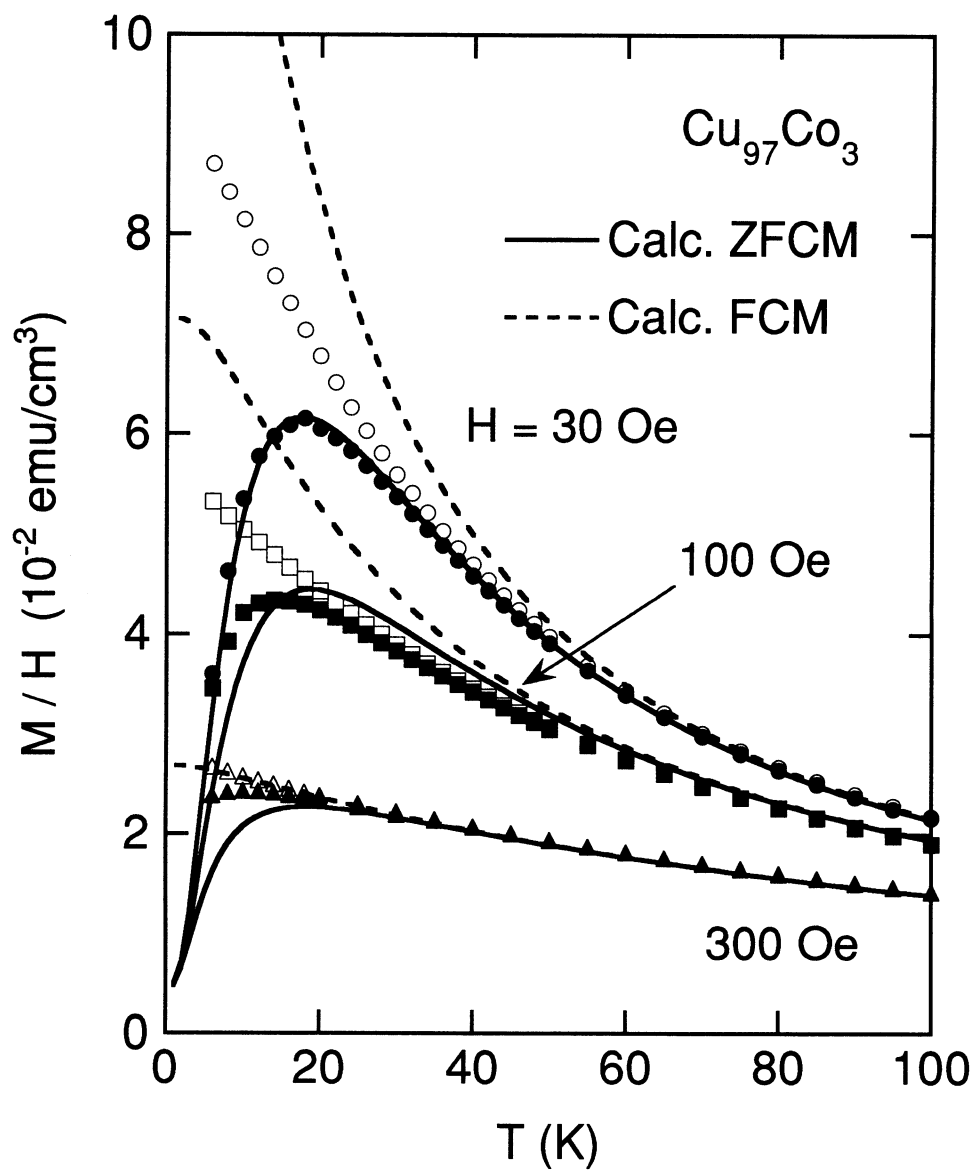


Fig. 6.11. Magnetic field dependence of FCM/ H and ZFCM/ H calculated for $\text{Cu}_{97}\text{Co}_3$ by the superparamagnetic blocking model using the parameters determined from the ZFCM data. The open and closed symbols show the experimental data for $\text{Cu}_{97}\text{Co}_3$ of FCM and ZFCM, respectively.

6.3 Magnetization curve

The solid curve (A) in Fig. 6.12 shows a calculated result of the magnetization curve for $\text{Cu}_{97}\text{Co}_3$ based on the superparamagnetic blocking model (eq. (5.27)) using the parameters determined from the susceptibilities data in Section 5.2. The calculated curve A clearly deviates from the experimental data with increasing field. This difference cannot explain the contribution from the isolated cobalt atoms in the copper matrix. The author therefore searched the values of $\langle V \rangle$, ε and σ that can describe to both magnetization curve and susceptibilities at high temperatures. Then the author obtained $\langle V \rangle = 3.5 \times 10^{-20} \text{ cm}^3$ ($\langle D \rangle = 40.6 \text{ \AA}$), $\varepsilon = 0.86 \%$, $\sigma = 0.87$ and $f(V_r)$ is the log-normal distribution function. The broken curve (B) in Fig. 6.12 shows the calculated magnetization curve using above values. The calculated curve B is in good agreement with the experimental data of $\text{Cu}_{97}\text{Co}_3$. The value of σ obtained from the magnetization curve is larger than that obtained from χ'_0 . This is due to the influence of interaction between the particles or to the distribution of K_u . However, the features of the susceptibilities and the magnetization of $\text{Cu}_{97}\text{Co}_3$ are well explained by the blocking model with no interaction between the particles and the distribution of K_u .

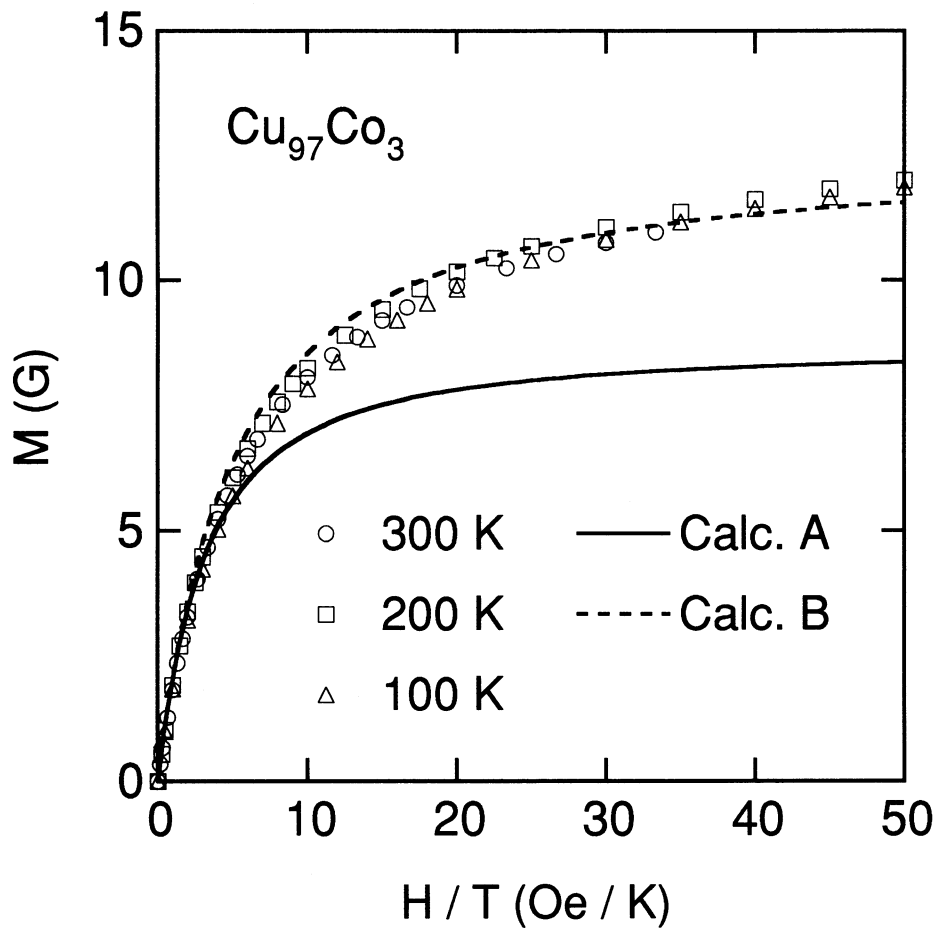


Fig. 6.12. Magnetization curves as a function of H/T calculated for $\text{Cu}_{97}\text{Co}_3$ by the superparamagnetic blocking model. The solid curve (A) shows the calculated result using the parameters determined from the susceptibilities data. The broken curve (B) shows the result of fitting the experimental data of the magnetization curve. The open symbols show the experimental data for $\text{Cu}_{97}\text{Co}_3$.

Section 7

Conclusion

The author made the following observations from detailed susceptibilities and magnetization measurements in $\text{Cu}_{97}\text{Co}_3$ alloy and from the data analysis.

(1) The linear susceptibility χ'_0 of has a spin-glass-like maximum and the nonlinear susceptibility χ'_2 has a negative peak at low temperature. However, the negative peak in χ'_2 of is very broad compared with that of spin glasses. At high temperatures, χ'_0 obeys the Curie law and χ'_2 is proportional to T^{-3} . This behavior of χ'_2 in $\text{Cu}_{97}\text{Co}_3$ is essentially different from the divergent behavior of χ'_2 in spin glasses.

(2) The temperatures dependence of susceptibilities (χ'_0 , χ''_0 , χ'_2 and χ''_2) in $\text{Cu}_{97}\text{Co}_3$ is well described quantitatively on the basis of the simplified superparamagnetic blocking model with no interaction between the particles. The broad peak of χ_2 in fine-particle systems can be explained by the summation of the nonlinear term of the Langevin function over the particle volume distribution, while the origin of the divergent behavior of χ_2 in spin glasses is the frustrated interaction between spins.

(3) The field-cooled (FCM) and zero-field-cooled (ZFCM) magnetization of $\text{Cu}_{97}\text{Co}_3$ exhibits the spin-glass-like behavior. However, the difference between FCM and ZFCM obviously appears far above the temperature at which the maximum in ZFCM occurs and FCM increases monotonously with decreasing temperature. Such behavior of the magnetization is caused by the distribution of the particle volume. The temperature dependence

of FCM and ZFCM in $\text{Cu}_{97}\text{Co}_3$ is also well described on the basis of the simplified superparamagnetic blocking model.

(4) The simplified superparamagnetic blocking model with any volume distribution gives χ'_2 proportional to T^{-3} at high temperatures. Therefore, the divergent behavior of χ'_2 in $\text{Au}_{96}\text{Fe}_4$ cannot be explained by the blocking model.

These results indicate that the origin of the magnetic properties of superparamagnetic fine particles and spin glasses is very different, though the behavior of the linear susceptibility and the magnetization of fine particles is similar to those of spin glasses. The nonlinear susceptibility χ_2 shows clearly the difference between the spin-glass transition and the progressive freezing of the particle moments.

Acknowledgements

I wishes to express my sincere gratitude to Professor Shoichi Nagata and Dr. Susumu Chikazawa for promoting this study and helpful discussions. I also wishes to express my gratitude to Professor Yoshihito Miyako and Dr. Toshifumi Taniguchi of Osaka University for the providing of the Au-Fe alloy, Professor Toshiro Sakakibara and Dr. Hiroshi Amitsuka of Hokkaido University for their help in measuring the magnetization. Finally, I also would like to thank Hirotohi Arisawa, Shuji Ebisu, Takashi Shirane, Noriaki Hasegawa, Kazuyuki Ohba, Masaki Takamatsu and Katumi Okafuji for their valuable help in this study.

Appendix A

Theory of Nonlinear Susceptibility for Spin Glass

The most fundamental theory for a phase transition is a mean field theory. In the case of spin glass transition, it has been difficult to construct the mean field theory since an order parameter has not been clear. The first attempt to make the mean field theory of spin glass was done by Edwards and Anderson.⁴⁾ The hamiltonian is

$$\mathcal{H} = -\frac{1}{2} \sum_{\langle ij \rangle} J_{ij} \mathbf{S}_i \cdot \mathbf{S}_j - H \sum_i S_i^z, \quad (\text{A.1})$$

where \mathbf{S}_i is the spin vector on site i , S_i^z is the component of \mathbf{S}_i along the applied field, $\sum_{\langle ij \rangle}$ denotes a sum over all nearest neighbor spins on sites i and j , and \sum_i denotes a sum over all spins on sites i . The exchange constants J_{ij} are randomly chosen according to a fixed distribution

$$p(J_{ij}) = \frac{1}{\sqrt{2\pi}J_0} \exp \left[-\frac{(J_{ij} - J)^2}{2J_0^2} \right], \quad (\text{A.2})$$

where J is a mean value and J_0 is a variance of the distribution. They averaged the free energy with the replica method and introduced the order parameter

$$q = \langle \langle S_i \rangle_T^2 \rangle_J, \quad (\text{A.3})$$

where $\langle \cdots \rangle_T$ is a thermal average and $\langle \cdots \rangle_J$ is a configuration average.

A Landau type phenomenological theory, which is equivalent to a mean field theory, has been extended to spin glass problems by Suzuki.²²⁾ The free energy functional was described by two order parameters, which are

magnetization m and Edwards-Anderson order parameter q as follows:

$$F(m, q) = F_0 + (am^2 + bm^4 + \dots) + (cq^2 + dq^3 + \dots) + (eqm^2 + \dots) - mH. \quad (\text{A.4})$$

The equilibrium values of m and q are determined from the following equations.

$$2(a + eq + \dots)m + 4bm^3 + \dots = H, \quad (\text{A.5})$$

$$2cq + 3dq^2 + \dots + em^2 = 0. \quad (\text{A.6})$$

For transition from paramagnetic phase to spin glass phase, the equation of the state has a following solution.

$$m = 0, \quad (\text{A.7})$$

$$q = -\frac{2c}{3d} + \dots \quad (\text{A.8})$$

The spin-glass transition temperature T_g is defined by

$$c(T_g) = 0. \quad (\text{A.9})$$

He showed that the spin-glass order parameter q is proportional to H^2 as

$$q = \chi_{\text{SG}} H^2 \geq 0, \quad (\text{A.10})$$

$$\chi_{\text{SG}} = -\frac{e}{2c(T)} \chi_0^2 \propto \frac{1}{c(T)} \geq 0. \quad (\text{A.11})$$

Therefore the conjugate field of q is a square of H and the order parameter susceptibility χ_{SG} diverges at T_g . He also showed the nonlinear susceptibility χ_2 is proportional to χ_{SG} in the vicinity of T_g . The magnetization m is expanded with respect to an applied magnetic field H in the vicinity of a spin-glass transition temperature T_g as

$$m = \chi_0 H + \chi_2 H^3 + \chi_4 H^5 + \dots, \quad (\text{A.12})$$

where χ_0 is the linear susceptibility, and χ_2, χ_4, \dots are the nonlinear susceptibilities. The relation between χ_{SG} and χ_2 near T_g is given by

$$\chi_2 = \frac{e^2}{c(T)} \chi_0^4 - 4b\chi_0^4 \propto -\chi_{\text{SG}} \leq 0. \quad (\text{A.13})$$

Thus χ_2 of spin glass diverges negatively at T_g .

The temperature dependence of χ_2 for the spin-glass transition near T_g is given as follows: The order parameters m and q are given as⁴⁾

$$m = \left\langle \tanh \left(\frac{xJ_0}{k_{\text{B}}T} \sqrt{zq} + \frac{H}{k_{\text{B}}T} \right) \right\rangle_{\text{G}}, \quad (\text{A.14})$$

$$q = \left\langle \tanh^2 \left(\frac{xJ_0}{k_{\text{B}}T} \sqrt{zq} + \frac{H}{k_{\text{B}}T} \right) \right\rangle_{\text{G}}, \quad (\text{A.15})$$

where z is the number of the nearest neighbor spins, k_{B} is the Boltzmann constant and

$$\langle Q(x) \rangle_{\text{G}} = \frac{1}{\sqrt{2\pi}} \int_{-\infty}^{\infty} Q(x) \exp \left(-\frac{x^2}{2} \right) dx. \quad (\text{A.16})$$

The spin-glass order parameter q is expanded with respect to H just above T_g as

$$q = \frac{H^2}{k_{\text{B}}^2 T^2 - zJ_0^2 \langle x^2 \rangle_{\text{G}}} + \dots = \chi_{\text{SG}} H^2 + \dots. \quad (\text{A.17})$$

Thus the order parameter susceptibility χ_{SG} is given by

$$\chi_{\text{SG}} = \frac{1}{k_{\text{B}}^2 T^2 - zJ_0^2} \approx \frac{1}{2k_{\text{B}}^2 T_g^2} \left(\frac{T_g}{T - T_g} \right), \quad (\text{A.18})$$

where

$$T_g = \frac{\sqrt{z}J_0}{k_{\text{B}}}, \quad (\text{A.19})$$

and

$$\langle x^2 \rangle_{\text{G}} = 1. \quad (\text{A.20})$$

The order parameter m is also expanded with respect to H just above T_g as

$$\begin{aligned} m &= \frac{H}{k_B^2 T} - \frac{zJ_0^2}{k_B^3 T^3} qH - \frac{H^3}{3k_B^3 T^3} + \dots \\ &\approx \frac{H}{k_B^2 T} - \frac{zJ_0^2}{k_B^3 T^3} \chi_{\text{SG}} H^3 - \frac{H^3}{3k_B^3 T^3} + \dots \end{aligned} \quad (\text{A.21})$$

Therefore the nonlinear susceptibility χ_2 is given by

$$\chi_2 = -\frac{zJ_0^2}{k_B^3 T^3} \chi_{\text{SG}} - \frac{1}{3k_B^3 T^3} \approx -\frac{1}{2k_B^3 T_g^3} \left(\frac{T_g}{T - T_g} \right). \quad (\text{A.22})$$

Thus the nonlinear susceptibility χ_2 diverges negatively at T_g obeying eq. (A.22). Similar results were obtained by Wada and Takayama²³⁾ using the Sherrington-Kirkpatrick model⁶²⁾ (infinite-ranged interaction model), and by Fujiki and Katsura²⁴⁾ using the Bethe approximation.

In general, the mean field theory and the Landau phenomenology neglect fluctuation effects. Including the fluctuation effects, physical quantities near T_g deviates from the results of the mean field theory. Then the temperature dependence of χ_2 for temperatures just above T_g is dominated by the following power law divergence:^{22, 24)}

$$\chi_2 = \Gamma t^{-\gamma}, \quad (\text{A.23})$$

$$t \equiv \frac{T - T_g}{T_g}, \quad (\text{A.24})$$

where t is the reduced temperature, γ (> 1)²⁴⁾ is the critical exponent, Γ is the critical amplitude.

References

- 1) J. W. Shih: Phys. Rev. **38** (1931) 2051.
- 2) O. S. Lutes and J. L. Schmit: Phys. Rev. **134** (1964) A676.
- 3) V. Cannella and J. A. Mydosh: Phys. Rev. **B6** (1972) 4220.
- 4) S. F. Edwards and P. W. Anderson: J. Phys. **F5** (1975) 965.
- 5) See, *e.g.*, K. H. Fischer and J. A. Hertz: *Spin glasses* (Cambridge Univ., Cambridge, 1991) p. 301,
- 6) E. P. Wohlfarth: Phys. Lett. **70A** (1979) 489.
- 7) R. W. Chantrell, M. El-Hilo and K. O'Grady: IEEE Trans. Magn. **27** (1991) 3570.
- 8) J. J. Becker: Trans. AIME **209** (1957) 59.
- 9) J. D. Livingston: Trans. Met. Soc. AIME **215** (1959) 566.
- 10) K. Krop, J. Mizia and A. Korbel: Acta. Met. **15** (1967) 463.
- 11) C. A. M. Mulder, A. J. van Duynveldt and J. A. Mydosh: Phys. Rev. **B23** (1981) 1384.
- 12) L. E. Wenger and P. H. Keesom: Phys. Rev. **B13** (1976) 4053.
- 13) S. Nagata, P. H. Keesom and H. R. Harrison: Phys. Rev. **B19** (1979) 1633.
- 14) F. Holtzberg, J. L. Tholence and R. Tournier: *Amorphous Magnetism II*, eds. R. A. Levy and R. Hasegawa (Plenum, New York, 1977) p. 155.
- 15) C. E. Violet and R. J. Borg: Phys. Rev. **149** (1966) 540.
- 16) J. L. Gittleman, B. Abeles and S. Bozowski: Phys. Rev. **B9** (1974) 3891.
- 17) J. L. Dormann, D. Fiorani, J. L. Tholence and C. Sella: J. Magn. & Magn. Mater. **35** (1983) 117.

- 18) R. Tournier, J. J. Veyssié and L. Weil: *J. Phys. Radium* **23** (1962) 672.
- 19) M. El-Hilo and K. O'Grady: *IEEE Trans. Magn.* **26** (1990) 1807.
- 20) M. El-Hilo, K. O'Grady and J. Popplewell: *J. Appl. Phys.* **69** (1991) 5133.
- 21) C. J. W. Koch, M. B. Madsen and S. Mørup: *Hyperfine Interact.* **28** (1986) 549.
- 22) M. Suzuki: *Prog. Theor. Phys.* **58** (1977) 1151.
- 23) K. Wada and H. Takayama: *Prog. Theor. Phys.* **64** (1980) 327.
- 24) S. Fujiki and S. Katsura: *Prog. Theor. Phys.* **65** (1981) 1130.
- 25) Y. Miyako, S. Chikazawa, T. Saito and Y. G. Youchunas: *J. Phys. Soc. Jpn.* **46** (1979) 1951.
- 26) S. Chikazawa, C. J. Sandberg and Y. Miyako: *J. Phys. Soc. Jpn.* **50** (1981) 2884.
- 27) S. Chikazawa, S. Taniguchi, H. Matsuyama and Y. Miyako: *J. Magn. & Magn. Mater.* **31–34** (1983) 1355.
- 28) T. Taniguchi, H. Matsuyama, S. Chikazawa and Y. Miyako: *J. Phys. Soc. Jpn.* **52** (1983) 4323.
- 29) T. Taniguchi and Y. Miyako: *J. Phys. Soc. Jpn.* **57** (1988) 3520.
- 30) R. Omari, J. J. Prejean and J. Souletie: *J. Phys. (Paris)* **44** (1983) 1069.
- 31) H. Bouchiat: *J. Phys. (Paris)* **47** (1986) 71.
- 32) D. Fiorani, J. L. Dormann, J. L. Tholence, L. Bessais and D. Villers: *J. Magn. & Magn. Mater.* **54–57** (1986) 173.
- 33) D. Fiorani, J. Tholence and J. L. Dormann: *J. Phys.* **C19** (1986) 5495.
- 34) D. Fiorani: *Magnetic Properties of Fine Particles*, eds. J. L. Dormann

- and D. Fiorani (North-Holland, Amsterdam, 1992) p. 135.
- 35) M. R. Corson: *Rev. Sci. Instrum.* **53** (1982) 1606.
 - 36) T. Bitoh, T. Shirane and S. Chikazawa: *J. Phys. Soc. Jpn.* **62** (1993) 2837.
 - 37) R. B. Goldfarb and J. V. Minervini: *Rev. Sci. Instrum.* **55** (1984) 761.
 - 38) H. Arisawa: Thesis for a Degree of Master of Engineering, Muroran Institute of Technology, Muroran, Hokkaido (1988).
 - 39) R. V. Chamberlin, M. Hardiman and R. Orbach: *J. Appl. Phys.* **52** (1981) 1771.
 - 40) R. V. Chamberlin, M. Hardiman, L. A. Turkevich and R. Orbach: *Phys. Rev.* **B25** (1982) 6720.
 - 41) L. Néel: *Ann. Geophys.* **5** (1949) 99.
 - 42) L. Néel: *Adv. Phys.* **4** (1955) 191.
 - 43) W. F. Brown, Jr.: *Phys. Rev.* **130** (1963) 1677.
 - 44) A. Aharoni: *Phys. Rev.* **B7** (1973) 1103.
 - 45) See, *e.g.*, E. Kneller: *Magnetism and Metallurgy*, eds. A. E. Berkowitz and E. Kneller (Academic, New York, 1969) Vol. 1, Chap. VIII, p. 393.
 - 46) E. C. Stoner and E. P. Wohlfarth: *Philos. Trans. R. Soc. London* **A240** (1948) 599.
 - 47) Y. Kimura and R. Hayakawa: *Jpn. J. Appl. Phys.* **31** (1992) 3387.
 - 48) R. W. Chantrell and E. P. Wohlfarth: *Phys. Stat. Sol. (a)* **91** (1985) 619.
 - 49) J. L. Dormann, J. Bessais and D. Fiorani: *J. Phys.* **C21** (1988) 2015.
 - 50) J. L. Dormann: *Magnetic Properties of Fine Particles*, eds. J. L. Dormann and D. Fiorani (North-Holland, Amsterdam, 1992)

p. 115.

- 51) E. P. Wohlfarth: J. Phys. **F10** (1980) L241.
- 52) J. Crangle: Philos. Mag. **46** (1955) 499.
- 53) R. Tournier and A. Blandin: Phys. Rev. Lett. **24** (1970) 397.
- 54) E. Vogt: *Magnetism and Metallurgy*, eds. A. E. Berkowitz and E. Kneller (Academic, New York, 1969) Vol. 1, Chap. VI, p. 251.
- 55) C. P. Bean, J. D. Livingston and D. S. Rodbell: J. Phys. Radium **20** (1959) 298.
- 56) D. S. Rodbell: J. Phys. Soc. Jpn. **17S** (1962) 313.
- 57) K. O'Grady, R. W. Chantrell, J. Popplewell and S. W. Charles: IEEE Trans. Magn. **MAG-16** (1980) 1077.
- 58) R. M. Bozorth: *Ferromagnetism* (Van Nostrand, New York, 1951) p. 849.
- 59) M. Ernst, J. Schelten and W. Schmatz: Phys. Stat. Sol. (a) **7** (1971) 469.
- 60) R. Pauthenet: J. Appl. Phys. **53** (1982) 2029.
- 61) X. Batlle, M. G. del Muro, J. Tejada, H. Pfeiffer, P. Gönert and E. Sinn: J. Appl. Phys. **74** (1993) 3333.
- 62) D. Sherrington and S. Kirkpatrick: Phys. Rev. Lett. **35** (1975) 1792.

List of Figures

Fig. 2.1	Ac susceptibility of spin-glass Au-Fe alloys and of Ni fine particles in SiO ₂ films as a function of temperature.	10
Fig. 2.2	Frequency dependence of low field ac susceptibility of a spin-glass Cu _{99.06} Mn _{0.94} alloy and of Fe fine particles in an amorphous Al ₂ O ₃ film.	11
Fig. 2.3	Specific heat of a spin-glass Cu _{0.988} Mn _{0.012} alloy and of Co fine particles in Cu-Co alloys.	12
Fig. 2.4	Temperature dependence of field-cooled and zero-field-cooled magnetization of spin-glass Cu-Mn alloys and of ferrofluid.	13
Fig. 2.5	Time decays of IRM(<i>t</i>) of a spin-glass Au ₉₂ Fe ₈ alloy and of ferrofluid.	14
Fig. 2.6	Mössbauer spectra of a spin-glass Au _{93.3} Fe _{6.7} alloy and of goethite fine particles at various temperatures.	15
Fig. 2.7	Nonlinear susceptibility χ_2 of a spin-glass Au _{98.5} Fe _{1.5} alloy and of Fe fine particles in an amorphous Al ₂ O ₃ film.	16
Fig. 3.1	X-ray diffraction patterns of Cu ₉₇ Co ₃ and Au ₉₆ Fe ₄ alloys.	18
Fig. 3.2	Schematic diagram of the measuring system for ac susceptibilities.	22
Fig. 3.3	Circuit diagram of the mutual inductance bridge (1).	23
Fig. 3.4	Circuit diagram of the mutual inductance bridge (2).	24
Fig. 3.5	Schematic cross section of the measuring coils.	25
Fig. 4.1	Temperature dependence of the in-phase linear (χ'_0) and nonlinear ($\frac{3}{4}\chi'_2 h_0^2$) susceptibilities of Cu ₉₇ Co ₃ alloy.	32

Fig. 4.2	Temperature dependence of the out-of-phase linear (χ_0'') and nonlinear ($\frac{3}{4}\chi_2''h_0^2$) susceptibilities of $\text{Cu}_{97}\text{Co}_3$ alloy.	33
Fig. 4.3	Inverse of the in-phase susceptibility $(\chi_0' - \chi_c)^{-1}$ of $\text{Cu}_{97}\text{Co}_3$ alloy as a function of temperature.	34
Fig. 4.4	In-phase susceptibility χ_0' of $\text{Cu}_{97}\text{Co}_3$ alloy as a function of T^{-1}	35
Fig. 4.5	Frequency dependence of the in-phase linear (χ_0') and non-linear ($\frac{3}{4}\chi_2'h_0^2$) susceptibilities of $\text{Cu}_{97}\text{Co}_3$ alloy.	36
Fig. 4.6	Frequency dependence of the out-of-phase linear (χ_0'') and nonlinear ($\frac{3}{4}\chi_2''h_0^2$) susceptibilities of $\text{Cu}_{97}\text{Co}_3$ alloy.	37
Fig. 4.7	In-phase linear (χ_0') and nonlinear ($\frac{3}{4}\chi_2'h_0^2$) susceptibilities of $\text{Cu}_{97}\text{Co}_3$ and $\text{Au}_{96}\text{Fe}_4$ as a function of temperature.	38
Fig. 4.8	Out-of-phase linear (χ_0'') and nonlinear ($\frac{3}{4}\chi_2''h_0^2$) susceptibilities of $\text{Cu}_{97}\text{Co}_3$ and $\text{Au}_{96}\text{Fe}_4$ as a function of temperature.	39
Fig. 4.9	Inverse of the in-phase susceptibility $(\chi_0' - \chi_c)^{-1}$ of $\text{Au}_{96}\text{Fe}_4$ alloy as a function of temperature.	40
Fig. 4.10	In-phase susceptibility χ_0' of $\text{Au}_{96}\text{Fe}_4$ alloy as a function of T^{-1}	41
Fig. 4.11	Log-log plot $-\frac{3}{4}\chi_2'h_0^2$ versus the reduced temperature t of $\text{Au}_{96}\text{Fe}_4$ above T_g	42
Fig. 4.12	Log-log plot of $-\frac{3}{4}\chi_2'h_0^2$ versus temperature for $\text{Cu}_{97}\text{Co}_3$	43
Fig. 4.13	Temperature dependence of the field-cooled (FCM/ H) and the zero-field-cooled (ZFCM/ H) magnetization/field for $\text{Cu}_{97}\text{Co}_3$ and $\text{Au}_{96}\text{Fe}_4$	45

Fig. 4.14 Magnetic field dependence of FCM/ H and ZFCM/ H of $\text{Cu}_{97}\text{Co}_3$ alloy.	46
Fig. 4.15 Magnetic field dependence of FCM/ H and ZFCM/ H of $\text{Au}_{96}\text{Fe}_4$ alloy.	47
Fig. 4.16 Initial magnetization curves of $\text{Cu}_{97}\text{Co}_3$ alloy at various temperatures.	49
Fig. 4.17 Magnetization curves of $\text{Cu}_{97}\text{Co}_3$ alloy at 6 K, 20 K and 50 K.	50
Fig. 4.18 Magnetization curves of $\text{Cu}_{97}\text{Co}_3$ alloy at 100 K, 200 K and 300 K.	51
Fig. 4.19 Initial magnetization curves of $\text{Cu}_{97}\text{Co}_3$ alloy as a function of H/T	52
Fig. 4.20 Initial magnetization curves of $\text{Au}_{96}\text{Fe}_4$ alloy at various temperatures.	53
Fig. 4.21 Magnetization curves of $\text{Au}_{96}\text{Fe}_4$ alloy at 6 K and 20 K. . .	54
Fig. 4.22 Magnetization curves of $\text{Au}_{96}\text{Fe}_4$ alloy at 50 K and 100 K.	55
Fig. 4.23 Initial magnetization curves of $\text{Au}_{96}\text{Fe}_4$ alloy as a function of H/T	56
Fig. 5.1 Schematic behavior of the linear susceptibility χ_{V0} and the nonlinear susceptibility χ_{V2} as a function of T/T_b	63
Fig. 5.2 Schematic behavior of the field-cooled and zero-field-cooled magnetization as a function of $T/T_b(H = 0)$ at various magnetic fields.	64
Fig. 5.3 $\text{Log}(\tau_m)$ versus T_p^{-1} plot for each susceptibility components of $\text{Cu}_{97}\text{Co}_3$ at $h_0 = 30$ Oe.	70

Fig. 5.4	$d(\chi'_0 T)/dT$ versus T plot for $\text{Cu}_{97}\text{Co}_3$ at $h_0 = 30$ Oe and at $\nu = 80$ Hz.	71
Fig. 5.5	Log-normal distribution function $f(V_r)$ and $V_r f(V_r)$ as a function of the reduced volume V_r	72
Fig. 5.6	$d(\chi'_0 T)/dT$ versus T plot for $\text{Au}_{96}\text{Fe}_4$ at $h_0 = 30$ Oe and at $\nu = 80$ Hz.	75
Fig. 5.7	Rectangular distribution function $f(V_r)$ and $V_r f(V_r)$ as a function of the reduced volume V_r	76
Fig. 5.8	Example of τ_0 dependence of $\chi_0''^{\text{max}}/\chi_0'^{\text{max}}$	77
Fig. 6.1	Temperature dependence of χ'_0 and $\frac{3}{4}\chi_2' h_0^2$ calculated for $\text{Cu}_{97}\text{Co}_3$ by the superparamagnetic blocking model.	82
Fig. 6.2	Temperature dependence of χ_0'' and $\frac{3}{4}\chi_2'' h_0^2$ calculated for $\text{Cu}_{97}\text{Co}_3$ by the superparamagnetic blocking model.	83
Fig. 6.3	Temperature dependence of χ'_0 and $\frac{3}{4}\chi_2' h_0^2$ calculated for $\text{Au}_{96}\text{Fe}_4$ by the superparamagnetic blocking model.	84
Fig. 6.4	Temperature dependence of χ_0'' and $\frac{3}{4}\chi_2'' h_0^2$ calculated for $\text{Au}_{96}\text{Fe}_4$ by the superparamagnetic blocking model.	85
Fig. 6.5	Frequency dependence of χ'_0 and $\frac{3}{4}\chi_2' h_0^2$ calculated by the superparamagnetic blocking model.	86
Fig. 6.6	Frequency dependence of χ_0'' and $\frac{3}{4}\chi_2'' h_0^2$ calculated by the superparamagnetic blocking model.	87
Fig. 6.7	Temperature dependence of FCM/ H and ZFCM/ H calculated for $\text{Cu}_{97}\text{Co}_3$ by the superparamagnetic blocking model using the parameters determined from the susceptibilities data. . .	91

Fig. 6.8	Temperature dependence of FCM/ H and ZFCM/ H calculated for $\text{Cu}_{97}\text{Co}_3$ by the superparamagnetic blocking model using the parameters determined from the ZFCM data.	92
Fig. 6.9	Temperature dependence of FCM/ H and ZFCM/ H calculated for $\text{Au}_{96}\text{Fe}_4$ by the superparamagnetic blocking model with the rectangular volume distribution function.	93
Fig. 6.10	Temperature dependence of FCM/ H and ZFCM/ H calculated for $\text{Au}_{96}\text{Fe}_4$ by the superparamagnetic blocking model with no particle volume distribution.	94
Fig. 6.11	Magnetic field dependence of FCM/ H and ZFCM/ H calculated for $\text{Cu}_{97}\text{Co}_3$ by the superparamagnetic blocking model using the parameters determined from the ZFCM data.	95
Fig. 6.12	Magnetization curves as a function of H/T calculated for $\text{Cu}_{97}\text{Co}_3$ by the superparamagnetic blocking model.	97

List of Tables

Table 3.1 Dimensions and the number of turns in the measuring coils. 26

Table 5.1 Summary of the obtained values of the parameters for
Cu₉₇Co₃ alloy. 73

Table 5.2 Summary of the obtained values of the parameters for
Au₉₆Fe₄ alloy. 78